MODELING AND FAILURE ANALYSIS OF COMPOSITE I-BEAMS FOR UAV WING SPAR DESIGN

By

Zachary Taylor Watkins

Bachelor of Science in Mechanical Engineering

The University of Oklahoma

Norman, OK

2019

Submitted to the Faculty of the
Graduate College of the
Oklahoma State University
in partial fulfillment of
the requirements for
the Degree of
MASTER OF SCIENCE
May 2021

MODELING AND FAILURE ANALYSIS OF

COMPOSITE I-BEAMS FOR UAV WING SPAR

DESIGN

Thesis Approved:

Dr. Andrew S. Arena

Thesis Adviser

Dr. Joseph P. Conner

Dr. Richard Geata

Dr. Jamey Jacob

ACKNOWLEDGEMENTS

First, I must thank my advisor Dr. Andy Arena. Through this research process, he has provided insight and guidance into areas I would have never considered. When I started this, I was student who had no idea how to perform proper research. Dr. Arena provided me with the instructional guidance to carry out research from the beginning ideas all the way to end, with both answers to current research and questions to be solved in future research.

I also must thank my friends in Stillwater and all over the country. I am sure they all got tired of me complaining how hard the work was and constantly blowing off plans to keep working, but through it all, their support helped me to keep pushing through. To everyone all over the country, thank you for that support. You have no idea how much I really needed it through this year-and-a-half process.

I must give one final thanks to my parents, Shawn and Tobie Watkins. Without them, I would not be where I am right now. Since I was a child, my parents have supported me in everything I do. They have instilled a strong work ethic and a sense of pride in all work I do. Seeing their example of hard work every day inspired me to constantly push myself and strive for greatness. I cannot express how thankful I am for them and everything they have done to support me through my educational and professional journey. I love you Mom and Dad, thank you for everything.

Name: ZACHARY TAYLOR WATKINS

Date of Degree: MAY 2021

Title of Study: MODELING AND FAILURE ANALYSIS OF COMPOSITE I-BEAMS FOR UAV WING SPAR DESIGN

Major Field: MECHANICAL AND AEROSPACE ENGINEERING

Abstract: In unmanned aerial systems (UAS), the composite I-beam using carbon fiber caps and a cross-grain balsa shear web is often used for the main spar. This manufacturing method is underdeveloped in analysis causing engineers to have to use intuition and iterative test procedures until a spar is made that meets the requirements for the flight envelope. Beyond analysis, the material properties of balsa wood with the geometry and loading unique to these I-beams is unknown. This research plans to experimentally determine the material properties of balsa wood and determine its failure modes to create and validate an analysis tool for the composite I-beams. The Wing Spar Analysis Program is created in MathCad that simulates bending of composite I-beams to determine the failure modes. The material properties of balsa wood are tested for tensile failure and shear failure. These material properties are then used to create prototype I-beams, using readily available materials, and composite I-beams, using carbon fiber caps and cross-grain balsa wood shear webs. The I-beams are tested in a three-point bender and the data is used to validate the Wing Spar Analysis Program. It is found that the Wing Spar Analysis Program gives a percent difference between experimental and expected stress in the range of 2.571% - 36.256% for composite I-beams of lengths between five and ten inches. Through visual inspection, it is also found that shear failure in the composite I-beams creates a vertical crack in the balsa wood shear web that causes a failure in the epoxy that bonds the I-beam together. It is also found that balsa wood is highly dependent on its thickness, where thicker balsa wood samples have a higher probability for defects and failure.

TABLE OF CONTENTS

Chapter Page

LIST OF TABLES

Table Page

LIST OF FIGURES

Figure Page

Figure Page

Figure Page

CHAPTER I

INTRODUCTION

In recent history, UAVs (Unmanned Aerial Vehicles) have seen a rise to prominence in both defense, commercial, and academic settings. These vehicles can be seen deployed in military settings across the globe, monitoring oil pipelines, and in university laboratories teaching undergraduate students the fundamentals of aircraft design. While these vehicles share many similarities with the manned aircraft seen flying all over the world, one area that is underdeveloped in UAVs is the structural engineering of the vehicles. Many of the guidelines used in designing the physical structure of the aircraft is all based off "rule of thumb" and "engineering intuition." The structural components of the aircraft will be designed and manufactured and then tested. If the component does not work, more material is added, and the test is performed again. This continues to happen until a component is found that does not break during testing. This method takes all the engineering out of the structural design of the aircraft and turns the process into "guess-and-check." This method is most prominent in designing the wing spars.

For years, a composite I-beam made using material with tensile and compressive strength for the caps with a balsa wood shear web has been used in UAVs to carry the loads experienced by the wing. Composite I-beams can be seen with spruce caps and balsa wood shear webs in RC aircraft made by modelers in their free time. The material in composite I-beams has changed to carbon fiber caps and balsa wood shear webs in professional UAVs and high speed, high g-loading

RC aircraft. At the same time, designers have been guessing the size needed for the caps and balsa wood, testing the wing, and going back to make the I-beam bigger when the wing fails. This method is a waste of time for the designer and little work has been done to understand the failure mechanisms associated with these composite I-beams despite how composite I-beams are widely used for UAV wing spars.

The research presented in this thesis will begin to change the "guess-and-check" method to a method rooted in engineering. Work done by Dr. AndY Arena and I have led to the development of an analysis tool has been created that uses the loading on wings of various geometries to determine the failure modes of the composite I-beam shear web. This research will attempt to validate the code by testing balsa wood and composite I-beams to understand the failure modes and validate this program. Once validated, this program can be used by future aircraft designers to create structurally efficient wing spars without having to go through the cycle of building and testing until something that doesn't break is found.

Goals and Objectives

This research has two goals. The first goal for this research is to understand the structural properties, structural interaction, and failure modes in composite I-beams using carbon fiber caps and a balsa wood shear web. This means that the individual material properties of balsa need to be understand, and then testing with composite I-beams can be performed to see the material interactions. The second goal is to create an analysis tool that uses the transformed area method that can analyze composite I-beams with reasonable certainty for designing UAV wing spars. To do this, four objectives are outlined that will lead to successfully achieving the goals:

1. Conduct an extensive literature review to over previous work done to understand the material properties of the individual materials, carbon fiber and balsa wood, and the interaction of the materials in composite I-beam spars used in UAV designs.

2. Develop the analysis program for a three-point bending loading scenario that utilizes the transformed-area method to analyze composite I-beam designs while also validating the program with theoretical loading scenarios that have been previously solved.
3. Conduct tensile and shear experiments for balsa wood to gain an understanding and create a database of material properties for balsa wood under tensile and shear loading.
4. Manufacture and test composite I-beams of various geometries using in-house three-point bending material tester to understand failure modes and to validate analysis program.

Outline

The following chapters will discuss the techniques utilized in developing the initial analysis tools as well as the experimental setup for the testing of the balsa and the composite I-beams. First, a thorough literature review will be discussed that includes an analysis of UAS structure and previous experiments with balsa wood. Second, there will be a discussion on the development of the analysis tool used to analyze the failure of the composite I-beams. Third, balsa wood will be tested for orientations and failure that are commonly seen in beam bending, particularly shear and normal. Fourth, the experimental setup will be detailed for the three-point bending tests of the composite I-beams. Finally, the analysis tool will be revised, and final tests will be done on full-scale composite I-beams to fully validate the analysis tool.

CHAPTER II

REVIEW OF LITERATURE

The literature review will focus on two areas. First, an overview of the use of composite I-beams for spar design will be discussed. This overview looks at the RC aircraft made by hobbyists as well as the tools and information they use when designing wing spars. This information was picked up by professional aircraft designers in academic and industry settings. With the overview known, an in-depth discussion occurs that describes the material properties of unidirectional carbon fiber and balsa wood that are used in composite I-beam spars for UAVs currently made. With the initial understandings of the material properties, experiments can be designed that will help to understand what is still unknown.

Background and Rationale for Composite UAV Spars

In aircraft structural design, the wing's main structural components are the skin, ribs, stringers, and spar. The skin creates a sealed surface for supporting aerodynamic pressure distributions that create aerodynamic loads. The ribs act as shape support to ensure the wing keeps its airfoil shape and work in tangent with the skin to resist aerodynamic loads. The stringers help the skin resist buckling failure by adding support to the skin and sub-dividing the skin into panels. The spar acts as the main load bearing component of the wing by carrying both ground loads and air loads [1]. While this research focuses on spar design and analysis, it is important to note that the other structural components serve important roles in the aircraft structure but will not be the focus of this literature review and research.

In the lifetime of an aircraft, it will experience various loads on and off the ground. On the ground, the aircraft experiences load due to its own weight and taxiing around the runway. In the air, the aircraft experiences load due to steady-level flight, flight maneuvers, and weather patterns [2]. The wing is the main lifting body on the aircraft, so the wing must be able to handle these loads without structural failure. This is where the wing spar comes into play. The spar is the main structural component and is designed to resist the loads in the air and on the ground [2]. These loads are experienced as direct, bending, shear, and torsional loads and the spar must be designed to handle these loads individually and as a combination of the loads.

There are numerous variables that come into play with the wing spar design, three of which are the weight, geometry, and materials. In the UAS field, it is even more important to keep all these variables in-mind due to the unique challenges that come in UAS flight operations. This study looks at the composite I-beam that has the ability to be optimize for all three variables. The composite I-beam used today uses thin layers of unidirectional carbon fiber tape for the caps of the beam and a cross-grain balsa wood shear web. This design utilizes the high tensile and compressive

strength of carbon fiber, the high shear strength of balsa wood, and the low weight of both materials in a unique geometry to create a spar that is light enough for use in UAS but can also resist the loads experienced in flight. A diagram of the composite I-beam spar design can be seen in Figures 1 and 2 below:

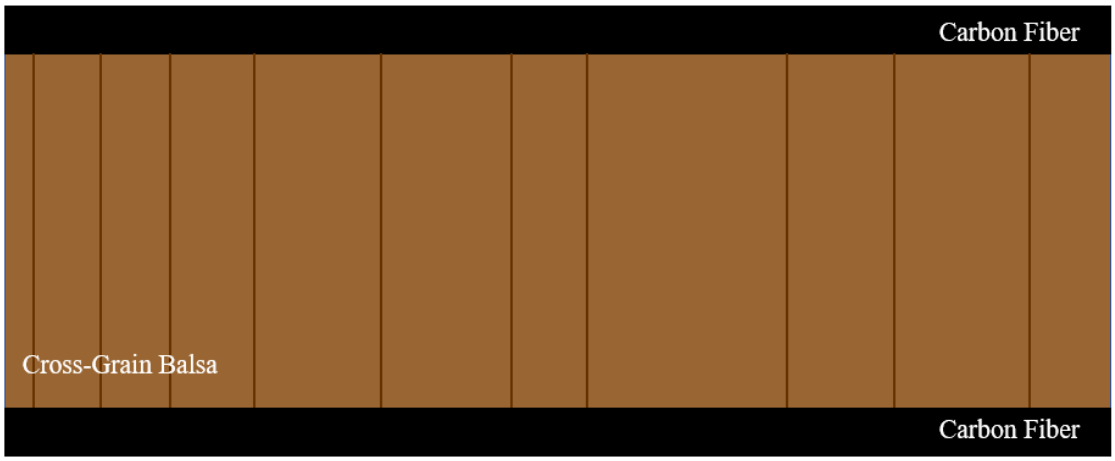

Figure 1: Side view of composite I-beam

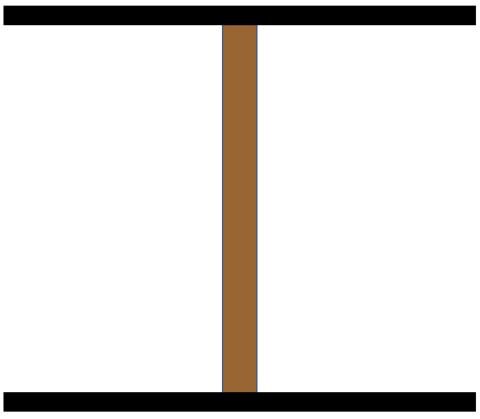

Figure 2: Front view of composite I-beam

This idea is not novel though. RC modelers have been using adding balsa wood shear web between spars made of hardwood for years [3]. By adding this material, the shear strength of the wing spar is increased. The composite I-beam design seen in Figure 3 and Figure 4 is more rudimentary compared to the carbon fiber and balsa wood I-beams. In Figures 3 and 4, the RC

aircraft designer uses the spruce spars as the caps to the I-beam and inserts the balsa wood between the two spars to create an I-beam. The idea is the same as using the carbon fiber and balsa wood I-beams. The spruce handles most of the normal stress from the flight load while the balsa wood takes the shear loading and increases the area moment of inertia to create a stiffer spar. It is important to note how the balsa wood is oriented. In Figure 1, the balsa wood is oriented with the grain structure vertically. This is known as cross-grain balsa. The balsa wood is oriented in this direction to add additional shear strength to the wing spar. The shear forces act perpendicularly to the grain direction. The grain direction creates the strength the balsa needs to resist the shear loads in the shear web. If the balsa is oriented in the opposite way, with grain direction running horizontally down the length of the wing, the shear loads will cause a failure down the length of the wing and the shear web becomes useless. In the forum post "Shear Webs used in Wings" Johnson specifically states, "I have seen designs that had webs arranged with the grain running span-wise. This is absolutely wrong and if you ever see this in a kit or a plan, then make the webs with the grain running vertically between the spars." [3]

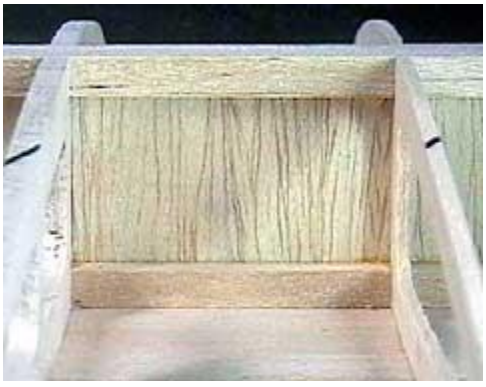

Figure 3: Composite I-beam found in RC airplane using spruce caps and balsa wood shear web [3]

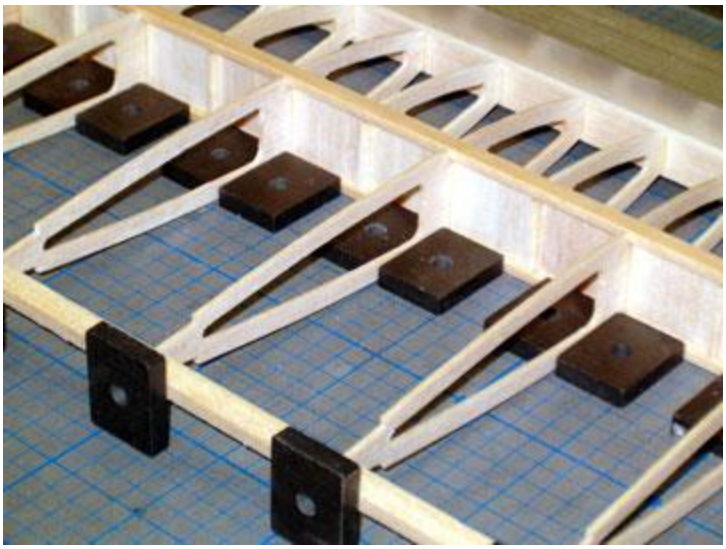

Figure 4: RC airplane wing spar using spruce and balsa wood

On the blog, "Dave Harding's Boehle (Bailey) Giant Blog," the RC modeler goes through iterative process of manufacturing spars, testing the spars, and rebuilding until a design can handle the loads associated with flight [4]. The modeler begins his design using the same methods in Figures 3 and 4. He uses spruce caps with a 3/32" balsa shear web at the root of the wing and a 1/16" balsa shear web for the rest of the wing. After testing his first design, he decides to add carbon caps to his spruce to again increase the stiffness of his wing spar. Figure 5 below shows his final wing with the noticeable carbon fiber caps added down the length of the wing spars.

Figure 5: RC airplane wing using carbon fiber caps, spruce, and balsa wood

Finally, as RC aircraft have increased their speed and g-loading, the manufacturers have turned to carbon fiber caps with balsa shear webs. These composite I-beams are designed to handle the high g-loading of flights. An example of this comes from the F5D Viper. The viper utilizes three layers of cross-grain balsa with carbon fiber sandwiched between the balsa to create the shear web. The aircraft also uses a piece of carbon uni-tape that is as thick as the composite skin. The uni-tape is manufactured at the same time as the composite skin where everything is layed-up together to create a single, homogenous skin [5]. The Figures below show examples of the Viper wing construction.

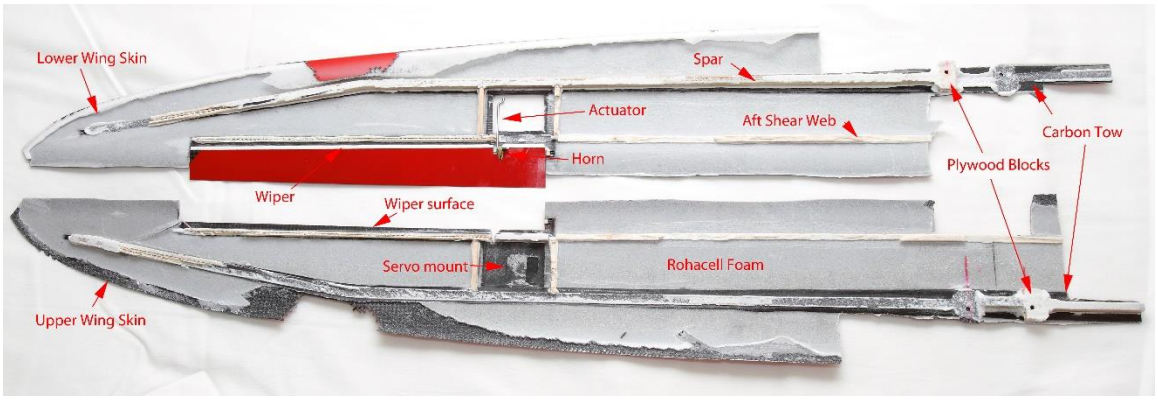

Figure 6: Viper wing structure

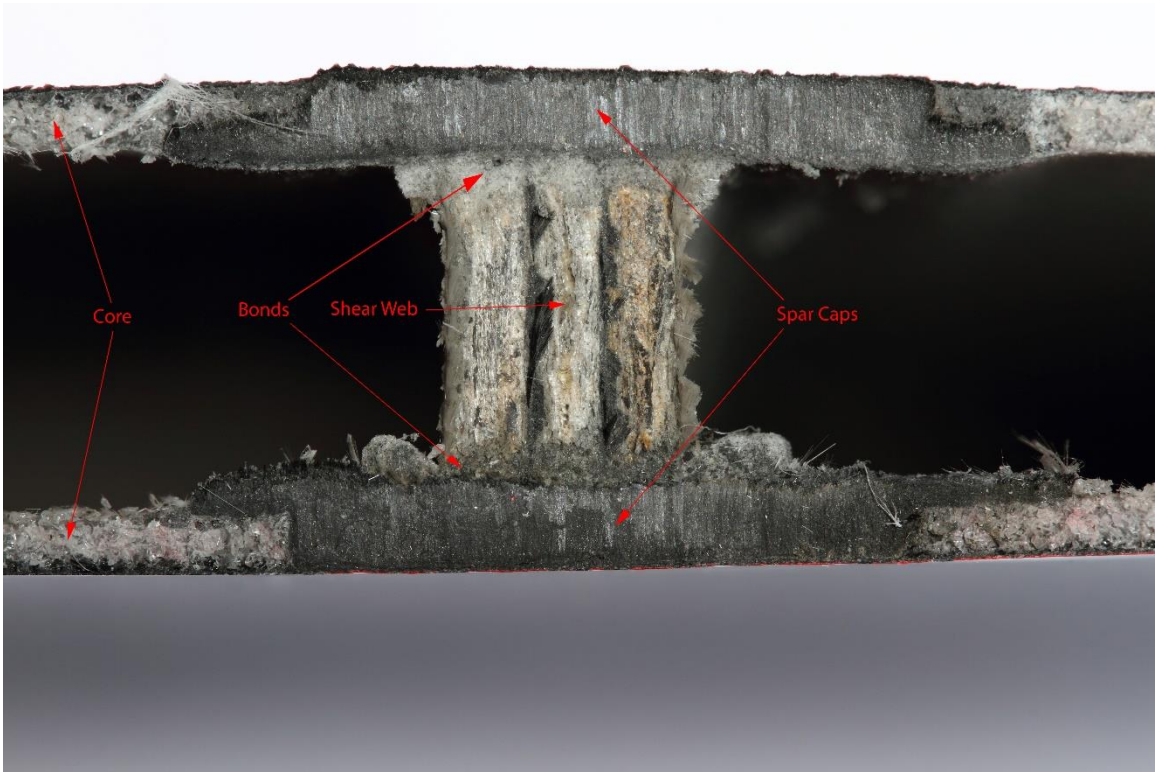

Figure 7: Viper wing spar

These spar designs are found in multiple RC kit-plane build guides and discussed in RC forums like RC Universe and RC Groups. While the composite I-beam method has been utilized for years using different woods and actual composite materials, little work has been done to characterize how these structures work. The designs are based upon the years of knowledge that is

passed down from RC modeler to RC modeler. Since the beginnings of UAV development came from the work done in the RC modeler universe, this method of wing spar construction was brought into UAVs. While this method has been used to great success, this success has its drawbacks. The main drawback being that there is no method for analyzing the composite I-beams, so the designs are based off intuition and former designs.

As stated, the composite I-beam spar is seen in UAV structural design for its effectiveness. At Oklahoma State University, the composite I-beam shear web has been used in aircraft for over 20 years. These wing spars can be seen in undergraduate capstone planes, seen in figure 6, for both Design/Build/Fly and Speedfest Outside of undergraduate senior design, these composite I-beams are used in research planes developed by graduate students for various projects.

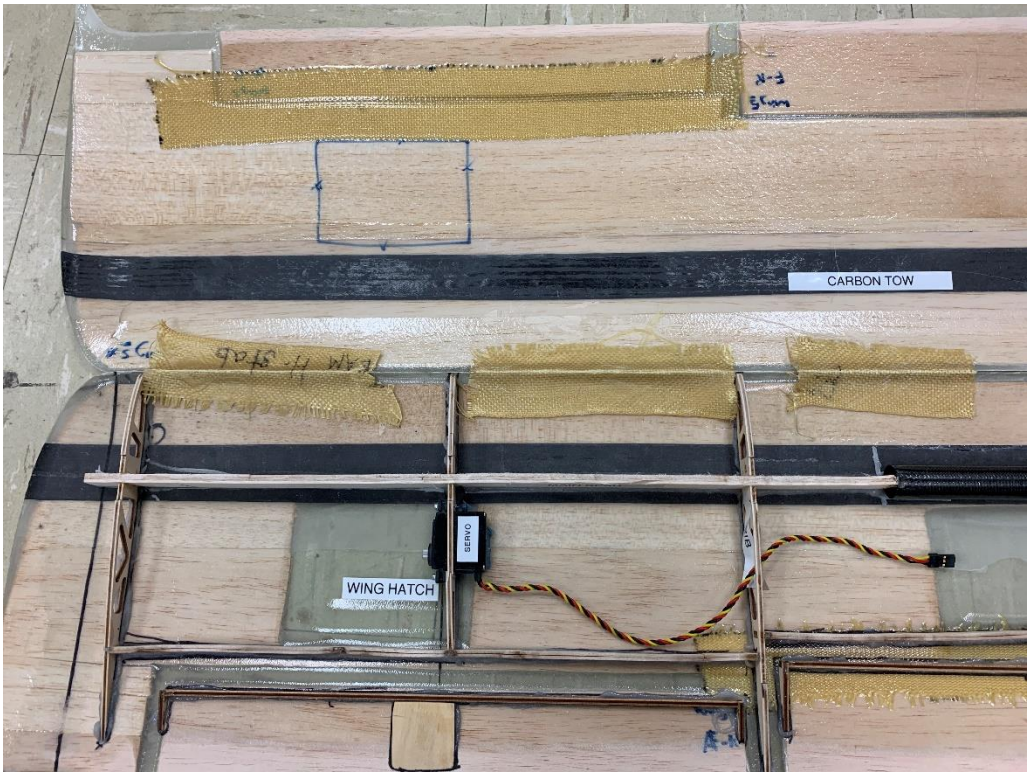

Figure 8: Composite I-beam spar used in Speedfest aircraft from 2019

The composite I-beam for aircraft spars has a long history in the RC and UAV world. With the adoption of UAVs for complex missions in both commercial and defense sectors, the composite I-beam has become widely adopted. Even with the use in industry application, the ability to analyze these wing spars is still underdeveloped. To continue pushing the boundaries on UAVs, an understanding of this wing structure needs to be made in order rapidly manufacture these aircraft as well as create spars that are structurally efficient for its intended aircraft.

Previous Research in Material Properties for Composite I-beams

To completely understand the failure modes of the composite I-beams, the materials used in its construction must be individually understood. For the purposes of this research, the materials analyzed are unidirectional carbon fiber and balsa wood. The following sub-sections will discuss the material properties of these materials to have a baseline understanding of the material before moving into analysis of these materials together in the I-beam.

Carbon Fiber Material Characterization

Figure 9: Carbon Fiber

Unidirectional carbon fiber, otherwise known as carbon uni-tape, makes up the flanges of the composite I-beam. In designing a composite I-beam, the flanges are responsible for taking the compressive and tensile stress when a bending load is applied. The carbon uni-tape is used for two reasons. First, carbon uni-tape is thin and light. One layer of carbon uni-tape is approximately 0.005" thick after the epoxy cycle is complete. Carbon uni-tape is also 3.07 oz/in^2 after the epoxy cycle is complete. Second, even though it is thin and lightweight, carbon uni-tape is strong in both compression and tensile loading. For the sake of this research, carbon fiber strips were bought that have already undergone the layup procedure to keep material properties consistent throughout the tests. This carbon fiber has a Young's Modulus of 19,575 ksi, an ultimate compressive strength of 174 ksi, and an ultimate tensile strength of 217 ksi [6].

Table 1: Material properties of carbon fiber [6]

Modulus of Elasticity	19575 ksi
Ultimate Compressive Strength	174 ksi
Ultimate Tensile Strength	217 ksi

It is important to know both the compressive and tensile ultimate strength of carbon fiber due to experiencing both tensile and compressive stresses during bending. When the I-beam is under a bending load, one side of the I-beam experiences a compressive stress while the opposite side experiences a tensile stress. When designing the I-beam, it is important to add thickness to the compressive side to avoid an early compressive failure. Practically, when designing the composite I-beam spar an aircraft, the compressive carbon flange will be thicker than the tensile carbon flange to compensate for the weaker compressive strength.

Balsa Wood Material Characterization

Balsa wood is a unique material when it comes to aircraft structural design. The material is known for having a high specific strength depending on the orientation of the grain structure.

Cross-grain balsa wood has been used in the shear webs of RC aircraft and UAVs for years, but little quantitative and qualitative data is known for cross-grain balsa. Before research is to be done regarding the failure of cross-grain balsa, the research already done needs to be understood. This knowledge allows assumptions and theories to be developed regarding future experiments and results of those experiments. This section will look at everything that is known about the material up to this point and why this is not enough to analyze the composite I-beams.

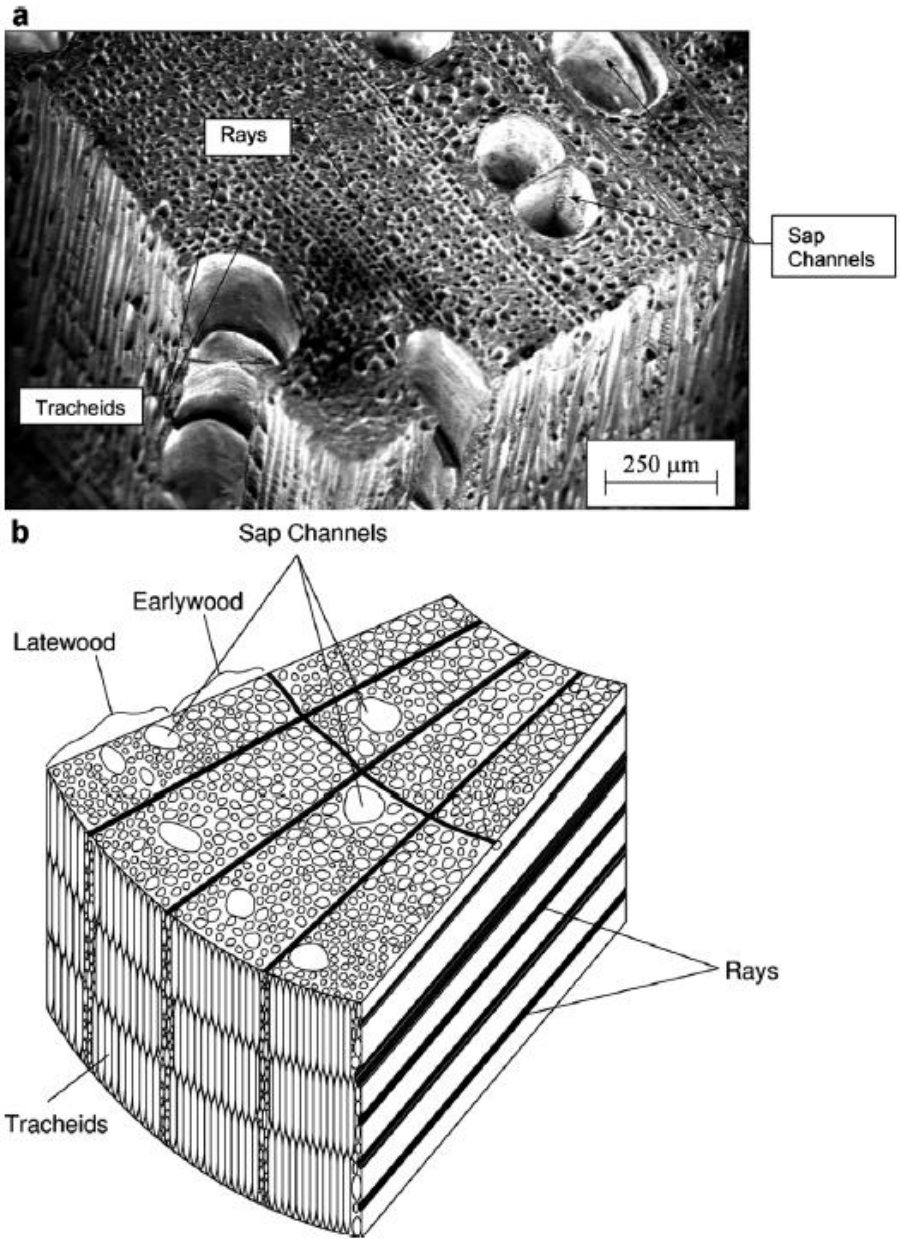

Figure 10: Balsa cellular makeup [7]

Balsa wood consists of fibers, rays, and vessels [8]. Vessels, also known as sap channels, makeup 3-9% of the material. These are long, tubular structures that run axially along the trunk of the balsa tree. They are approximately 380 µm in length and 200-350 µm in diameter. They are responsible for transporting fluids, mostly water, from the roots to the crown of the tree. Rays, also known as parenchyma, are brick-like cells that makeup 20-25% of the material. They are

approximately 30 µm in length and 20-50 µm in diameter. They run radially from the center of the tree trunk out to the bark. They are responsible for storing the nutrients of the tree and add radial strength for the tree. Fibers, also known as tracheids, are the long prismatic cells of the tree that make up 66-76% of the material. They have a hexagonal cross-section that are approximately 700 µm in length and 20-40 µm in diameter. The primary purpose of the fibers is to add mechanical support to the tree. The fibers are the primary strength component of the tree [8].

In Figure 5, a figure is provided to see the ideal make-up of the material. It is easy to distinguish the large sap channels in the balsa wood. The tracheids are also noticeable as the small pores seen surrounding the sap channels and moving vertically along the wood. Finally, the rays can be seen in the cross-section of the cut-out and run lengthwise down the piece. This figure is ideal though, it is better to look at actual balsa to see the make-up of the material. Figures 6, 7, and 8 show the balsa make-up from different angles of the material. Figure 6 shows the balsa wood looking directly at a sample of the wood. This image clearly shows all aspects of the balsa with the sap channels as the large holes, the tracheids as the bunched-up pores that look similar to a cell wall, and the rays as dark lines running at a slight angle vertically along the sample. Figure 7 shows the side view of a circular cutout. This figure clearly shows the sap channels and the rays since they are charred from a laser cut. Figure 8 shows the side view of cutout using a laser. The sap channels are easily seen as the large holes. The rays can be seen as the discolored lines running a slight angle vertically along the section.

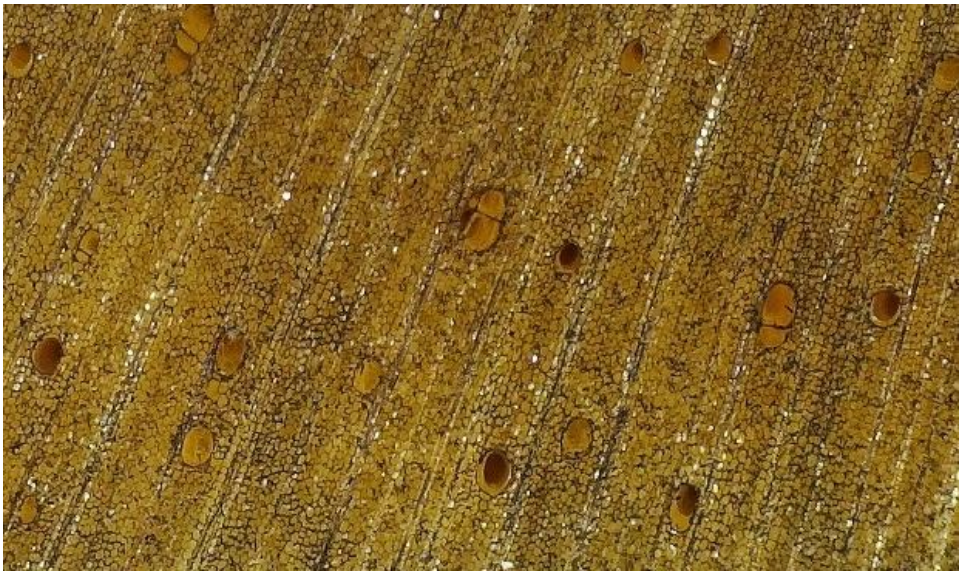

Figure 11: Balsa wood cellular makeup

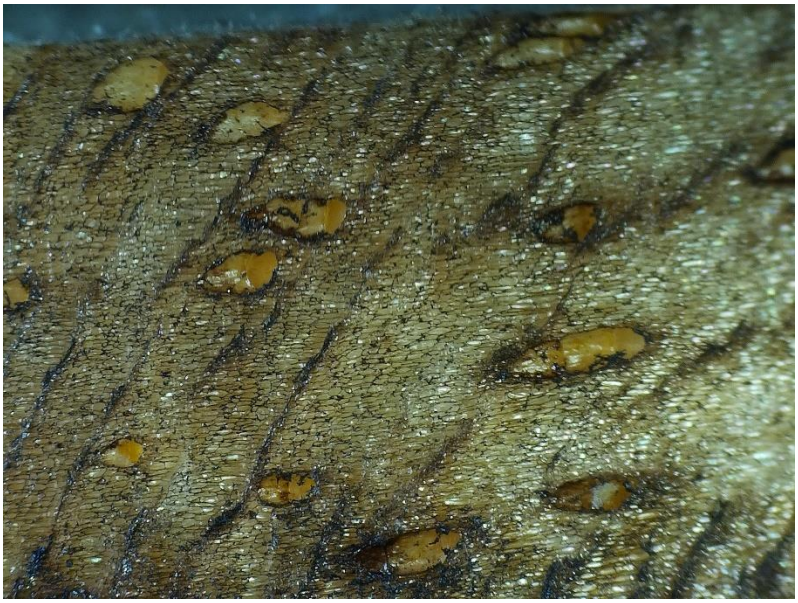

Figure 12: Side view of balsa wood section

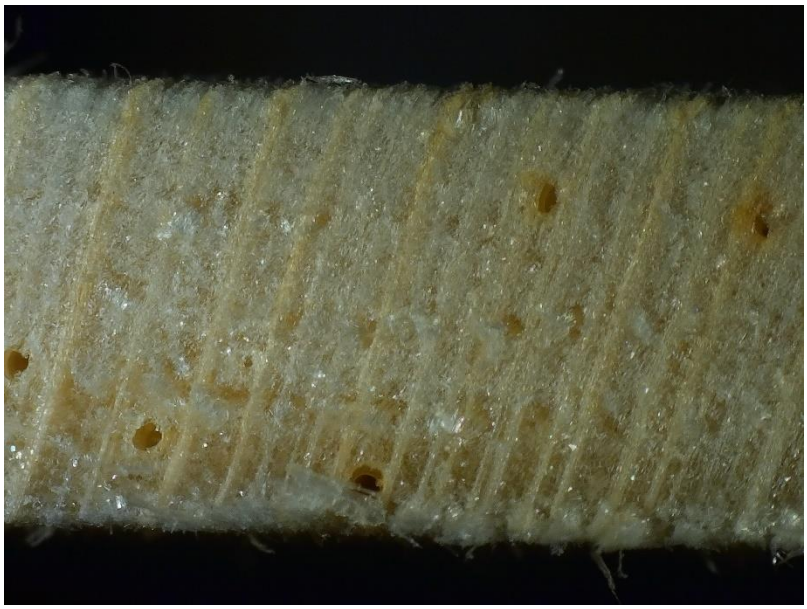

Figure 13: Cross-grain of balsa wood cellular makeup

Balsa wood's cellular makeup causes the material to be an orthotropic material showing different mechanical properties depending on the grain direction. When balsa is oriented to where a bending load is applied perpendicular to the grain direction, this is said to be cross-grain balsa. When the balsa is oriented to where the bending load is applied parallel to the grain direction, this is said to be with-grain balsa. Cross grain balsa exhibits high shear strength, but low tensile/compressive strength. With-grain balsa exhibits low shear strength, but high tensile/compressive strength.

Balsa Wood Material Testing

Balsa's applications extend beyond aircraft structures. Balsa wood has been used in civil engineering applications and as a core material in composite manufacturing. Because of this, organizations have put resources into understanding the material properties of balsa wood. Testing so far has been performed based off *ASTM D143-14: Standard Test Methods for Small Clear Specimens of Timber*. These test methods utilize a primary specimen of 2 by 2-in cross section and a secondary specimen of 1 by 1-in cross section [9]. The primary specimen has the advantage of

many growth rings, being less influenced by earlywood and latewood differences compared to smaller specimens, and is large enough to represent a large portion of the sample material. These primary specimens are used for impact bending, compression perpendicular to the grain, hardness, shear parallel to the grain, cleavage, and tension perpendicular to the grain. The secondary specimens are used for compression parallel to the grain and static bending tests.

This standard of testing is good for understanding balsa as a general material but begins to fail when using balsa in shear web analyses. Since shear webs use balsa that is very thin, the behavior of the material needs to be understood under these particular loading and geometry scenarios. Additionally, *ASTM: D143-14* does not test for shear perpendicular to the grain which is the most important material property for the loading of the shear web. Many experiments have been performed to determine material properties of balsa wood, but the shear strength perpendicular to the grain is often overlooked since shear loading of balsa perpendicular to the grain does not fail like a standard shear failure [10]. Instead of shearing, many researchers have found that shear loading perpendicular to the grain causes a crushing failure in the balsa. Because of this, the data and results are often omitted from the literature. Even though balsa under a shear load perpendicular to the grain does not behave in a standard way, it is important to get a general understanding of the failure mode in this configuration and to obtain data that quantifies the failure. This is because that shear loading perpendicular to the grain is the primary loading of the balsa used in the shear webs.

Where balsa samples for shear and tensile properties have been largely underdeveloped, determining the Young's modulus has been extensive. The Young's Modulus is the relation between and stress and strain in the elastic region of the material and this property also varies depending on the grain orientation of the balsa wood sample. The Young's Modulus varies depending on if the force is applied longitudinally, tangentially, or radially to the grain direction. The image below gives a reference for these axes:

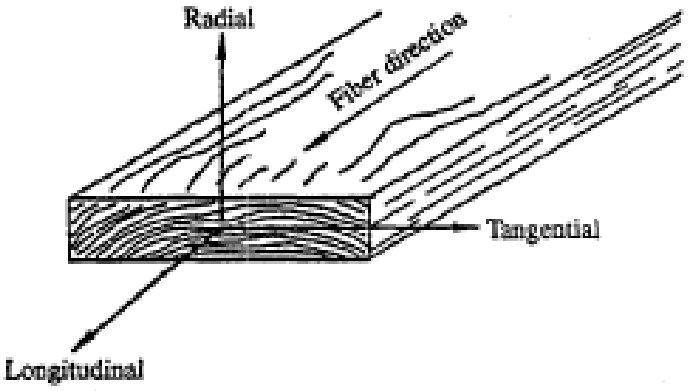

Figure 14: Balsa wood orthotropic axes [11]

The values for Young's Modulus are related by ratios determined by the Young's Modulus in Bending. The Young's Modulus in Bending is related to the Young's Modulus in the longitudinal axis by [11]:

$$E_L = 1.10 \cdot E_B$$

Where E_L is the Young's Modulus in the longitudinal axis and E_B is the Young's Modulus in Bending. The other axes can then be related using [11]:

$$\frac{E_T}{E_L} = 0.015$$

$$\frac{E_R}{E_L} = 0.046$$

Where E_T is the Young's Modulus in the tangential axis and E_R is the Young's Modulus in the radial axis. The material properties of balsa wood have been compiled for this thesis. The figure below shows the compiled list based off multiple sources:

Table 2: Known Properties of Balsa Wood [11]

Modulus of Elasticity in Bending (E_B)	493128 psi
Modulus of Elasticity Along Longitudinal Axis (E_L)	542441 psi
Modulus of Elasticity Along Tangential Axis (E_T)	8137 psi
Modulus of Elasticity Along Radial Axis (E_R)	24952 psi
Modulus of Rupture in Bending	3132815 psi
Compressive Strength Parallel to Grain	2161 psi

Even with the values known, future tests will be done to understand the tensile and shear properties of balsa. It is important to understand the tensile strength with grain direction perpendicular to the applied force and shear strength with grain direction both parallel and perpendicular. The balsa strength data will be used in performing experiments to understand failure modes of balsa individually and as a material used in composite I-beams. Throughout the thesis, the terms cross-grain and with-grain balsa will be used. Cross-grain refers to balsa wood with grain direction perpendicular to the force direction and with-grain refers to balsa wood with grain direction parallel to the force direction.

It is still important to know the previous experiments done and data obtained regarding their material properties because of the testing limits in this research. The tests performed only looked at the shear strength and tensile strength of thin balsa at various grain directions. Figures like compressive strength are unable to be obtained through the testing because of hardware and software limitations. The test stand used is simple in nature in that the user can only perform pull tests with a related force. This means that no displacement can be obtained from the data and that no compressive loads can be applied. These limitations are known and will be discussed in future chapters.

As important as the quantitative data for balsa wood is, it is just as important to understand qualitative data for failure through pictures and videos of failure. The orientation of the grain heavily effects the failure mode of the balsa wood. Within the different grain orientations, there are multiple failure modes. For compression, the failure modes can be seen in Figure 13 below. The failure modes for compression are:

(a) Crushing

(b) Wedge splitting

(c) Shearing

(d) Splitting

(e) Crushing and splitting

(f) rolling

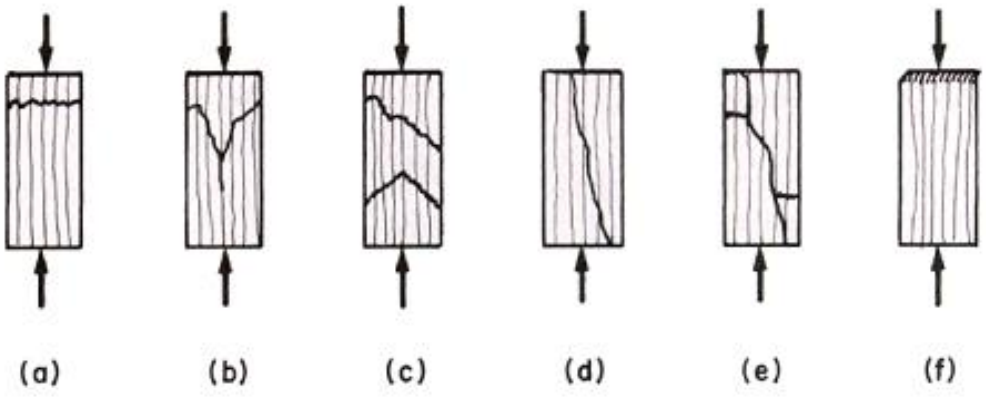

Figure 15: Failure modes for compression of wood with grain direction parallel to force direction [12]

For tensile failure with the grain direction parallel to the force direction, the failure modes can be seen in Figure 14 below. The failures modes are:

(a) Splintering tension

(b) Combined tension and shear

(c) Shear

(d) Brittle tension

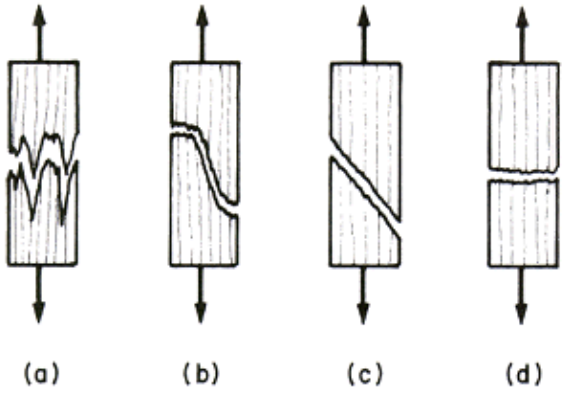

Figure 16: Failure modes for tension of wood with grain direction parallel to force direction [12]

Tensile failure with grain direction perpendicular to the force direction, Figure 15 below shows the three failure modes. The failure modes are:

(a) Tension failure of earlywood

(b) Shearing along a growth ring

(c) Tension failure of wood rays

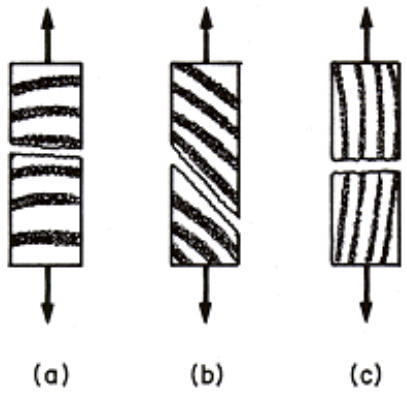

Figure 17: Failure modes for tension of wood with grain direction perpendicular to force direction [12]

For wood under flexural load, like what would be found in a three-point bending test, the failure modes can be seen in Figure 16. The failure modes are:

(a) Simple tension

(b) Cross-grain tension

(c) Splintering tension

(d) Brash tension

(e) Compression

(f) Horizontal shear

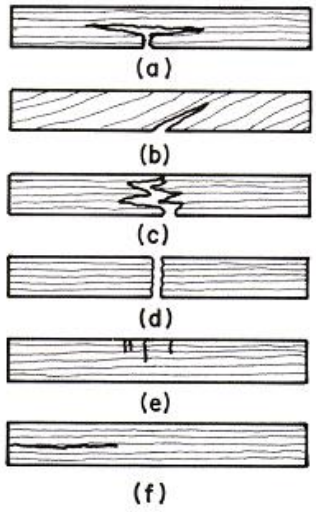

Figure 18: Failure of wood under bending load [12]

The interesting thing to note in these failure modes, especially under a flexural load, is there is little discussion regarding cross-grain shear failure. In the composite I-beams, the balsa wood is high amounts of cross-grain shear stress with very low tensile or normal stress since the carbon fiber takes most of that load. The research regarding the failure modes of balsa wood is incomplete. Material testing of balsa wood has focused entirely of testing large test specimen to determine material properties which lead to inconsistencies when using thin pieces of balsa wood. When testing cross-grain direction, the material tests are underdeveloped due to unusual failure

modes that are inconsistent with the tensile and shear failure modes usually experienced. This information gives a good beginning understanding and early framework, but the research here will attempt to understand the shear failure mode of cross-grain balsa to better understand the design and analysis of the composite I-beams.

CHAPTER III

DEVELOPMENT OF WING SPAR ANALYSIS PROGRAM

This section will look at the three-step process used in developing the analysis tool used in predicting the failure mode of the composite I-beams. The program, known as the Wing Spar Analysis Program, was written in house at the Design and Manufacturing Lab at Oklahoma State University. The primary theory used in developing this program is the transformed area method. The transformed area method allows a beam made from two or more materials to be mathematically transformed to create a theoretical beam made from a homogenous material that can be analyzed using flexure formula and Hooke's law.

The program takes the inputs of aircraft operating envelope and I-beam material and geometry. It calculates the aerodynamic loads on the wing, transforms the I-beam into the homogenous material using the transformed area method, and calculates the stress and strain of the I-beam. This analysis does not focus on the flight loads, instead the program has been modified to simulate three-point bending loads to mimic the Design and Manufacturing Lab's in-house three-point bending machine.

Mechanics of Materials Theory

The calculations for the code are divided into two sections, “Shear and Moment Calculations” and “Spar Calculations.” The “Shear and Moment Calculations” calculates the loading, shear, and moment along the length of the beam under a three-point bending scenario. The “Spar Calculations” uses the transformed area method to convert the composite beams into a theoretical single material to calculate angular slope, deflection, stress, shear, and strain. The following sub-sections will give detailed descriptions of the theory and analysis of the Wing Spar Analysis Program.

Shear and Moment Calculations

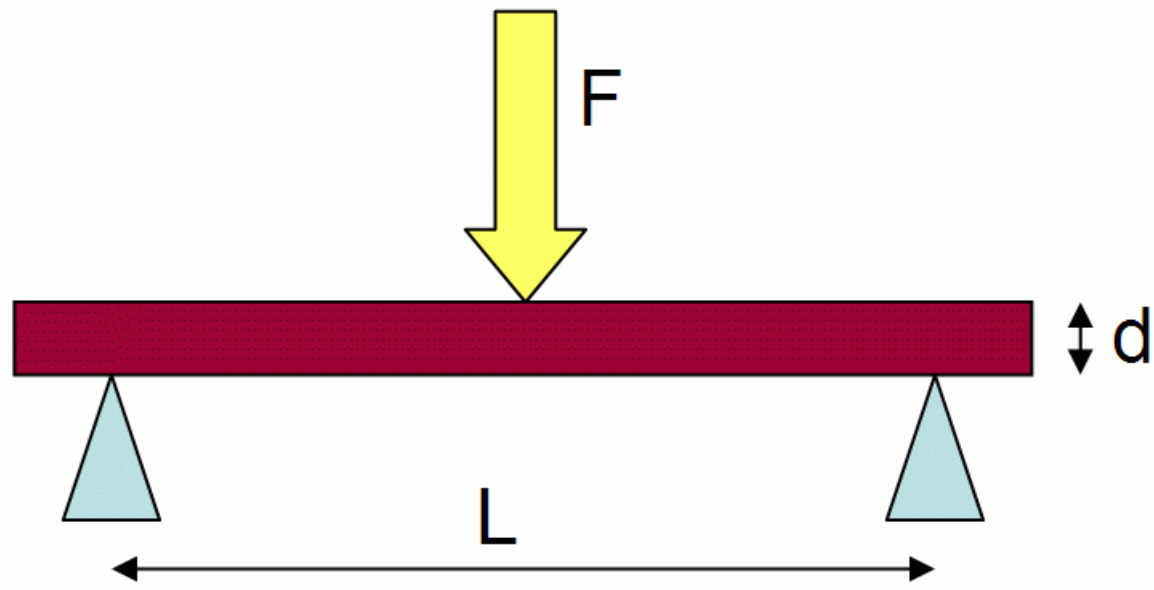

Figure 19: Beam Under Three Point Bending

In the analysis, the first step in determining the stress and strain of the I-beam, the loading, shear, and moment diagrams down the length of the beam need to be determined. To develop the loading, shear, and moment along the length of the beam, singularity functions are used. Singularity functions are used to describe the loading across the length of the beam by using a single function

to describe moments, point loads, or distributed loading. The loading equation is written, and the shear function can be found by taking the first derivative of the shear function and the moment function can be found by taking the second derivative of the loading equation [12]. The loading equation is shown below:

$$w(x) = -F_2 \cdot \langle x - 0 \rangle^{-1} + F_1 \cdot \langle x - \frac{L}{2} \rangle^{-1} - F_2 \cdot \langle x - L \rangle^{-1}$$

Where $w(x)$ is the loading as function of x-position down the length of the beam, F_2 is the reaction force at the end supports of the beam, F_1 is the applied force by the test stand, and L is the length of the beam. By taking the first derivative of this equation, the shear function can be found. The shear function is shown below:

$$V(x) = F_2 \cdot \langle x - 0 \rangle^{0} + F_1 \cdot \langle x - \frac{L}{2} \rangle^{0} + F_2 \cdot \langle x - L \rangle^{0}$$

Where $V(x)$ is the shear loading as a function of x-position down the length of the beam. By taking the second derivative of the loading equation, the moment equation can be found. The moment equation shown below:

$$M(x) = F_2 \cdot \langle x - 0 \rangle^{1} - F_1 \cdot \langle x - \frac{L}{2} \rangle^{0} + F_2 \cdot \langle x - L \rangle^{0}$$

Where $M(x)$ is the moment loading as a function of x-position down the length of the beam. This method is used because it is easy to implement in the MathCAD code using an if-else statement to determine the loading for various parts of the equation depending on the exponent of the specific part of the equation. While calculating the loading, shear, and moment of the beam, the equations are also used to graph the Shear Diagram and Moment Diagram for the beam geometry. An example of the two diagrams is shown below:

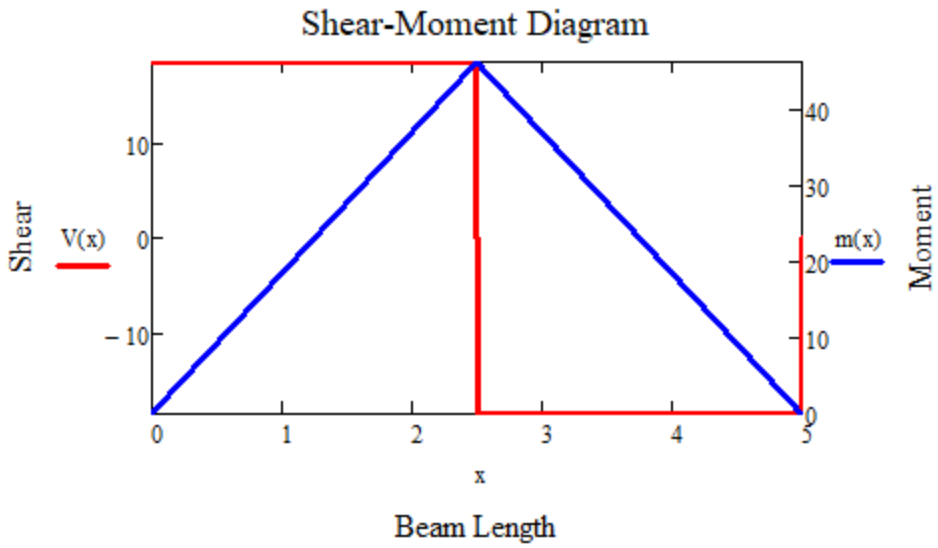

Figure 20: Shear and Moment Diagram as a fucntion of beam length

With the calculated loading, shear, and moment singularity functions the beam deflection as a function of horizontal length can be found by taking the fifth derivative of the loading equation [12]. The equation is as follows:

$$\delta(x) = \frac{1}{EI}\left\{\left[\frac{F_2}{6}\right]\cdot\langle x-0\rangle^3 - \left[\frac{F_1}{6}\right]\cdot\langle x-\frac{L}{2}\rangle^3 + \left[\frac{F_2}{6}\right]\cdot\langle x-L\rangle^3 + \left[\left(\frac{-F_2\cdot L^3}{6\cdot L}\right)+\left(\frac{F_2\cdot\frac{L^3}{2}}{6\cdot L}\right)\right]\cdot x\right\}$$

Where E is the modulus of elasticity for the cap material and I is the total area moment of inertia for the beam.

With the basic loading, shear, and moment diagrams calculated, the next logical step is to start the stress analysis. With the multiple materials used in the I-beams, this is not possible without using the transformed area method.

Spar Calculations using the Transformed Area Method

This program relies on the flexure formula for determining stresses stress and subsequent strains, shown below [12]:

$$\sigma_{max} = \frac{Mc}{I}$$

$$\sigma = -\frac{My}{I}$$

Where σ is the normal stress, M is the moment, c is the distance farthest from the neutral axis, I is the area moment of inertia of the beam, and y is the distance from the neutral axis where stress is determined. This equation is incredibly powerful for finding the maximum stress in bending beams while also being able to find stress at various locations along the I-beam. The downfall of the equation is that it is developed for use in homogenous materials only. Without an advanced method of analyzing two or more materials, the flexure formula cannot be used. A method must be used to convert the composite materials into a form where the flexure formula can be utilized.

The transformed area method is used to convert a composite structure made of two or more materials into a single homogenous material to be used for stress and strain analysis [12]. Assuming that both materials being analyzed are linearly elastic, the I-beam can be analyzed using the flexure formula and Hooke's Law.

$$\sigma = E \cdot \varepsilon$$

In the case of the composite I-beams, the carbon fiber caps work to carry the tensile and compressive loads that are more prevalent in the top and bottom of the beam. The cross-grain balsa shear web carries the shear loading of the beam while carrying almost zero of the normal stress. Without changing into a single homogenous material, the stress distribution along the cross-section of the I-beam is not linear. One would see high stress in the cap and at the boundary of the carbon

fiber cap and the balsa wood shear web, there would be a jump to near-zero along the height of the balsa wood shear web. Finally, at the boundary of the balsa shear web and the bottom carbon fiber cap, one would see another increase in stress. It is important to remember that the strain stays the same for the beam whether it is a composite material or homogeneous. This stress distribution makes it difficult to perform the calculations necessary for determining the failure mode of the beam.

To create a beam of a single homogenous material, the transformed area method will be used to change the geometry of the beam. In the case of the composite I-beams, the cross-sectional area of the I-beam can be decreased by making the shear web width to create a geometry that forces a linear distribution of normal stress. This is done by using a dimensionless number called the transformation factor. The transformation factor is a ratio of the two materials elastic moduli.

$$n = \frac{E_1}{E_2}$$

Where E_1 is the elastic modulus of the first material and E_2 is the elastic modulus of the second material. The convention is to have E_1 be the elastic modulus of the less stiff material and E_2 be the elastic modulus of the stiffer material. By multiplying different geometric dimensions in the composite I-beam by the transformation factor, a theoretical homogenous material can be created that allows the engineer to simplify the stress-strain analysis of the structure. Multiplying the width of the shear web by the transformation factor changes the width to create a thinner core.

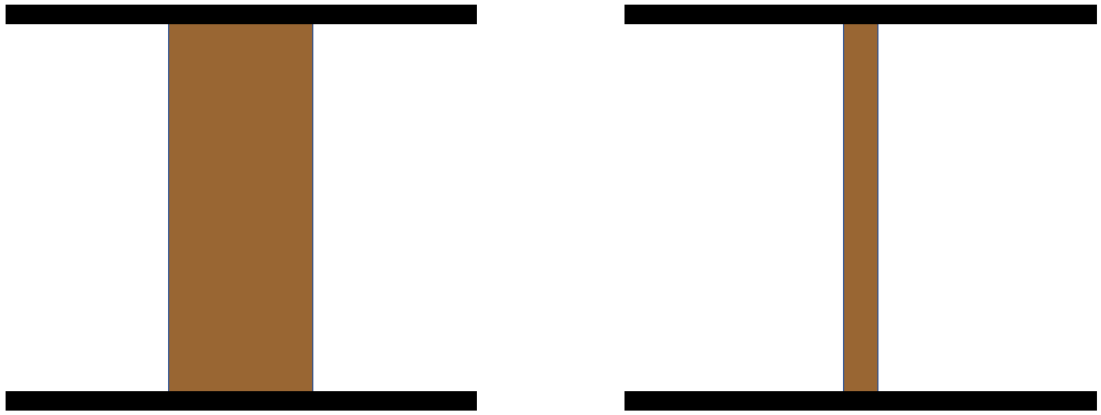

Figure 21: Transformed area method geometry change

Multiplying the geometry associated with the shear web, the thickness, and thus the area, of the shear web will be decreased to create a homogenous material. By decreasing the area of the shear web, an equivalent load to the carbon fiber caps is created. To create this mathematically homogenous material, the following process is used (refer to the image below for reference):

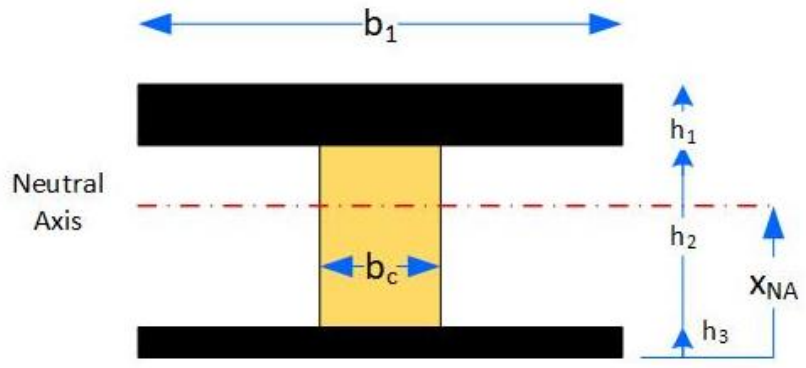

Figure 22: Geometric Variables for I-Beam Calculations

First, the transformation factor is determined:

$$n = \frac{E_c}{E}$$

Where n is the transformation factor, E_c is the Young's Modulus of the core material, and E is the Young's Modulus of the cap material. The transformed geometry of the cross-sectional area can be found using the transformation factor. The equations are as follows:

$$b_{c,new} = nb_c$$

$$A_1 = h_1 b_1$$

$$A_2 = h_2 b_{c,new}$$

$$A_3 = h_3 b_1$$

$$x_{NA} = \frac{A_1\left(h_3 + h_2 + \frac{h_1}{2}\right) + A_2\left(h_3 + \frac{h_2}{2}\right) + A_3 \cdot \frac{h_3}{2}}{A_1 + A_2 + A_3}$$

$$A_x = A_1 + A_2 + A_3$$

Where b_c is the width of the core material, $b_{c,new}$ is the transformed width of the core material, A_1 is the area of the top cap, h_1 is the height of the top cap, b_1 is the width of the top cap, A_2 is the transformed area of the core material, h_2 is the height of the core material, A_3 is the area of the bottom cap, h_3 is the height of the bottom cap, x_{NA} is the neutral axis, and A_x is the total transformed area. The area moments of inertia for the various components can be found and then added together to get the total area moment of inertia.

$$I_1 = \frac{b_1 {h_1}^3}{12} + A_1\left[\left(h_3 + h_2 + \frac{h_1}{2}\right) - x_{NA}\right]^2$$

$$I_2 = \frac{\frac{b_c \cdot E_c}{E} \cdot {h_2}^3}{12} + \left(x_{NA} - h_3 - \frac{h_2}{2}\right)^2$$

$$I_3 = \frac{b_1 \cdot {h_3}^3}{12} + A_3\left(x_{NA} - \frac{h_3}{2}\right)^2$$

$$I = I_1 + I_2 + I_3$$

I_1 is the area moment of inertia of the top cap, I_2 is the transformed area moment of inertia of the core material, and I_3 is the area moment of inertia of the bottom cap, I is the total area moment of intertia. The final piece of geometric values that needs to be found is Q to be used in shear stress calculations. These are found from the following equations:

$$Q_c = A_1\left[\left(h_3 + h_2 + \frac{h_1}{2}\right) - x_{NA}\right]$$

$$Q_t = A_3\left(x_{NA} - \frac{h_3}{2}\right)$$

$$Q_{max} = A_1\left[\left(h_3 + h_2 + \frac{h_1}{2}\right) - x_{NA}\right] + \left[(h_3 + h_2 - x_{NA}) \cdot b_c \cdot \frac{h_3 + h_2 - x_{NA}}{2}\right]$$

Where Q_c is the Q in the cap under compressive stress, Q_t is Q in the cap under tensile stress, and Q_{max} is the max Q. With the geometric values found, the normal stress, shear stress can be found as a function of the length of the beam and the shear buckling coefficient can be found:

$$\sigma_t(x) = \frac{(m(x) \cdot x_{NA})}{I}$$

$$\sigma_c(x) = \frac{[m(x) \cdot (h_1 + h_2 + h_3 - x_{NA})]}{I}$$

$$\tau_{max}(x) = \frac{V(x) \cdot Q_{max}}{I_{real} \cdot b_c}$$

$$\tau_f(x) = \frac{V(x) \cdot Q_{max}}{I_{real} \cdot b_c}$$

$$\tau_{buckle} = 8 \cdot E_c \cdot \left(\frac{b_c}{h_2}\right)^2$$

Where $\sigma_t(x)$ is the normal tensile stress as a function of the horizontal length, $\sigma_c(x)$ is the normal compressive stress as a function of horizontal length, $\tau_{max}(x)$ is the maximum shear stress as a function of horizontal length, I_{real} is the total area moment of inertia without the transformation factor, $\tau_f(x)$ is the shear stress in the web-cap joint as a function of horizontal length, and τ_{buckle} is the shear buckling coefficient. The value for normal tensile stress, normal compressive stress, max shear stress, and shear stress in the web-cap joint can be found at all points down the length of the beam while the shear buckling coefficient serves as a constant limit dependent on the geometry of the beam.

With these calculations, the Wing Spar Analysis Program also graphs the normal tensile and compressive stress as function of horizontal length while also showing the ultimate compressive and tensile strength of the material for reference.

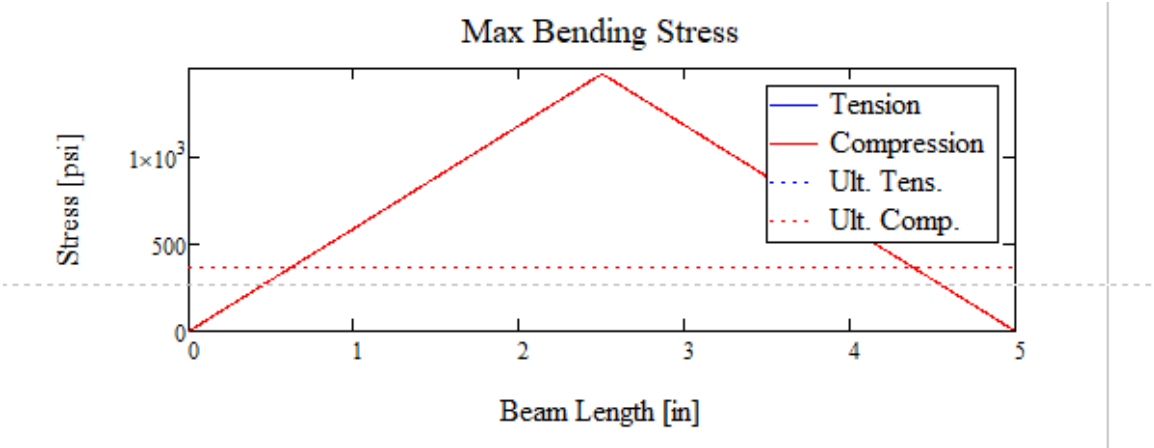

Figure 23: Bending stress a function of beam length

The Wing Spar Analysis Program also graphs the maximum shear stress as a function of horizontal length while also showing the ultimate shear strength of the core material along with the shear buckling coefficient for reference.

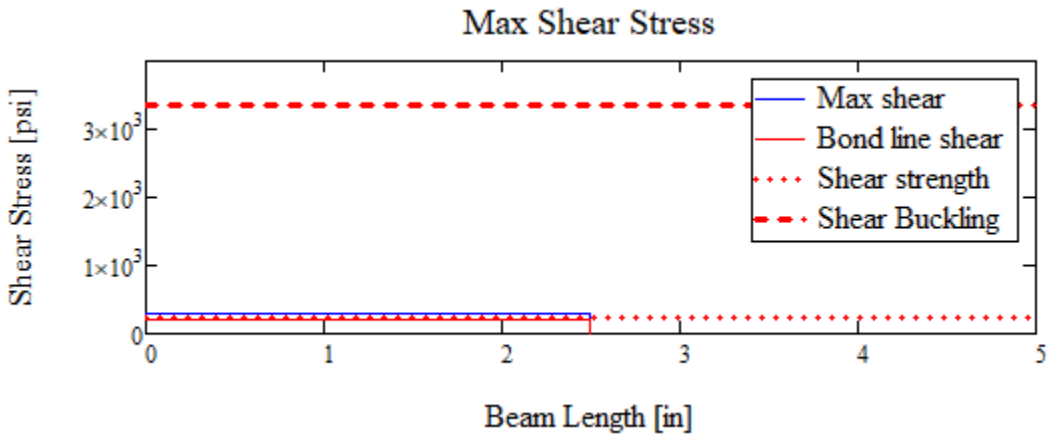

Figure 24: Maximum shear stress as a function of beam length

Finally, the "3PB Analysis" program creates images based off the input geometry for the real and transformed beam along with the cross-sectional normal stress distribution for the real and transformed beam.

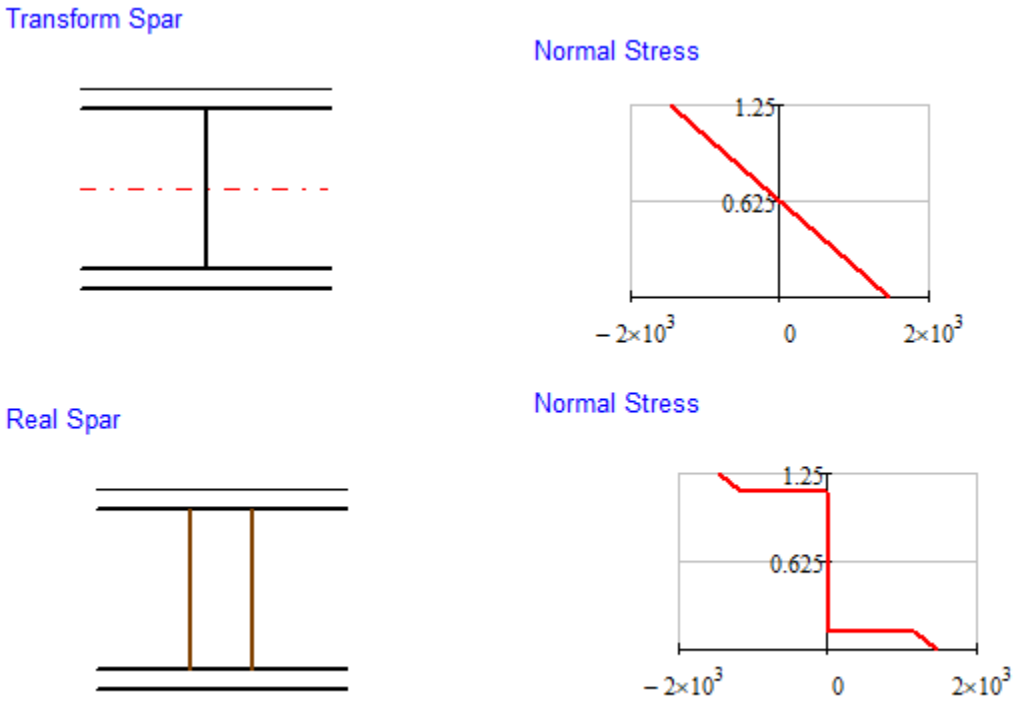

Figure 25: Transformed and real cross-section of beams with associated stress distribution

This theory is utilized in a more complex loading scenarios for determining the failure mode of a full aircraft. The Wing Spar Analysis Program utilizes aerodynamic data and wing geometry to determine the failure mode and is more complex in nature. The simplicity of the modified Wing Spar Analysis Program for three-point bending allows for easy testing, quick iteration, and gives full confidence that if the theory used in this code matches three-point bending experiments, then the theory will translate into the Wing Spar Analysis Program when used with full aircraft loading.

Wing Spar Analysis Program Usage and Explanation

While the theory in the Wing Spar Analysis Program is important to understand, the theory cannot stand alone. This section gives a detailed account of the how the program is used and discusses the definition behind the outputs.

First, the user inputs the material properties necessary for the calculations. This includes the Young's Modulus of the spar cap material and the shear web material, the ultimate compressive and tensile strength of the cap material, and the ultimate shear strength of the shear web material. So far, the material discussed for the composite I-beams have focused on carbon fiber and balsa wood. These are the main materials used in future testing and for aircraft designs, but any material can be input if the material properties are known. Second, the user inputs the geometry of the beam being tested. This geometry includes the spar cap thickness for the top and bottom of the I-beam, the width of the spar cap, the height of the shear web, and the width of the of the shear web. Third, the user will input the length of the beam being tested and the force that is applied. These are the inputs necessary for computing the failure mode of the beam.

Once the inputs are entered, the program can be run. It first calculates the load, shear, and moment as a function of length using singularity functions and graphs the results of the shear and moment. It does this by taking the force input and applying it to the center of the beam. The code

then creates a uniform material and transformed cross-section using the transformed area method for calculating stresses and displacements. Finally, the code solves for the compressive, tensile, shear, and shear buckling along the beam.

From these calculations, the code will output a status that is related to the failure modes possible. This includes “0.5% Strain Warning,” “COMPRESSIVE FAILURE!,” “TENSILE FAILURE!,” “SHEAR FAILURE!,” “SHEAR BUCKLING!,” or “Within Limits.” A “COMPRESSIVE FAILURE!,” signifies that there is compressive failure in the top cap of the I-beam due to the applied loading. A “TENSILE FAILURE!,” signifies that there is a tensile failure in the bottom cap of the I-beam due to the applied loading. A “SHEAR FAILURE!,” signifies that there is a shear failure in the shear web material of the I-beam due to the applied loading. A “SHEAR BUCKLING!,” signifies that there is a shear buckling failure in the shear web material of the I-beam due to the applied loading. A “Within Limits.” signifies that the I-beam will not fail due to the applied loading and is designed to handle the expected loads. The code also outputs graphs that show the bending and shear stress along the beam shown in Figure 22.

Initial Validation

Once the program was written, it was important to perform preliminary validation of the program using examples that already have known solution. Examples from mechanics of materials textbooks were used to validate the program. The preliminary validation would show mistakes in the program if output solutions are incorrect with the theory found in literature. If errors were found, the program would need to be modified more. The examples tested were a square aluminum beam, rectangular I-beam beam, aluminum I-beam, and a composite I-beam.

The first test showed a 1” by 1” square cross-section beam made of aluminum. This was input into the code using 0.05” thick spar caps with a 1” width and a 0.9” tall shear web with 1” thickness. This input creates a square beam for the code even though the inputs are still for an I-

beam geometry. These inputs are used to see if the code can do a basic beam bending calculation for a homogenous symmetric beam. The comparison between the methods can be seen in Figure 22.

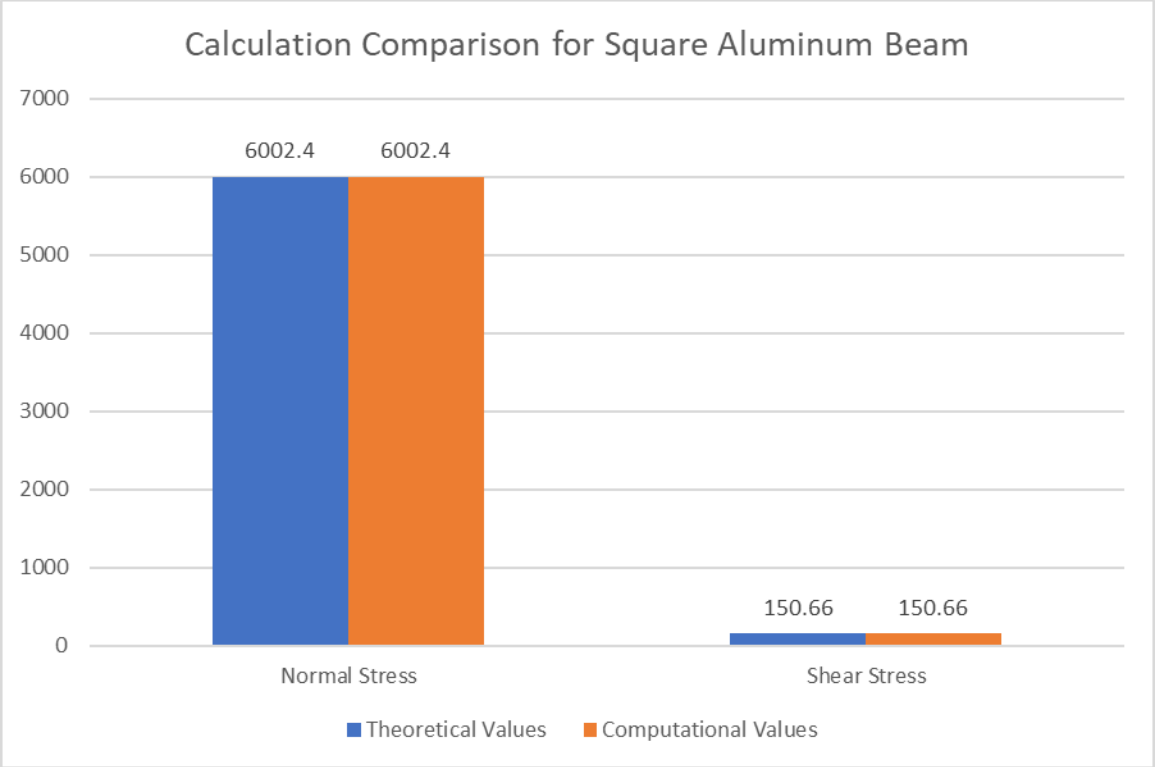

Figure 26: Calculation comparison for square aluminum beam

The second test was performed with a 2.02" x 1" rectangular cross-section beam made of aluminum. This was input into the code using 0.01" thick spar caps with a 1" width and a 2" tall shear web with a 1" thickness. This input creates a rectangular beam for the code even though, again, the inputs are still for an I-beam. These inputs are used to add complexity to the first validation problem and see if the beam could calculate the correct values for a homogenous rectangular beam. The comparison between the methods can be seen in Figure 23 below.

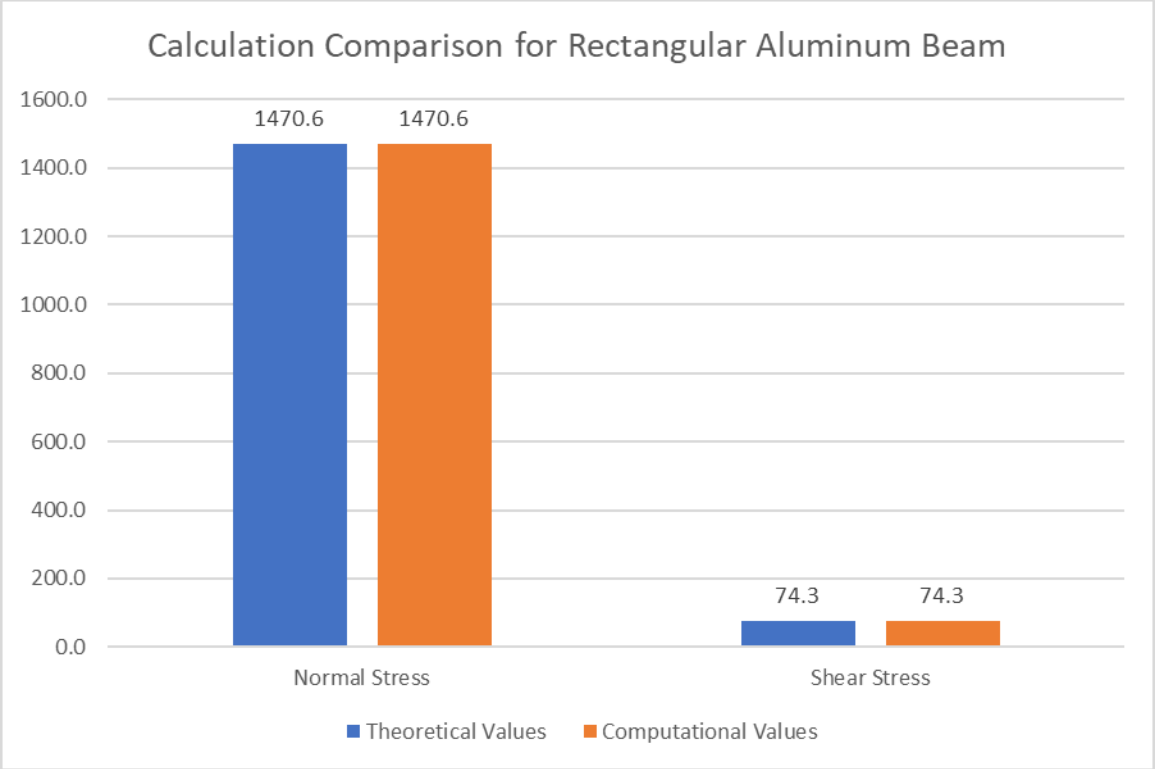

Figure 27: Calculation comparison for rectangular aluminum beam

The third test was performed with a fully aluminum I-beam. The spar caps are 0.1" thick and 1" wide. The shear web is 2" tall and 0.5" wide. These inputs match the inputs required for the I-beam and was used to test the calculation requirement of the code to see if it could compute the correct values for a homogenous I-beam. The comparison between the methods can be seen in Figure 24 below.

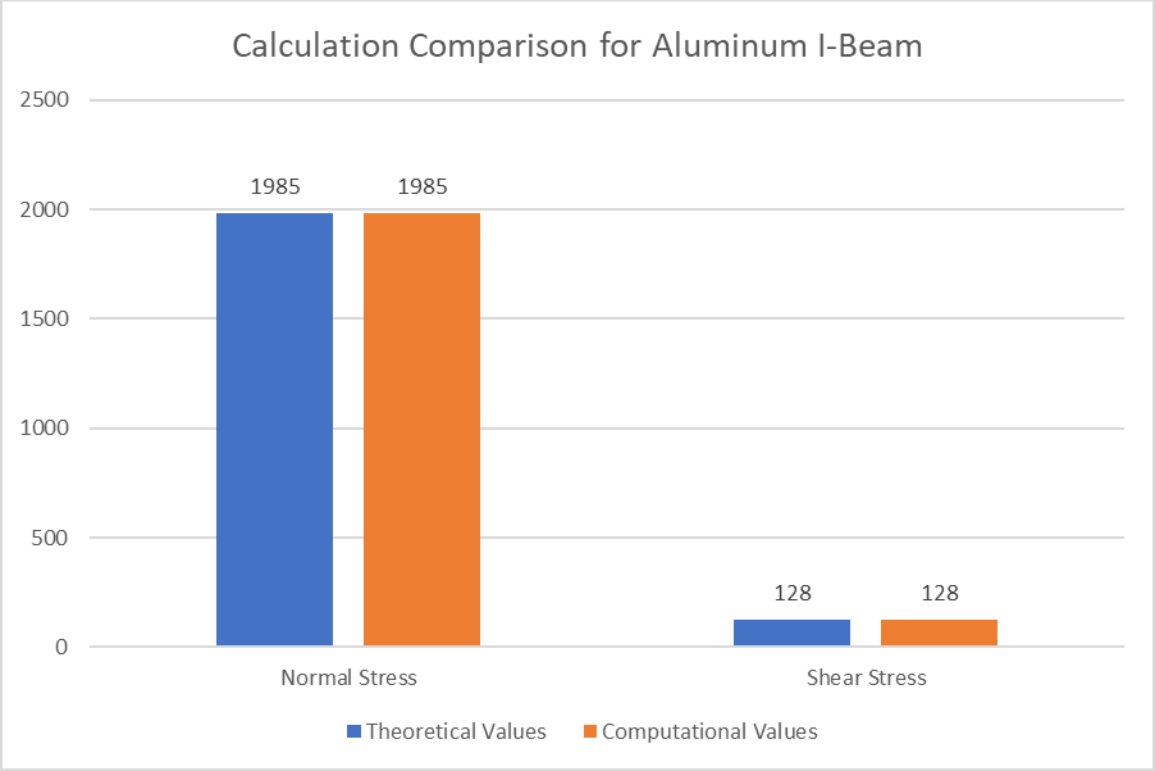

Figure 28: Calculation comparison for aluminum I-beam

The final validation was a composite I-beam with carbon fiber spar caps and a balsa wood shear web with material properties found from the literature review. This was done to see if the code could compute the stresses and deformation of the beam using the transformed area method. The comparison between the methods can be seen in Figure 25 below.

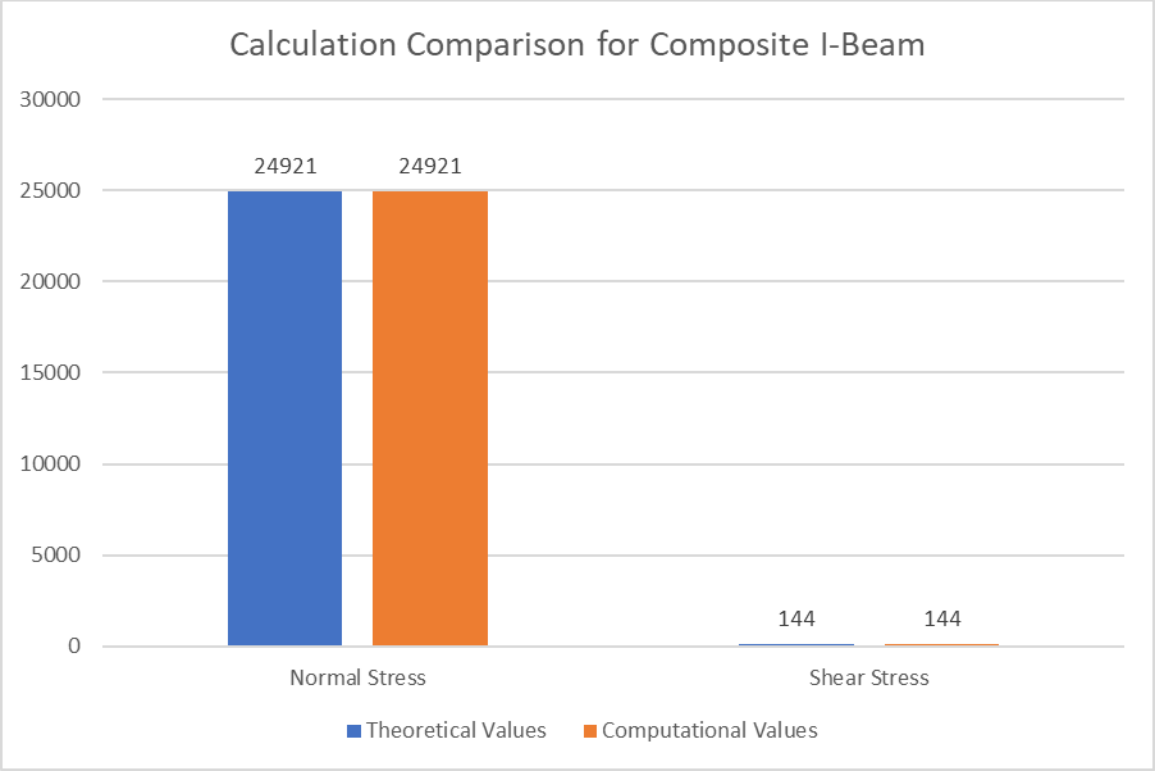

Figure 29: Calculation comparison for composite I-beam

The ability of the code to match known examples found in standard mechanics of material literature with materials that have known properties give confidence that the code functions correctly and the theory will work for the analysis moving forward. This shows that the transformed area method theory functions for both homogenous and composite beams. The only unknown left in the analysis code is the material properties of the balsa wood with small thicknesses under loading in the cross-grain direction.

CHAPTER IV

BALSA MATERIAL TESTING AND RESULTS

Before testing composite I-beams with balsa wood shear webs, material properties of thin balsa wood must be expressed. Determining the shear strength of cross-grain balsa wood is the most important material property that needs to be determined, but the tensile strength of cross-grain balsa and the shear strength of with-grain balsa will also be determined to allow for comparison between different grain directions. This section will look at the experiments and results from the tensile and shear testing of balsa and how those values vary for different dimensions and densities. The importance of understanding the material properties of thin balsa cannot be stated enough. Due to the lack of previous research in the shear and tensile properties of cross-grain balsa, rigorous testing needs to be performed. These tests will give the understanding of balsa wood used in the shear webs and give the building blocks for analyzing the full composite I-beam structure. This testing will lead to a database of balsa properties that are to be referenced for the spar analysis program to get the most accurate analysis results.

The experiments will focus on the tensile testing of balsa wood with grain direction perpendicular to the force direction and shear testing with grain direction both parallel and perpendicular to the force direction. With these results, a database of balsa wood material properties can be created based off the density and geometry of the balsa wood.

Material Testing Reasoning and Introduction

Due to a lack of understanding in the failure modes of the composite I-beam shear web, it was determined that testing for both tensile and shear failure of balsa wood needs to be performed. In beam bending, tensile and shear failure are two of the most common forms of failure. Compression is also a common form of failure in beam bending, but due to the inability to test for compressive failure with the testing facilities at the Design and Manufacturing Lab, this failure mode will not be investigated.

The first sections in this chapter will look at the tensile testing performed, the experimental methodology, and discuss the results obtained. After tensile testing, the shear testing will be discussed including the experimental methodology and the results obtained. Interesting trends are noticed regarding the ultimate strength of the material in relation to density. Even more interesting, deviation in material properties is noticed as the thickness of balsa is increased from 0.125” to 0.25”. In summary, the 0.25”-thick balsa is weaker than 0.125” balsa wood but these results will be discussed in more detail in future sections.

Tensile Testing Experimental Setup

A large amount of effort was put into testing balsa wood in tensile loading to understand the material properties of cross-grain. As discussed in the Literature Review, there is a wide range of testing methods and a wide range of results for the material properties of balsa. Because of this, tests were set up specifically for the balsa used in the shear webs. This includes size, geometry, density, and loading scenarios. To accurately test balsa wood in shear web scenarios, testing was performed with 0.125”- and 0.25”-thick balsa wood samples.

The first tests performed were tensile tests. Utilizing the Vernier Structures & Materials Tester with wishbone balsa samples, tensile tests were performed to determine the tensile strength

of balsa wood. The tensile test samples were designed based off ASTM D-143-14 [9]. Figure 28 below shows the Solidworks model of the test sample with the associated dimensions.

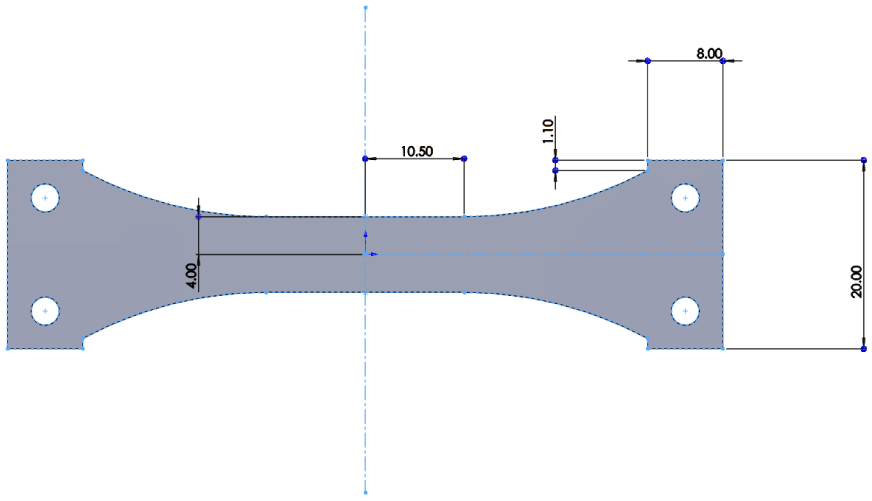

Figure 30: Tensile test sample model

The tensile test samples were designed based off the associated standard: ASTM D-143-14 [9]. The ASTM standard calls for a much-larger sample than what could fit in the Vernier Structure and Material Tester. To accommodate the sizing of the Vernier Structure and Material Tester, ratios were developed to determine the relationship between the dimensions of the wishbone. Changing one dimension would allow all the dimensions to be sized down and allow for testing within the constraints of the environment.

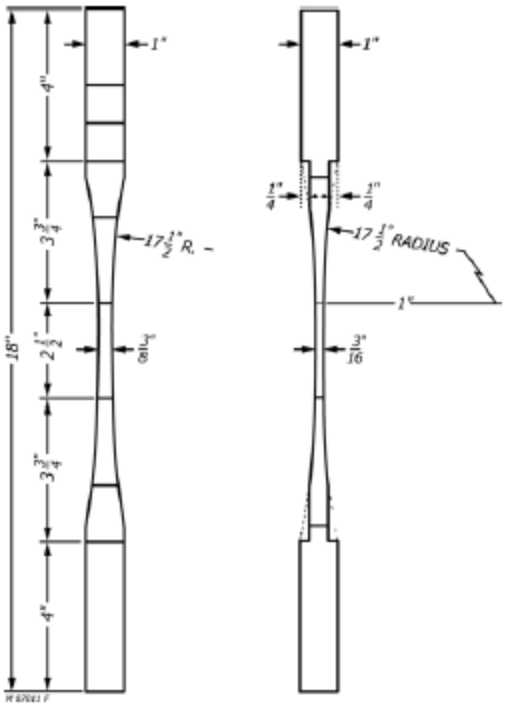

Figure 31: Standard tensile sample geometry [9]

The tensile test samples had a rectangular, plywood doubler glued to the ends to increase the strength of the material at the mounting holes. The mounting holes are an area subject to stress concentrations. In preliminary testing, the test sample would fail at the mounting holes instead of the center of the wishbone. The test sample is then mounted to 3D-printed supports to allow for a resting place on the top of the Material Tester and a way for the Material Tester to apply a tensile force. The following images show the physical tensile test sample, the 3D printed mounts, and the complete test setup.

Figure 32: Tensile test sample

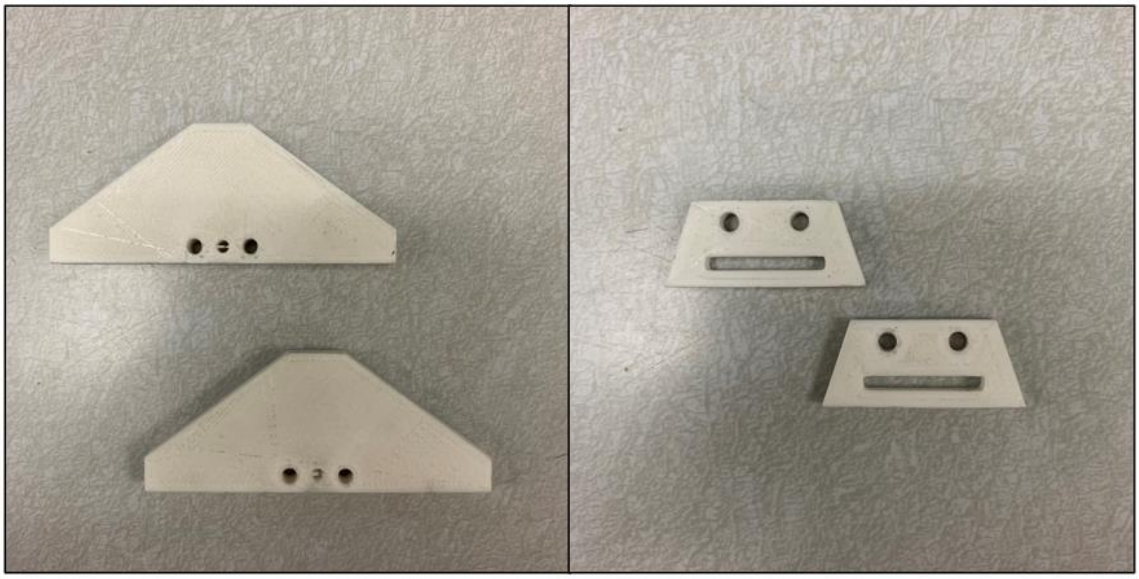

Figure 33: 3D printed testing mounts

Figure 34: Tensile test setup

The top 3D-printed piece is a pyramid that fixes the test sample to the crossbeams on the Vernier Structure and Material Tester. The bottom two pieces have bolt holes to be mounted to the bottom of the test sample and a slot that gives the U-bolt a place to mount and apply force.

The tests were performed with Regular and Aero Light balsa ordered from National Balsa. It is important to note that the difference between Regular and Aero Light balsa is mainly due to different densities. Aero Light balsa is handpicked to a controlled density of 4-7 lb/ft^3 [13] where Regular balsa has a larger range of density and is usually heavier. This is not always true though; sometimes regular balsa can have densities in the same range of Aerolight. This range of balsa densities give a good distribution on the material properties over a large range of weight and densities.

Tensile Test Experimental Methodology

- Design tensile test samples using Solidworks
- Cut out tensile test samples and doublers using laser cutter
- Construct tensile test samples by super-gluing doublers to mounting holes
- Mount test samples to the Vernier Structure and Material Tester
    - Use #4-40 nuts and bolts to fasten 3D-printed bottom and top supports to the test sample
    - Place the 3D-printed top support on the Vernier Structure and Material Tester support beams
    - Mount the U-Bolt to the 3D-printed bottom piece by sliding the tab through the slot and fastening the nuts on both sides of the U-bolt
- Plug Vernier Structure and Material Tester DAQ into computer with installed LabQuest 3 software and make sure it is reading data
- Apply force until the force measurement goes slightly positive then de-load slightly and zero the measurement
- Begin recording data
- Slowly turn the level to apply a force
- Once failure occurs, stop the data recording and de-load the Vernier Structure and Materials
- Save data and export to a file that can be analyzed in Microsoft Excel
    - Save as a ".gmbl" file for the LabQuest 3 software
    - Export as a ".txt" file for analysis in Microsoft Excel
- This process is repeated for all of the samples

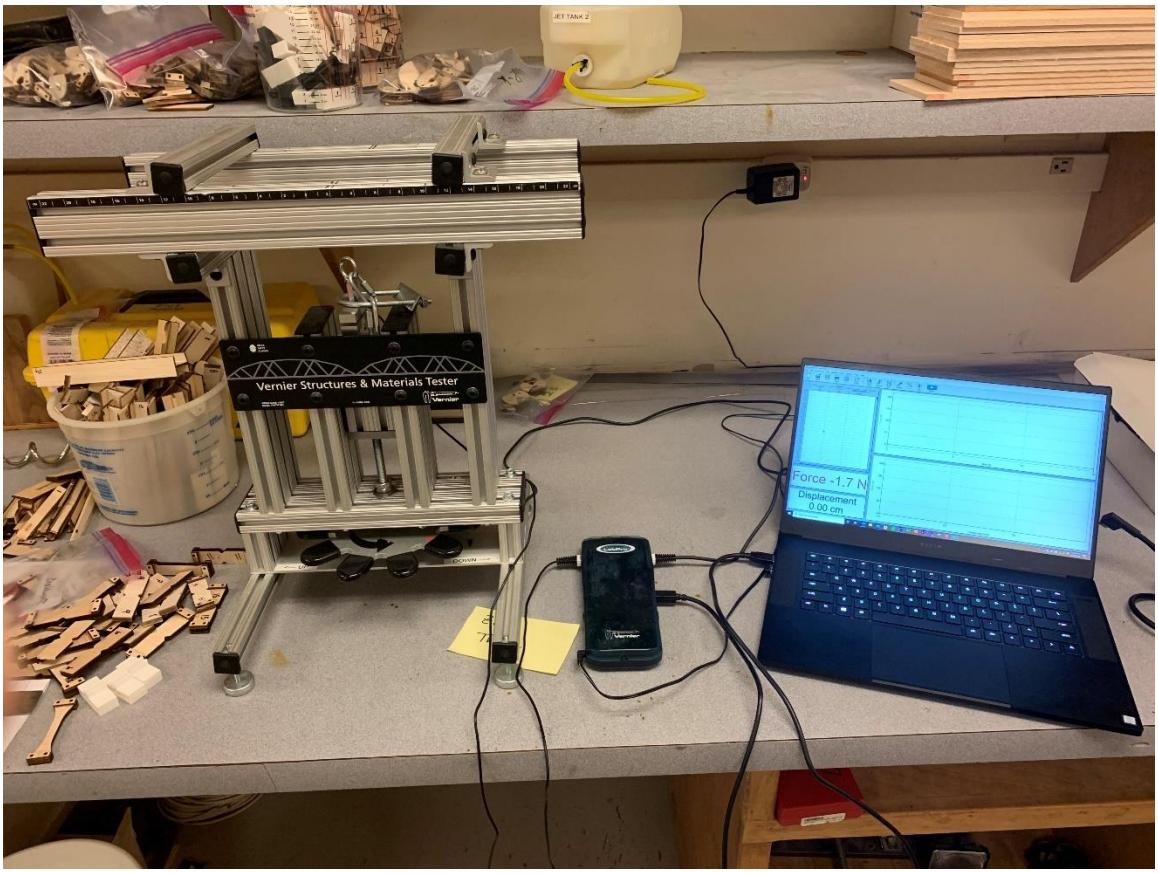

Figure 35: Hardware assembly setup

Tensile Test Results

The tensile tests for grain direction perpendicular with the force produce expected failure visualizations with the balsa wood failing around the middle of the wishbone along the grain direction. This type of failure in wood material is known as a tension failure of earlywood. [14] It is important to know the tensile strength of the material when force is perpendicular to the grain direction because the moment applied to the beam in three-point bending could possibly cause a tensile failure in this grain direction when designing the composite I-beams. An image of a sample post-test is shown below:

Figure 36: With-grain Tensile Test Failure

As the load is applied to the test sample, stress on the sample rises briefly and then levels out. This is the yield stress of the material and occurs early in the load application. After this yield stress, there is another rise until the ultimate tensile stress of the balsa wood is reached where failure is meant, and the stress drops to zero. All samples follow this same pattern with slight variation. An image of the graphs showing force vs. time is shown below:

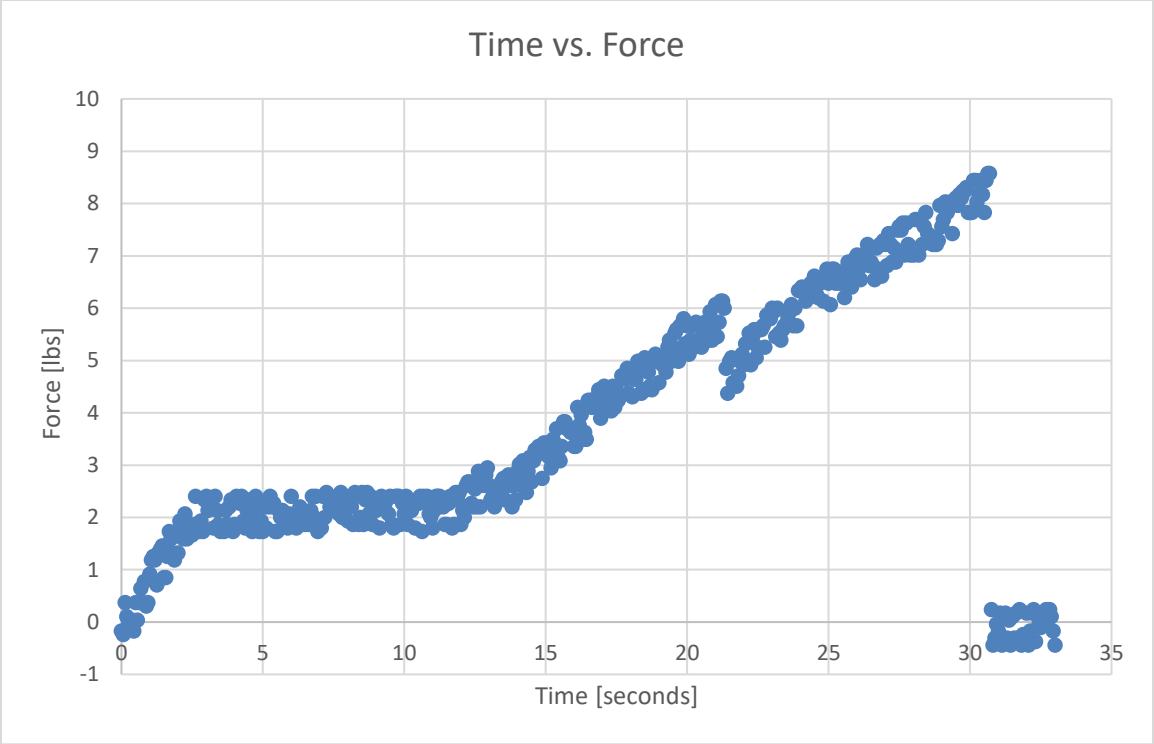

Figure 37: Force vs. Time for 0.125" Tensile Sample

One will also notice slight dips in the ultimate stress area. These are areas where the material "gives out." It is as thought the balsa wood experiences a small crack that does not cause failure, since more force can be applied until ultimate failure, but it is something to be cognizant of moving forward. This phenomenon could also be attributed to the test sample settling in place on the Vernier Structure and Material Tester. As load is applied, the sample shifts to in its mounts to fit into place perfectly.

One trend was noticed as testing was performed: there is variation in ultimate tensile strength of the balsa wood compared to the density of the balsa wood. After initial tests were performed, the ultimate tensile strength of the material increases as the density of the wood increases. This led to more testing in an attempt to make baseline values for the strength of the balsa wood depending on the measured density of the material. This trend is shown in Figure 36 below:

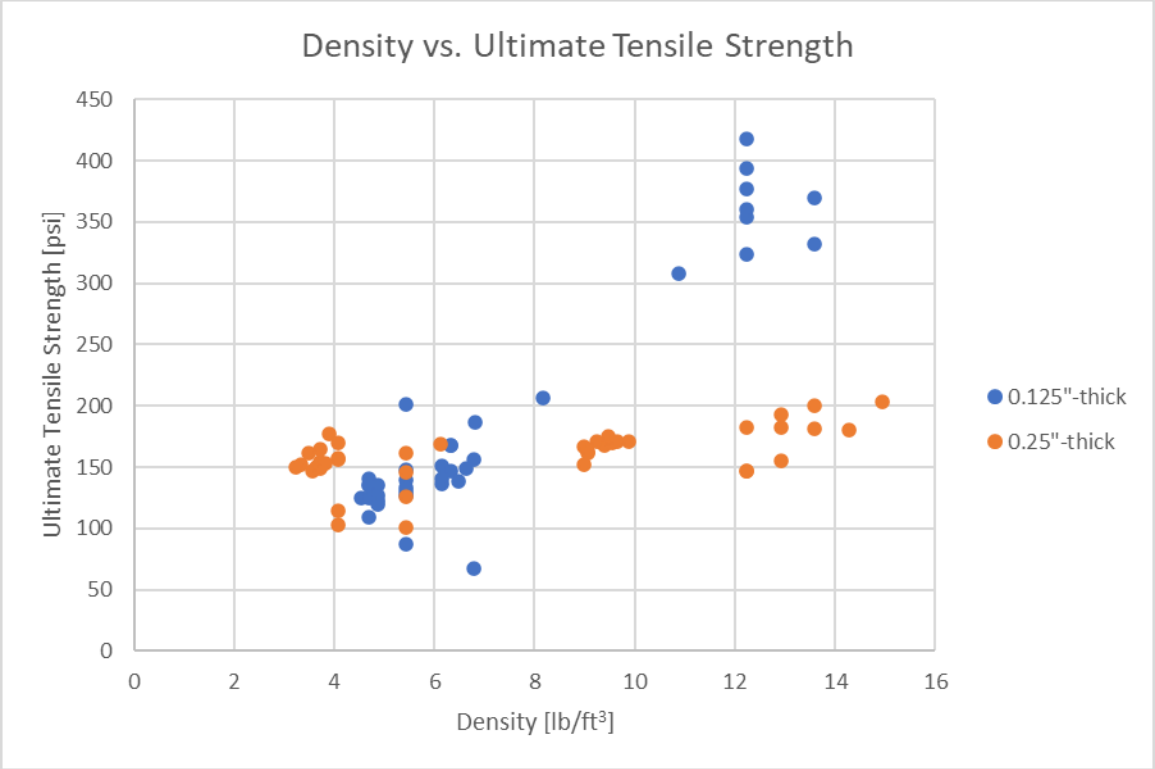

Figure 38: Density vs. Ultimate Tensile Strength of Balsa Wood

The noticeable trend in this data comes from the higher density end of the balsa wood. When the balsa wood gets into the higher densities, above 10 lb/ft^3, there is a split. This split is caused by differences in 0.125" and 0.25" balsa wood. The high density, 0.125" density continues to increase in ultimate tensile strength while the high density, 0.25" stagnates and does not increase with density. This is not intrinsic and is a strange trend in the data. It is expected that as the density of the balsa wood increases, there would also be an increase in the tensile strength of the material. This is not what is seen though. At a density starting at approximately 12 lb/ft^3, there becomes a split where some of the tests specimens continue to increase in tensile strength while the others do not increase or decrease. The noticeable reason this happens is due to the material being used; the balsa wood that continues to increase in tensile strength is 0.125" thick and the balsa wood that continues to stay at around 150-200 psi is 0.25" thick balsa wood. It is believed that the 0.25" thick balsa wood is worse quality compared to the 0.125" thick balsa wood. This is believed to happen

for two reasons. 0.125” balsa is strongly scrutinized by the manufacturers and distributers because it is most used by the RC Modelers purchasing the material. The shear webs used by the RC modelers almost never use anything bigger than 0.125” thick balsa wood so the seller makes sure to use high quality wood for this dimension of balsa. RC modelers rarely use 0.25” thick balsa and if it is used, it is used for components such as leading-edge shaping. Since the 0.25” thick balsa is not being used for structural components, the quality control on the wood is not to a high standard.

Another reason why the 0.25” balsa wood does not reach high tensile strengths is due to the material makeup. It is believed that the thicker wood is going to have more area for defects and sap channels at the fracture area. Figure 37 shows the difference between the two thicknesses

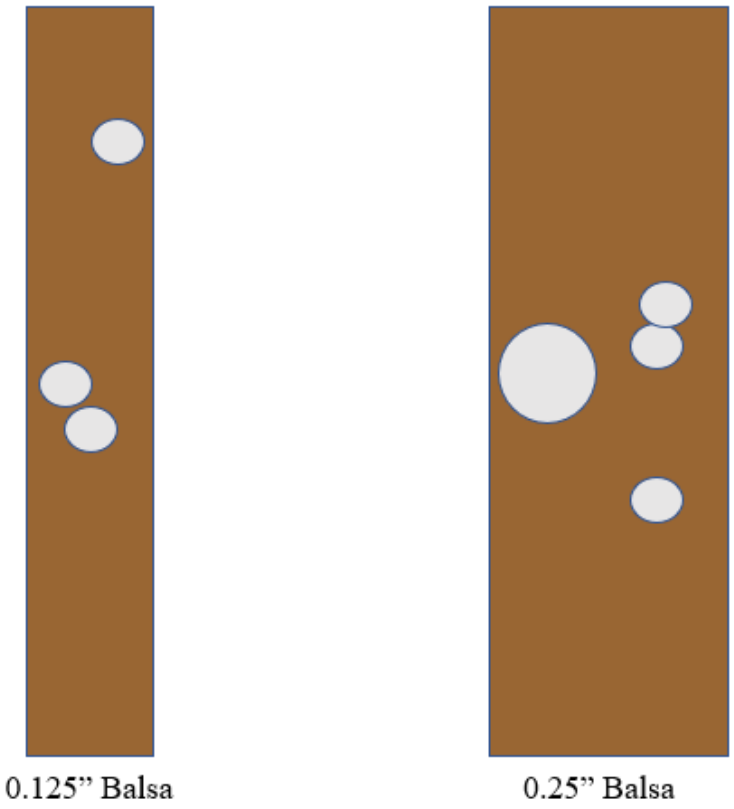

Figure 39: Comparison between 0.125" and 0.25" balsa wood

It is easy to see the difference between the two here. These materials are the same density, so the 0.125” thick balsa wood will have less sap channels and impurities to keep the density while the 0.25” balsa would have more sap channels and impurities. This leads to weak points in the 0.25” thick balsa wood and make them more likely to fail and a lower tensile strength. This gives the initial impression that 0.125” thick balsa should be used for all shear webs and that if a thicker shear web is needed, it is better to laminate 0.125” thick balsa pieces together to get the desired thickness.

Shear Test Experimental Setup

Understanding the shear properties of balsa wood is most important for the design and analysis of the shear webs. Since the shear web takes a large amount of the shear stress in the composite I-beam design, a concrete understanding of balsa’s failure modes while in shear as well as knowledge of the ultimate shear stress is important to making accurate wing spars.

The experimental test setup for shear testing is very similar to the previous tensile tests. The difference being that the shear tests use a different geometry for the test sample. In order to test solely for the shear strength of balsa wood, a sample needs to be developed that can fit two requirements:

1. Fit within the dimensional requirements of the Vernier Structure and Material Tester.
2. Be loaded by only shear stresses when a tensile force is applied.

The following image shows the geometry used to conduct the shear tests.

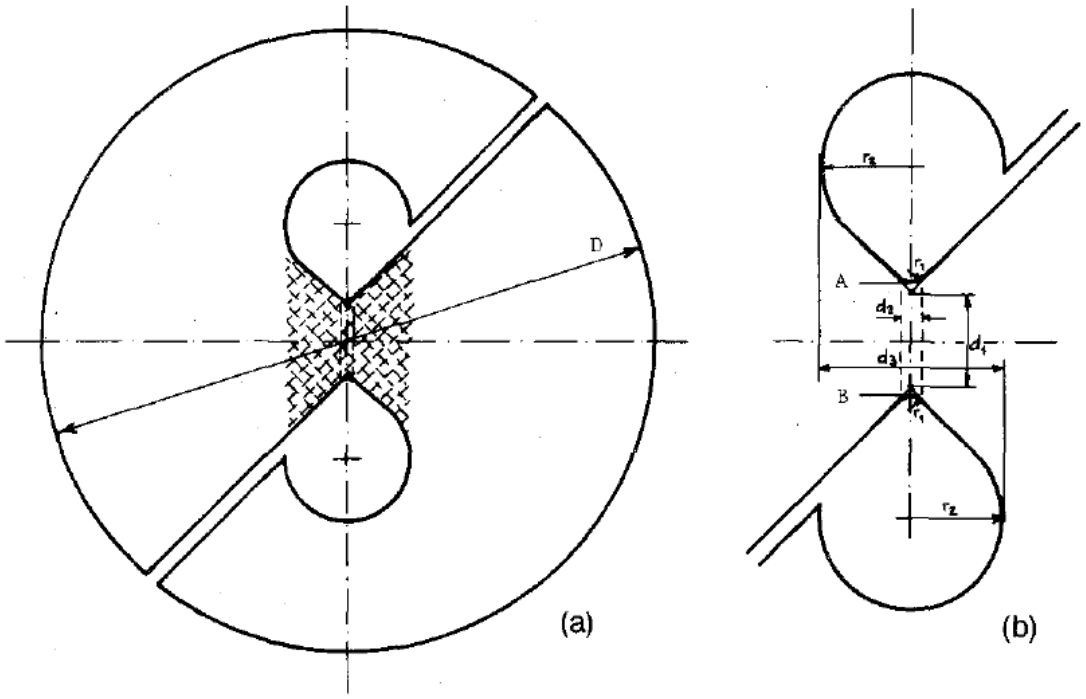

Figure 40: Shear test sample geometry [15]

This design is unique because of its ability to load the test sample with no principal stresses and only a shear stress. Based off the previous image, the test sample is a circular plane with antisymmetric cutouts. The critical section of the sample is the narrow section at the center. The rectilinear portions of the cutouts are oriented at ±45° and so the principal stresses are oriented in these directions. The normal and shear stresses on section AB are [15]:

$$\sigma_x = \sigma_y = \frac{P_\alpha sin\alpha}{A}$$

$$\tau = \frac{P_\alpha cos\alpha}{A}$$

If the applied load is completely vertical and the angle (α) is zero, this creates a situation where the test sample is subjected to only shear loading with the normal stresses equal to zero [15].

$$\sigma_x = \sigma_y = 0$$

$$\tau = \frac{P_0}{A}$$

The dimensions for the sample are based off a set of equations and ratios. When these equations are manipulated, one can create a sample of any size if the equations continue to hold. The equations are as follows [15]:

$$\frac{d_1}{d_2} = \frac{d_1}{\sqrt{2}r_1} = 5$$

$$\frac{d_1}{d_3} = \frac{d_1}{2r_1} = \frac{1}{2}$$

$$D = 10d_1$$

The dimensions used were:

d_1 = 0.2 in

d_2 = 0.04 in

d_3 = 0.4 in

r_1 = 0.028 in

r_2 = 0.2 in

D = 2 in

A Solidworks model of the shear test specimen is shown below (units are in inches):

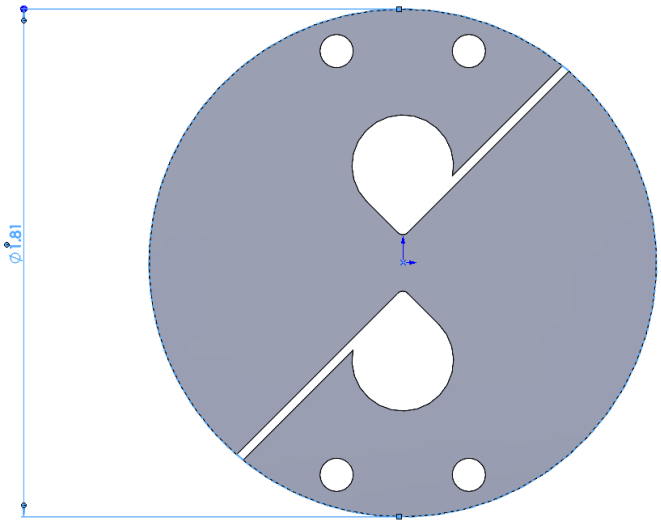

Figure 41: Shear test specimen mode showing diameter

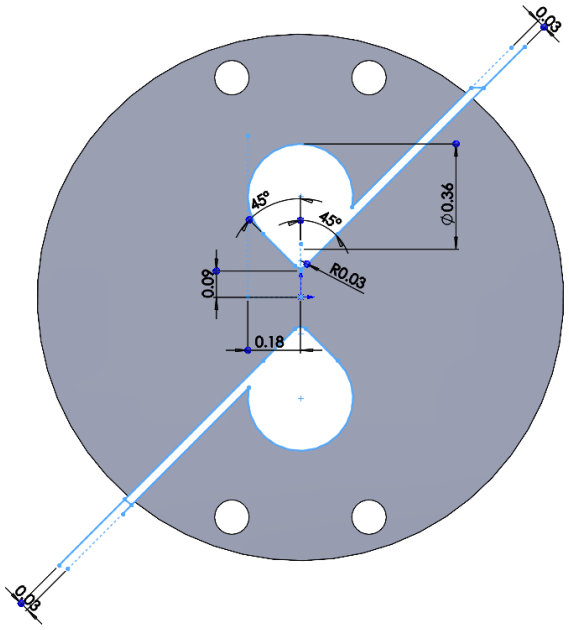

Figure 42: Shear test specimen showing internal cut dimensions

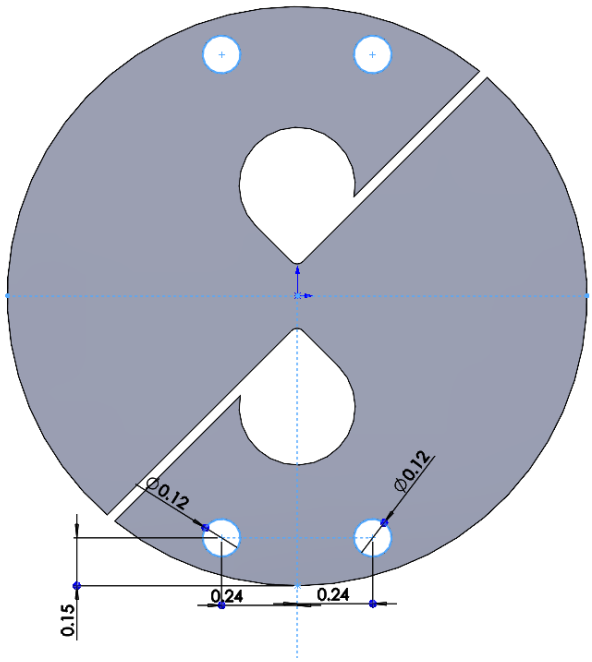

Figure 43: Shear test specimen showing mounting hole dimensions

Two methods were used for creating the samples for with-grain and cross-grain shear testing. For with-grain, a plywood doubler similar to the ones used in tensile testing was bonded to the mounting holes of the sample. For cross-grain, a plywood doubler was applied to the test samples with purple CA glue on both sides that only allowed for a 0.125" gap for the failure to occur. During preliminary tests, it was found that for cross-grain shear testing, the balsa would experience a tensile failure along the grain instead of the desired shear failure. This gives the premature theory that the shear strength of balsa is higher than the tensile strength of balsa. This means that one would see tensile failure before the balsa ever fails in pure shear, but this will be discussed later. For with-grain shear failure, the doublers were only applied to the holes to add extra strength where the mounting occurs.

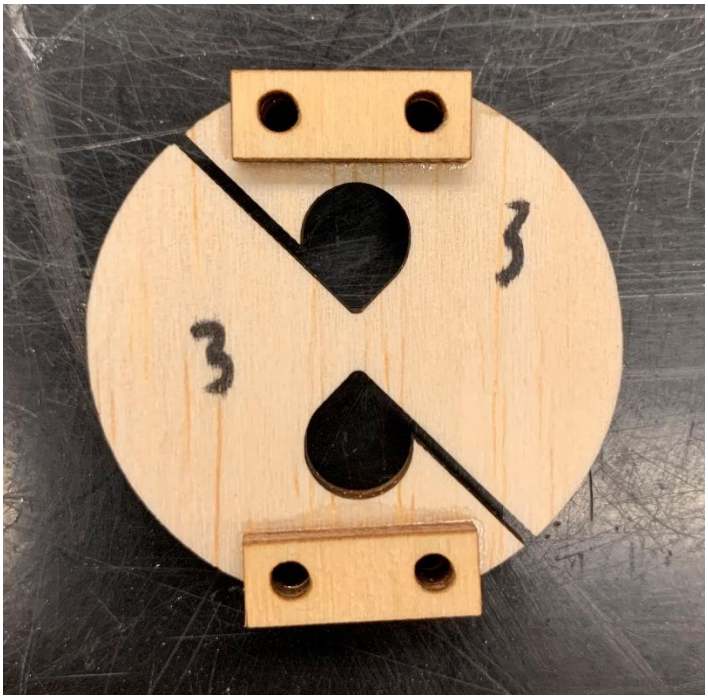

Figure 44: Physical with-grain shear test sample

Figure 45: Physical cross-grain shear test sample

These tests were again performed with both Aero Light and Regular balsa to give a large range of weight and densities. The same 3D-printed mounting parts are used to mount the test samples to the stand and to apply the loads.

Shear Test Experimental Methodology

- Design shear test samples using Solidworks
- Cut out shear test samples and doublers using laser cutter
- Construct shear test samples by super-gluing doublers to mounting holes
- Mount test samples to the Vernier Structure and Material Tester
    - Use #4-40 nuts and bolts to fasten 3D-printed bottom and top supports to the test sample
    - Place the 3D-printed top support on the Vernier Structure and Material Tester support beams
    - Mount the U-Bolt to the 3D-printed bottom piece by sliding the tab through the slot and fastening the nut on both sides of the U-bolt

Figure 46: Cross-Grain shear test setup

- Plug Vernier Structure and Material Tester DAQ into computer with installed LabQuest 3 software and make sure it is reading data
- Apply force until the force goes slightly positive then de-load slightly and zero the measurement
- Begin recording data
- Slowly turn the level to apply a force
- Once failure occurs, stop the data recording and de-load the Vernier Structure and Materials
- Save data and export to a file that can be analyzed in Microsoft Excel
    - Save as a ".gmbl" file for the LabQuest 3 software
    - Export as a ".txt" file for analysis in Microsoft Excel
- This process is repeated for all of the samples

Shear Test Results

Shear test results are similar to those found in the tensile test results. To summarize, a relationship between density and ultimate shear strength is found where the shear strength of the balsa wood is dependent on both the density and thickness of the balsa wood. To completely understand the results of the shear tests, the visual failure modes will be discussed first followed by a discussion of the quantitative data.

Visual Analysis of Shear Failure

With-grain shear tests and cross-grain shear tests have interesting failure modes that are not completely expected. Both samples will be visually inspected to give a clear understanding of what these failure modes look like. The with-grain shear samples will be looked at first. Figure 47 below gives an example of a with-grain shear failure:

Figure 47: With-grain Shear Test Failure

The shear tests with grain direction parallel to the force direction are less important because this is not how the balsa wood shear webs in the I-beams are designed. These are still important to know though for baseline material properties, future testing, and for comparison between composite I-beam testing. This testing will also serve to validate the Wing Spar Analysis Program in future work and could be used for different structures outside of aircraft wing spars.

The failure mode is what is expected of the specimen loaded in this way. As the load is applied, the stress increases in the specimen until the ultimate shear stress is reached and failure occurs along the grain at the fracture area. This creates a “clean break” along the grains. This type of failure is known as shear failure from previous literature review [14]. This is comparable to common shear failures seen for homogenous materials like aluminum or steel.

The shear tests for cross-grain balsa samples produce unexpected failures. These shear failure in these samples is not commonly seen in the shear testing of homogenous materials. Figure 48 below gives an example of a cross-grain shear failure:

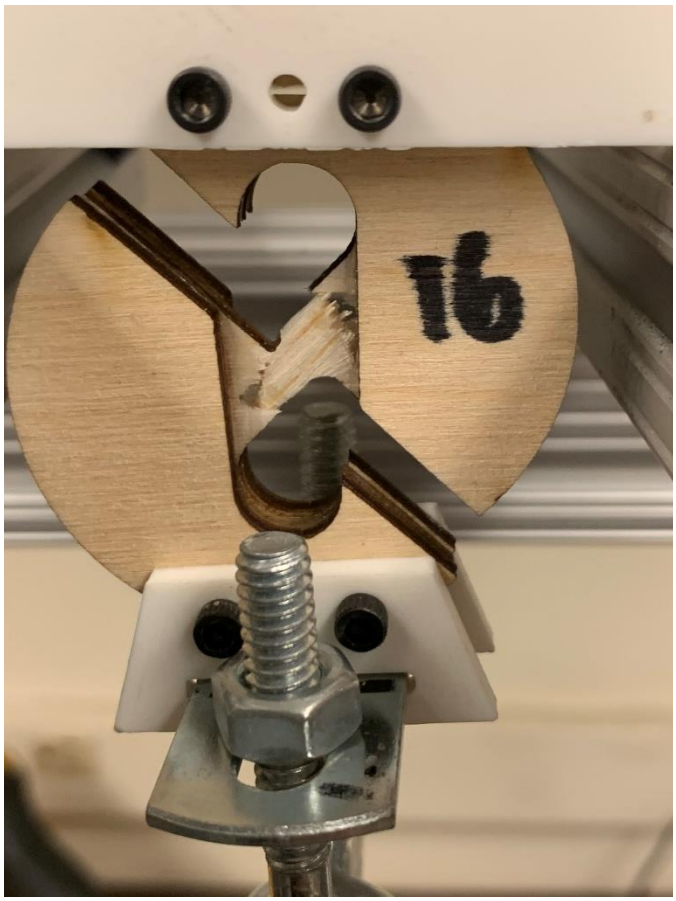

Figure 48: Cross-grain Shear Test Failure

The important thing to notice is that this is not a clean shear break like what was seen in the samples with grain direction parallel to the force direction. There is also no specified failure mode for this as defined in the Literature Review [14]. The best way to describe the failure mode is that the load applied pulls the grains apart until the cross-section is so weak that the material fails. The best description for it so far is a "tensile failure in the grain caused by shear loading." As the force in the vertical direction is applied from the Vernier Structure and Material Tester, the balsa begins to fail along the grain direction. The tensile strength in the grain direction that is perpendicular to the applied load begins to fail. As the crack begins to propagate, this causes a failure in the section where the middle is pulled apart instead of a creating a vertical shear failure. Figures 49 through 51 show the loading scenario all the way from initial loading to final failure.

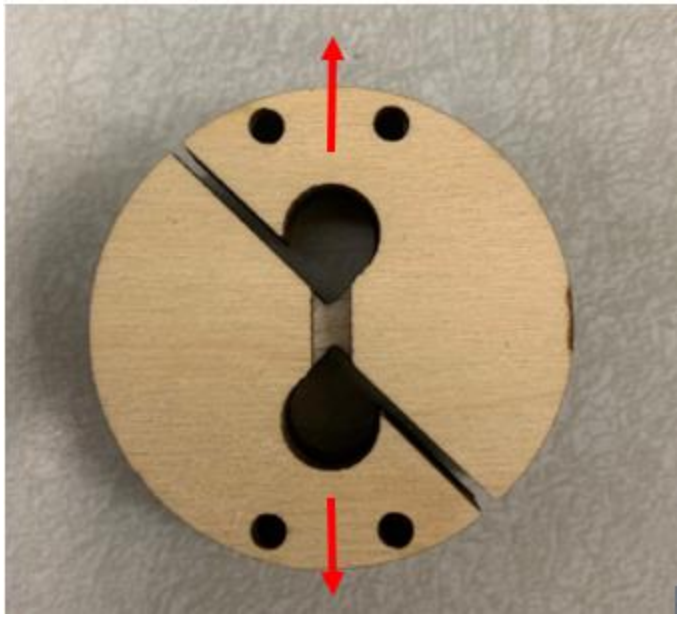

Figure 49: Force application from Vernier Structures and Material Tester

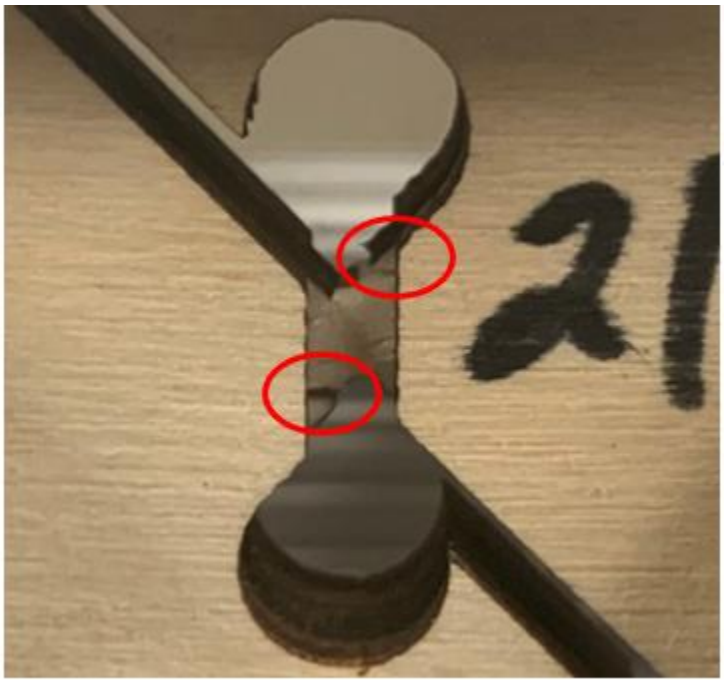

Figure 50: Initial crack propagation in shear test sample

Figure 51: Complete failure of shear test sample

The ultimate stress the material can take under a shear load is still much higher than that under a tensile load, but the failure is not what is expected from shear loading due to the non-homogeneity of the balsa material and the drastic difference in the strength of the grain direction from perpendicular to parallel grain direction in relation to the load direction.

Numerical Analysis of Shear Failure

To gain a complete understanding for shear failure of balsa wood, the numerical understanding is just as important as the visual understanding. Numerical analysis gives definitive values of the shear strength of the balsa shear web and allows for the accurate design and analysis of composite I-beams.

The Vernier Structure and Material Tester applies load and the records the raw data of time vs. force. As the load is applied to the test sample, stress on the sample rises briefly and then levels out. This is the yield stress of the material and occurs early in the load application. After this yield stress, there is another rise until the ultimate shear stress of the balsa wood is reached where failure

is met, and the stress drops to zero. All samples, both cross- and with-grain, follow this same pattern with slight variation. This trend is shown in Figure 52 below.

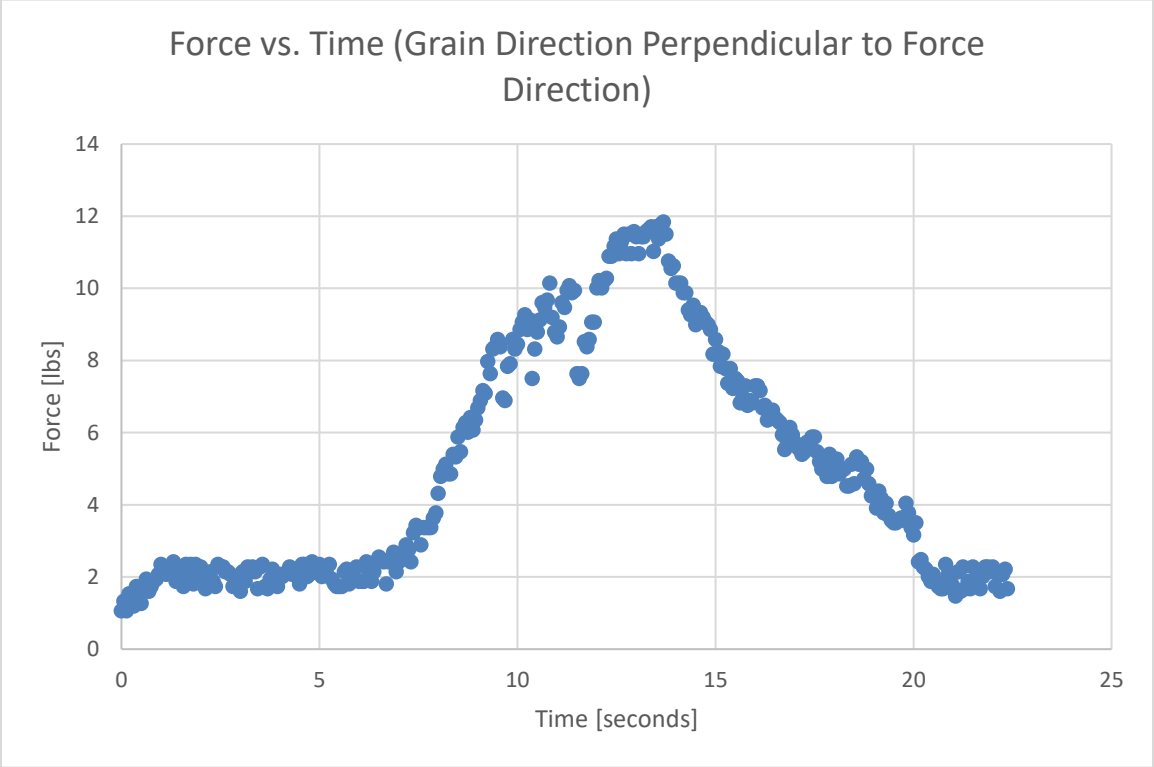

Figure 52: Force vs. Time for 0.25" Thick Shear Sample

Understanding the individual trend of the shear test samples is important, but it is more important to understand how the shear strength varies with density. The strength variation with density allows the engineer to design their wing spar regarding the measured density of the balsa wood. Figure 53 shows the variation of balsa wood with grain direction perpendicular to the applied shear force.

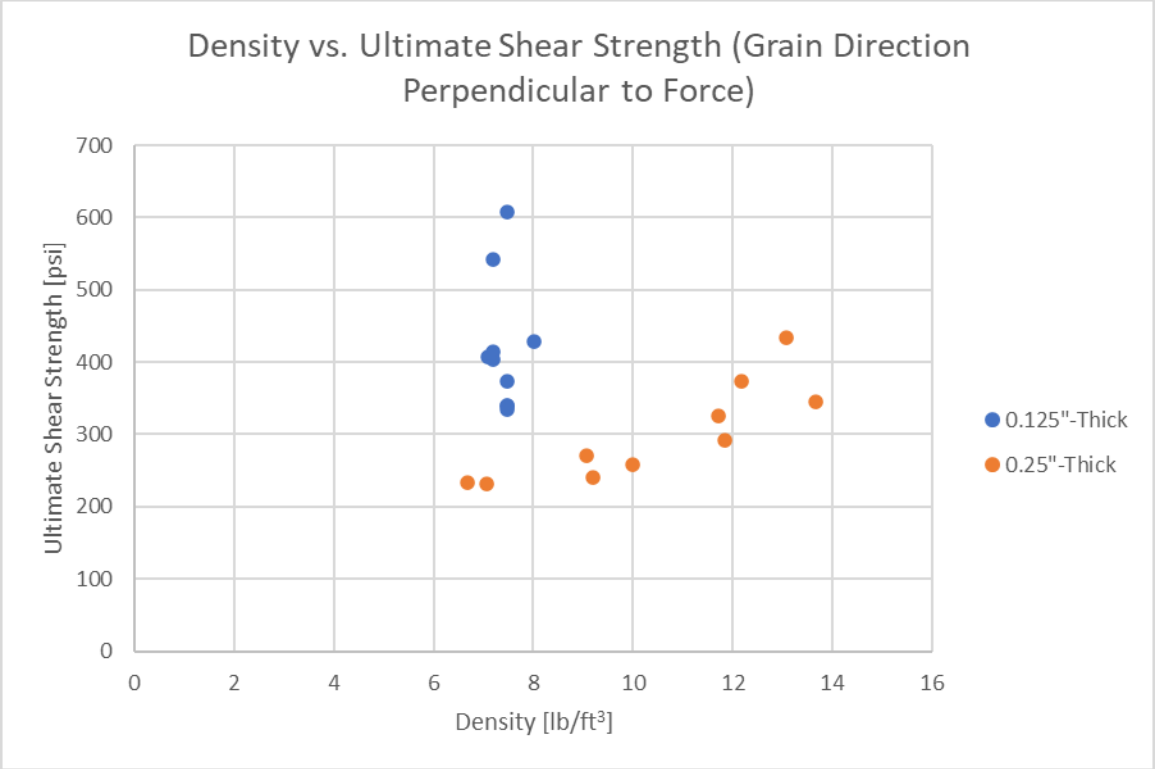

Figure 53: Density vs. Ultimate Shear Strength for Grain Direction Perpendicular to Force

One trend was noticed as testing was performed: there is variation in ultimate shear strength of the balsa wood compared to the density of the balsa wood, but there is also variation in ultimate shear strength compared to the thickness of balsa wood. The marks in blue represent 0.125”-thick balsa wood while the orange represents 0.25”-thick balsa wood. Immediately, it is noticeable that the 0.125”-thick balsa wood has a higher ultimate shear stress compared to the 0.25” thick balsa wood. At a density range of 6-8 lb/ft^3, the 0.125”-thick balsa is in the range of 300-600 psi while the 0.25”-thick balsa wood is approximately 225-250 psi. The 0.25”-thick balsa wood only breaks into the 400 psi shear strength range when a density between 12-14 lb/ft^3 is reached. This trend agrees with the trend noticed in tensile testing. The 0.125”-thick balsa wood is a better quality of material that can handle higher loading compared to the 0.25”-thick balsa wood.

Similar trends were noticed for balsa wood when testing for ultimate shear strength when the grain direction is parallel to the force. There is more variation in material properties for this

orientation and it can also be seen that very high-density balsa begins to break the trend. Again, this is attributed to the difference in material quality discussed in the tensile test results section. This orientation for balsa is never used for making composite I-beams due it being more susceptible to shear failure and shear buckling which creates a shear fracture across the length of the I-beam. Figure 52 below shows the variation between density and shear strength for balsa wood with grain direction parallel to the applied shear force.

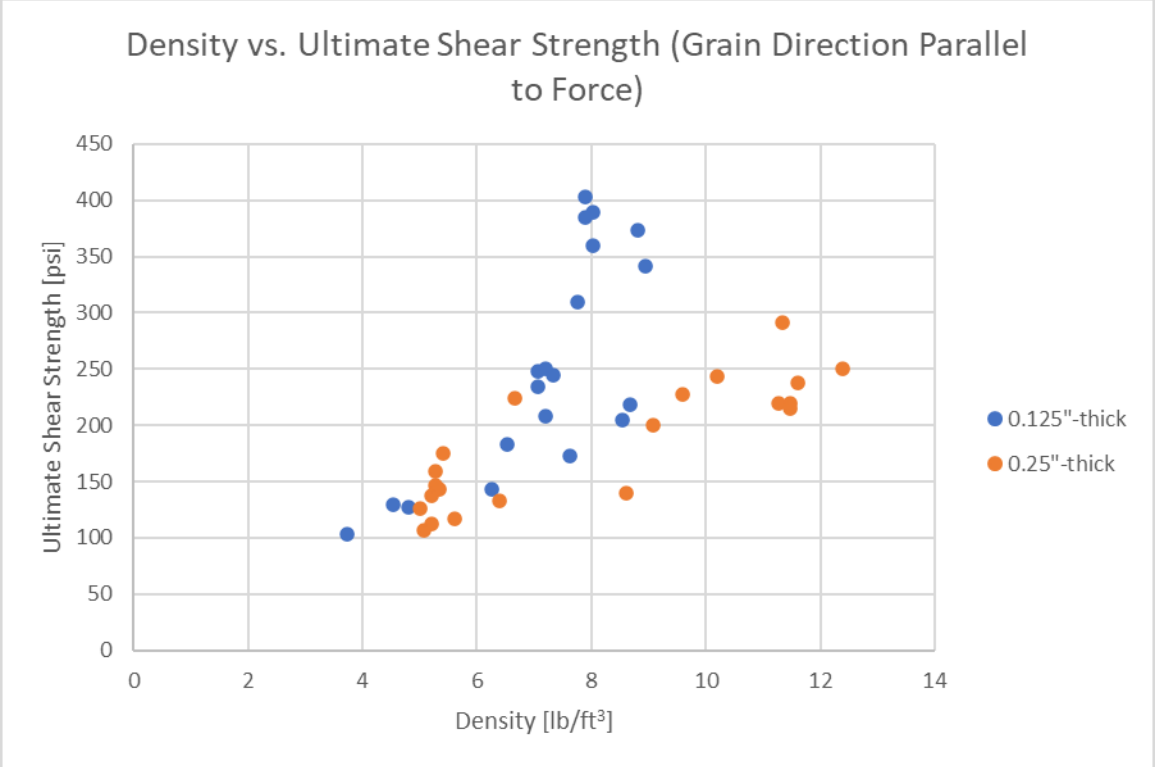

Figure 54: Density vs. Ultimate Shear Strength for Grain Direction Parallel to Force

One interesting take away from the full shear analysis is the divergence in balsa wood shear strength when the balsa wood gets to a density of approximately 10 lb/ft^3. This trend is noticed for balsa wood in cross-grain and with-grain shear testing as well as cross-grain tensile testing. This means that this is not just an irregularity in the tests or data, but a repeatable phenomenon of balsa wood. This trend comes from the fact that the balsa wood of this density is commonly 0.25”-thick. With the bigger thickness comes the possibility of more imperfections in the material. There are

more sap channels and weak points in the material compared to the 0.125”-thick material found from 4 lb/ft^3 to 10 lb/ft^3. Now, this seems counterintuitive. A higher density balsa is made of more tracheids since this material component is most prominent in balsa wood and is responsible for determining its density. But, the failure area doubles in size in 0.25-inch balsa wood compared to 0.125-inch thick balsa. In the failure area, there is more room for imperfections in the material due to the increased area. In the future, more testing will need to be done to understand the material properties of balsa wood as thicker material gets used. The most common material used in the research performed at Oklahoma State University is 0.125-inch-thick balsa wood so that is what most of the research will look at..

Based off both the ultimate tensile and shear stress of the balsa in relation to density, a reference to balsa material properties based off density of the material was added to the wing spar analysis program since the strength of the I-beam is dependent on the balsa wood material properties. The database takes the average values for the material properties of balsa wood for densities starting at 4 lb/ft^3 and goes up to 10 lb/ft^3 in increments of 1 lb/ft^3.

Conclusions from Balsa Material Testing

The difference in the tensile and shear strength of balsa wood is the most interesting conclusion found through material testing of balsa wood. As the thickness of balsa wood increases above 1/8”-thick, the non-homogeneity of balsa wood becomes more apparent. Impurities in the balsa wood material composition increase effecting the overall strength of the material. This leads to initial recommendation that when designing the shear webs for UAVs, it is better to laminate 1/8”-thick sheets of balsa wood together instead of buying thick material. Lamination is the process of bonding sheets together with either super glue or epoxy to increase the thickness until the desired thickness is achieved. For example, if a 3/8”-thick shear web is needed for the loading of the wing, it is better to laminate 3 pieces of 3/8” thick balsa wood together instead of buying a 3/8”-thick

piece of balsa wood. Figure 55 shows an example of this shear web applied to the F5D Viper RC aircraft. This aircraft laminates three 1/8”-thick balsa pieces together with carbon fiber between the layers to achieve the desired thickness necessary for the high g-loading of the aircraft.

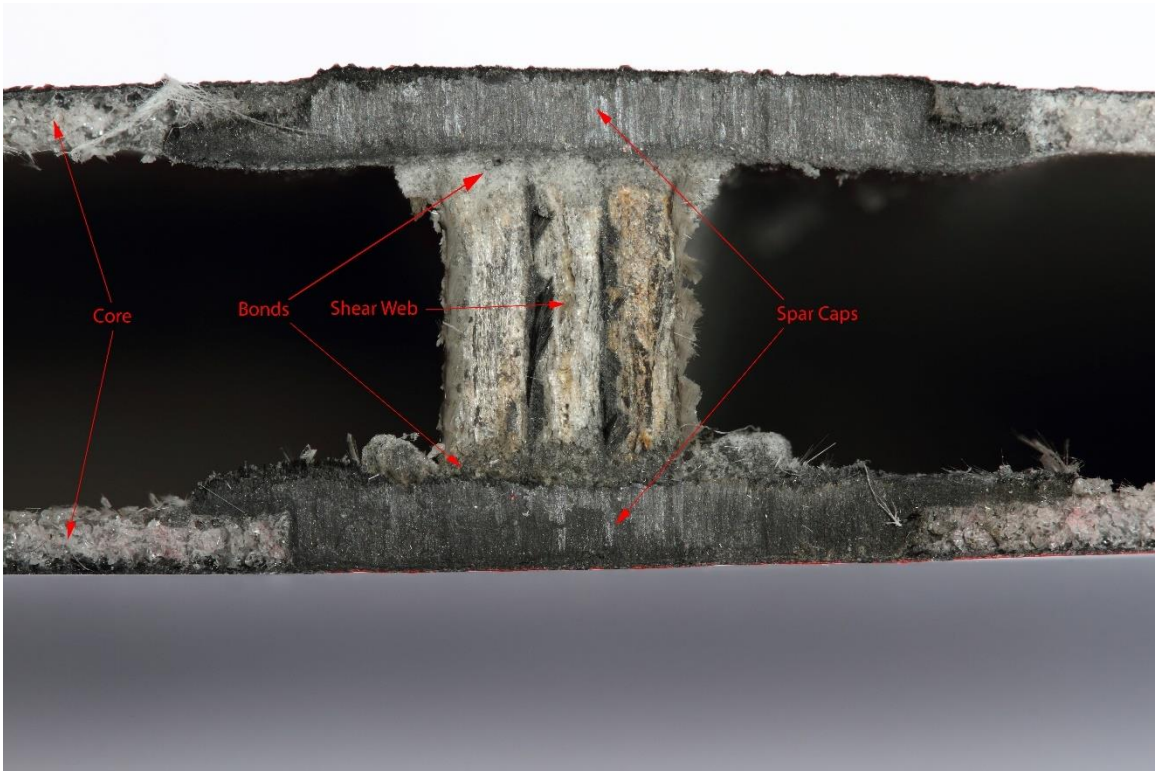

Figure 55: F5D Viper shear web [5]

CHAPTER V

I-BEAM TESTING AND RESULTS

The final phase of testing introduces the three-point bending of composite I-beams. Three point-bending accurately simulates the bending loads found in flight. By performing three-point bending tests, characterizing the failure of I-beams is easy to do by using the Vernier Structure and Materials Tester. Before testing composite I-beams made of carbon fiber and balsa wood, prototype I-beams were made to get a better understanding of the manufacturing, testing, and results. These prototype I-beams were made using plywood I-beams caps with balsa wood shear webs. Once the testing was performed on the prototype I-beams and an understanding was gained, the composite I-beams were made and tested following standard three-point bending testing procedure. The results for the composite I-beams have given a visal understanding of how the cross-grain balsa wood shear webs failure under load and have given validation that the transformed area method used in the Wing Spar Analysis Program can be used to design composite I-beams used in aircraft.

This chapter will look at the experimental setup, methodology, and results for these tests. This includes how the geometry was chosen, how the I-beams were manufactured, how the experiments were performed, and the results of the experiments. The results will then be compared to the Wing Spar Analysis Program to validate the results and perform further development of the code.

Prototype I-Beam Experimental Setup

Understanding the failure modes of composite I-beams is one of the main goals of this research, but before testing of composite I-beams with carbon fiber caps and balsa wood shear webs, it is important to characterize the failure modes with known samples. I-beams were made with on-hand materials that could be manufactured easily with quick turnaround. Three sets of I-beams were made with the goals of characterizing three failure modes:

- Set One: Cross-grain shear failure in shear web
- Set Two: With-grain shear failure in shear web
- Set Three: Tensile failure in I-beam cap

Set One and Set Two were constructed using 0.125" thick plywood caps with both cross-grain and with-grain balsa shear webs. With the high tensile and compressive strength of the plywood caps, this will ensure a shear failure in the balsa wood shear webs. Plywood has a Young's Modulus of $1.01*10^6$ psi [16], an ultimate compressive strength of 4500-6000 psi [17], and a ultimate tensile strength of 4000-5000 psi [17]. The lower end range of the material property values were used to add a factor of safety to the calculations. It is important to know what a shear failure in the web looks and behaves like to understand shear failures in the carbon fiber and balsa I-beams used in aircraft wings.

Set One was split into three subsets with three samples in each subset to test a total of 9 I-beams. One subset was made using 0.125" thick, 0.5" wide plywood caps and a 0.125" thick, 0.5" tall cross-grain balsa shear web with a total length of five inches. The second subset was made using 0.125" thick, 0.5" wide plywood caps and a 0.125" thick, 0.35" tall cross-grain balsa shear web with a total length of five inches. The third subset was made using 0.125" thick, 1.0" wide plywood caps with 0.125" thick, 0.75" tall cross-grain balsa shear web with a total length of seven inches.

Set Two was also split into three subsets with three samples in each subset. All subsets in Set Two use the same dimensions and those in Set One. The difference between the two is that the shear web in Set Two is with-grain balsa. These were constructed using CA glue to bond together balsa wood pieces and to bond to the shear web and caps together.

Set Three was constructed using 0.125” thick with-grain balsa caps and cross-grain balsa shear webs. The low tensile and compressive strength of the with-grain balsa woods caps compared to the higher shear strength of the cross-grain balsa wood shear web ensures a tensile failure in the caps will occur before a shear failure in the webs. This is important to understand how a tensile failure in carbon fiber caps looks and behaves like to understand tensile failure in the I-beams used in aircraft wings. While this is a less common failure in aircraft wings, it is still important to understand the behavior for design and analysis of the composite I-beams.

Set Three was split into three subsets with three test samples in each subset to test a total of nine samples. The first subset was made using 0.125” thick, 1” wide with-grain balsa wood caps and 0.125” thick, 1.0” tall cross-grain balsa wood shear webs with a total length of 7.5”. The second subset was made using 0.125” thick, 1” wide with-grain balsa wood caps and 0.125” thick, 1.0” tall cross-grain balsa wood shear webs with a total length of 5.0”. The third subset was made using 0.125” thick, 1” wide with-grain balsa wood caps and 0.25” thick, 1” tall cross-grain balsa wood shear webs with a total length of 5.0”. These were constructed using CA glue to bond together balsa wood pieces and to bond to the shear web and caps together. Figure 56 below shows a graphic of the I-beam geometry while Figures 57 through 59 show the physical samples used.

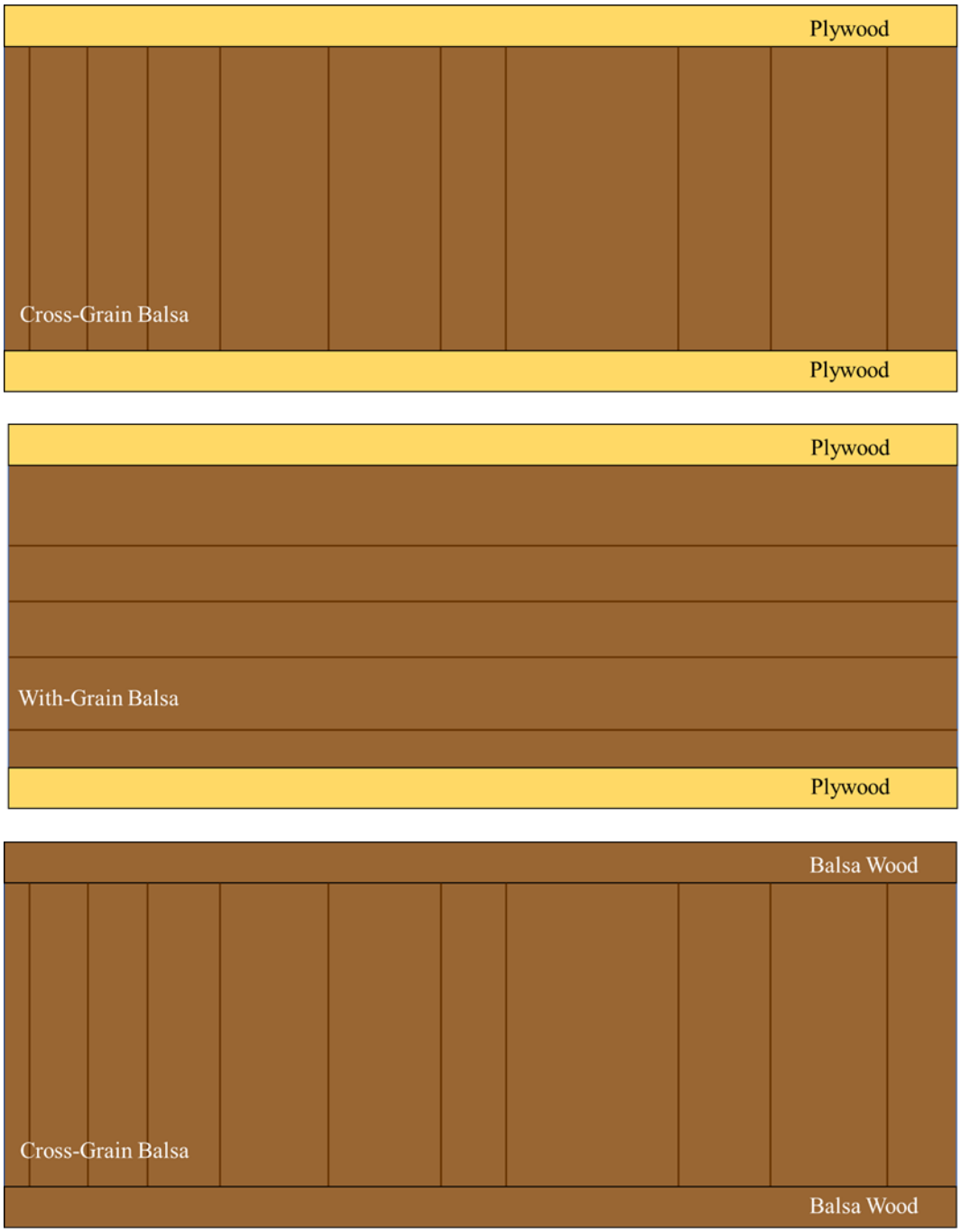

Figure 56: Simplified graphic of prototype composite I-beams

Figure 57: I-beams with plywood caps and cross-grain balsa wood shear webs

Figure 58: I-beams with plywood caps and with-grain balsa wood shear webs

Figure 59: I-beams with with-grain balsa wood caps and cross-grain balsa wood shear webs

Prototype I-Beam Experimental Methodology

In order to perform accurate, repeatable experiments with the prototype composite I-beams, a strict experimental methodology was followed. Following this methodology allowed for efficient testing and the ability to compare quantitative and qualitative data across all samples. The experimental methodology is as follows:

- Design I-beam components using Solidworks
- Cut out I-beam components using laser cutter
- Construct I-beam using given materials
- Mount I-beams to the Vernier Structure and Material Tester
    - Allow for 0.25” space for I-beam to rest on support beams
    - Place the U-bolt in the center of the I-beam

- Plug Vernier Structure and Material Tester DAQ into computer with installed LabQuest 3 software and make sure it is reading data
- Apply force until the force goes slightly positive then de-load slightly and zero the measurement
- Begin recording data
- Slowly turn the level to apply a force
- Once failure occurs, stop the data recording and de-load the Vernier Structure and Materials
    - For testing shear failure in cross-grain balsa wood shear webs, failure will appear as small cracks laterally in the shear web. This will not be a complete failure of the sample. Once could keep applying load until a tensile failure occurs for complete failure.
    - For shear failure in with-grain balsa wood shear webs, failure will appear as a long crack that propagates longitudinally down the I-beam. This will be a complete failure of the I-beam.
    - For tensile failure of the with-grain balsa wood caps, the failure will appear as a tensile failure in the bottom cap that propagates laterally up the I-beam until the whole I-beam is broke. This will be a complete failure of the I-beam.
- Save data and export to a file that can be analyzed in Microsoft Excel
    - Save as a ".gmbl" file for the LabQuest 3 software
    - Export as a ".txt" file for analysis in Microsoft Excel
- This process is repeated for all of the samples

Prototype I-Beam Results

Two sets of results were obtained from the three-point bending tests of the prototype composite I-beams: visual and analytical results. The visual results will be analyzed first to

characterize the three failure modes that were tested. After the visual analysis, the data recorded by the Vernier Structure and Material Tester will be analyzed to obtain time vs. force and stress-strain graphs. The results obtained will also be used to compare the stress failure value to the Wing Spar Analysis Program value to get an initial accuracy.

Visual Analysis of Prototype Composite I-beams

One of the main takeaways from the prototype composite I-beam testing was to get a visual understanding of what a cross-grain shear failure, with-grain shear failure, and tensile failure look like in composite I-beams. There are many examples of what these failures look like in more common materials, like concrete in civil engineering applications, but because of the unique material composition of balsa wood it is important to see exactly how balsa wood fails under these loading scenarios. Figures 60 through 62 show examples of the different failure modes for the different I-beams sets.

Figure 60: Prototype I-Beam cross-grain shear failure

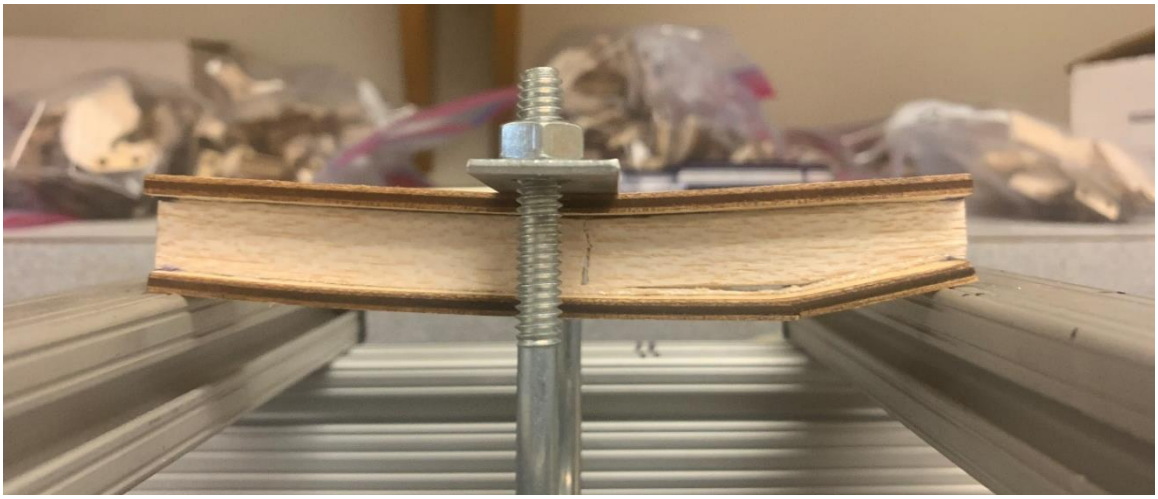

Figure 61: Prototype I-Beam with-grain shear failure

Figure 62: Prototype I-Beam tensile failure

The failure of most interest is the cross-grain shear failure in the shear web. This failure is characterized by small lateral cracks in the balsa wood shear web followed by delamination in the adhesive bonding the shear web to the caps. It is important to state the delamination in the adhesive is not immediate. One will see small cracks appear at different locations along the length of the beam. As more load is added and the displacement increases, the adhesive will delaminate. What is interesting is that the onset of these cracks do not cause a complete failure of the I-beam. The I-beam can still handle increased loading until either the caps fail, or a shear failure occurs in the

glue bond. What happens is that the crack appears in the shear web and this causes a higher deflection in the I-beam. The deflection increases because the shear web is no longer a continuous material. These cracks will continue to appear at different points in the shear web until either the deflection is too high and the glue bonding the shear web and caps together fails in shear from the difference in deflection of the materials or the caps reach their tensile strength limit. More often, the glue bond fails in shear before the ultimate tensile strength of the caps are reached.

After testing the first nine samples, the Vernier Structure and Materials Tester was found to have a problem. The Vernier Structure and Materials Tester has a displacement sensor that calculates displacement based off rotation of the wheel. When the data was being analyzed, the displacement values created a saw-tooth pattern graph. The sensor was analyzed a programming error was found. After reprogramming the sensor and creating a different user interface in the software, measurements for displacement were able to be recorded with 0.01-centimeter resolution. With this change, nine more samples were tested to see if this data could be collected correctly for future tests with the composite I-beams.

The failure in the with-grain balsa shear webs is easily noticed. A crack propagates longitudinally down the length of the beam. With-grain balsa wood has a very low ultimate shear stress, and the failure is observed at very low loading. This crack immediately causes a complete failure. A vertical crack is also shown near the center of the beam. The failure of the balsa wood shear web is appearing to be a combination of two flexural failure modes: horizontal shear and brash tension [14]. This orientation is not used in aircraft for two reasons: not being able to handle large flight loads and the quick failure of a full wing as the cack propagates down the full length of the I-beam.

The tensile failure of the caps is catastrophic. A tensile failure occurs when the ultimate tensile strength of the cap material is reached before the ultimate shear failure of the shear webs.

This starts as a common tensile failure in the bottom cap. This crack in the cap causes a large lateral crack in the shear web and subsequently a crack in the top cap. This sequence of events is near instantaneous and is only seen when video-taped in slow motion or when the loading is stopped as soon as failure occurs. The flexural failure of the full balsa wood I-beam appears to be the brash tension failure mode in both the caps and the shear web . Tensile failure of the caps in an aircraft is very uncommon because of the high tensile strength of carbon fiber, but it is still important to know how this failure occurs if ever experienced in flight. This kind of failure is catastrophic for the aircraft and will result in failure at the wing root where the loading is higher and cause.

Numerical Analysis of Prototype Composite I-beams

The Vernier Structure and Material Tester takes the raw data of force, time, and displacement. With this data, force vs. time and stress-strain graphs can be made using the equations:

$$\sigma = \frac{F}{A}$$

$$\varepsilon = \frac{l}{l_0}$$

The force vs. time graphs were found for every sample tested and the stress vs. strain graphs were found in the samples made after the initial prototype testing. As discussed in the last subsection, problems with the displacement sensor on the Vernier Structure and Material Tester added additional samples to tests. The initial samples only have time vs. force graphs while the additionally samples have both time vs. force and stress-strain graphs. Time vs. force and stress-strain graphs have been made for the samples tested. The following images show these graphs for the various I-beams. Since the cross-grain failure is most important, these graphs have been displayed in more detail with each subset getting its own graph. The with-grain shear failure and tensile failure graphs have been combined into single graphs.

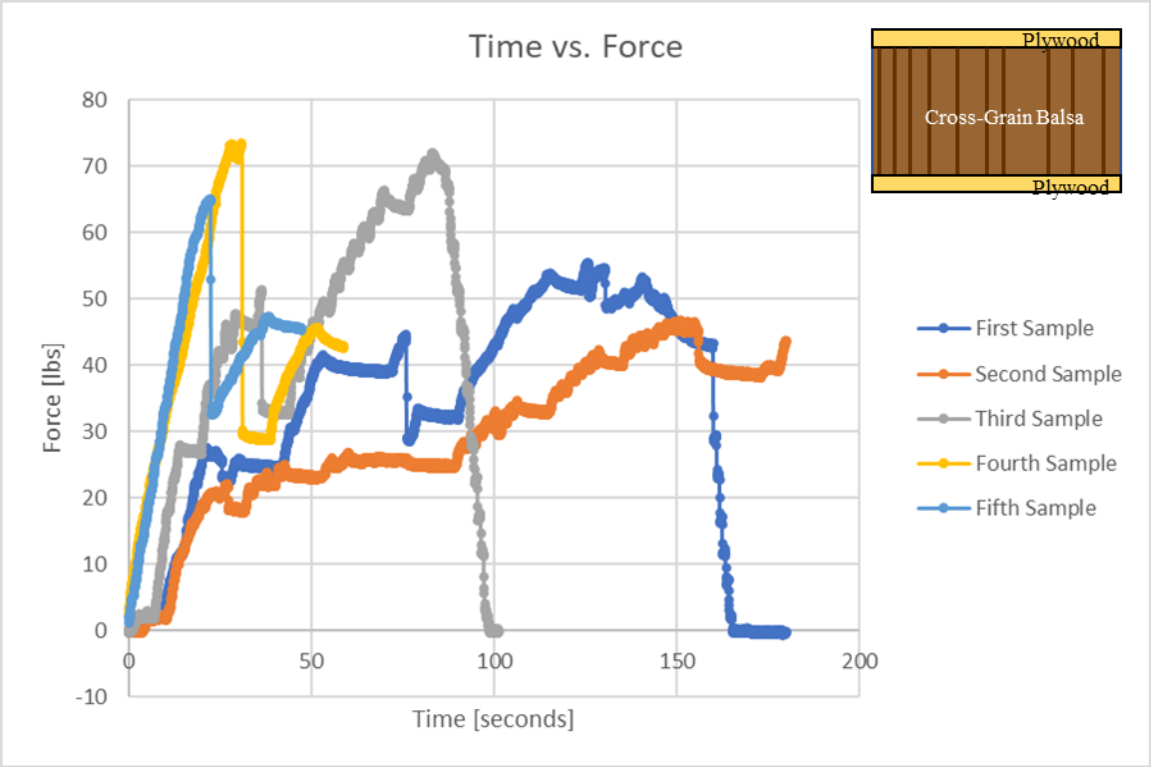

Figure 63: Time vs. Force for first cross-grain shear tests

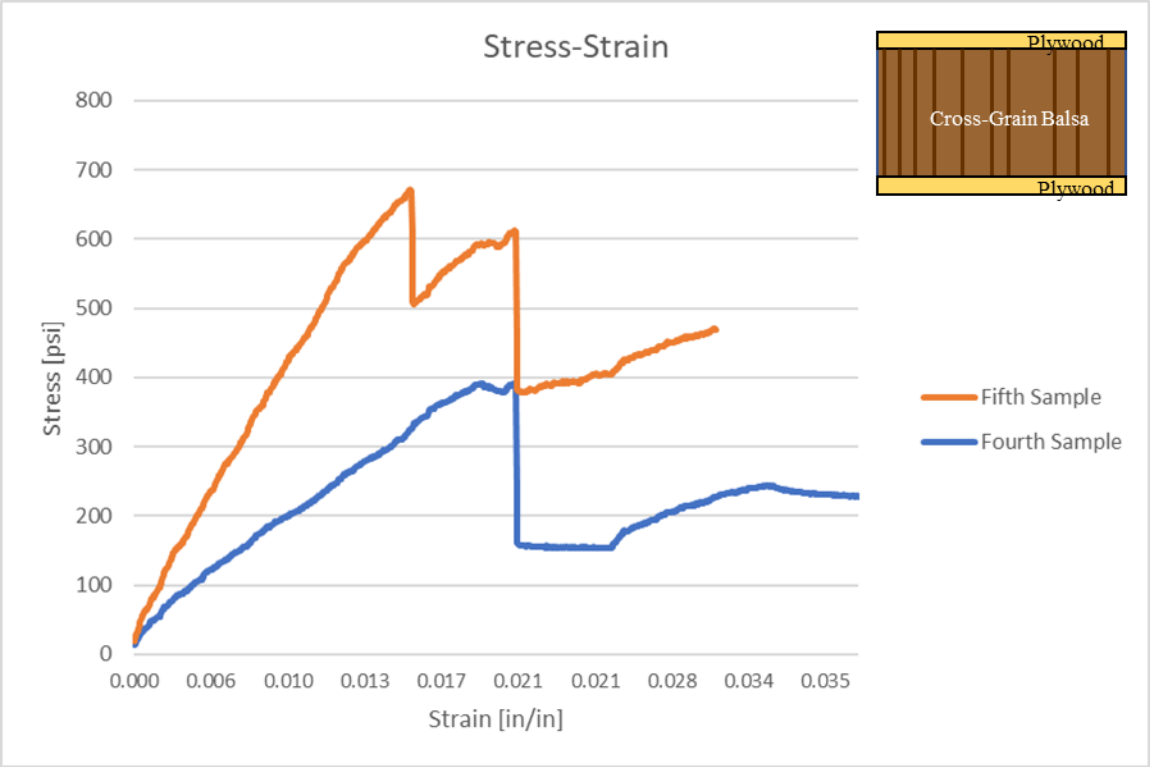

Figure 64: Stress-Strain for first cross-grain shear failure tests

The stress-strain graphs for the two samples with cross-grain balsa and plywood caps are in Figure 64. Two things are instantly noticed in this data. The first is the difference in the maximum stress experienced by the I-beams. The fourth sample shows a maximum stress of about 400 psi and the fifth sample shows a maximum stress of about 675 psi. These differences are attributed to the balsa shear webs. With the diversity in material properties of balsa wood due to the material composition of the wood, a large range of ultimate stresses is expected. It is interesting that the difference between the two samples is over 200 psi. This gives preliminary understanding that a factor of safety needs to be built into the wing spar analysis program to account for the range of material properties in the balsa wood.

The second interesting trend in this data is the increase in the stress after the fracture. Force was applied after the fracture to pronounce the fracture and see how the beam reacted. In the fifth sample, the stress went back to 600-psi, close to the 675-psi breaking stress. The prototype

composite I-beams can handle more stress even after the fracture since the whole shear web has not failed and the I-beam shape stays intact. This gives the preliminary theory that a shear failure in the shear web is not catastrophic. With these results, it is possible that a shear failure in the shear web will not result in ultimate failure of the wing and the aircraft could still fly.

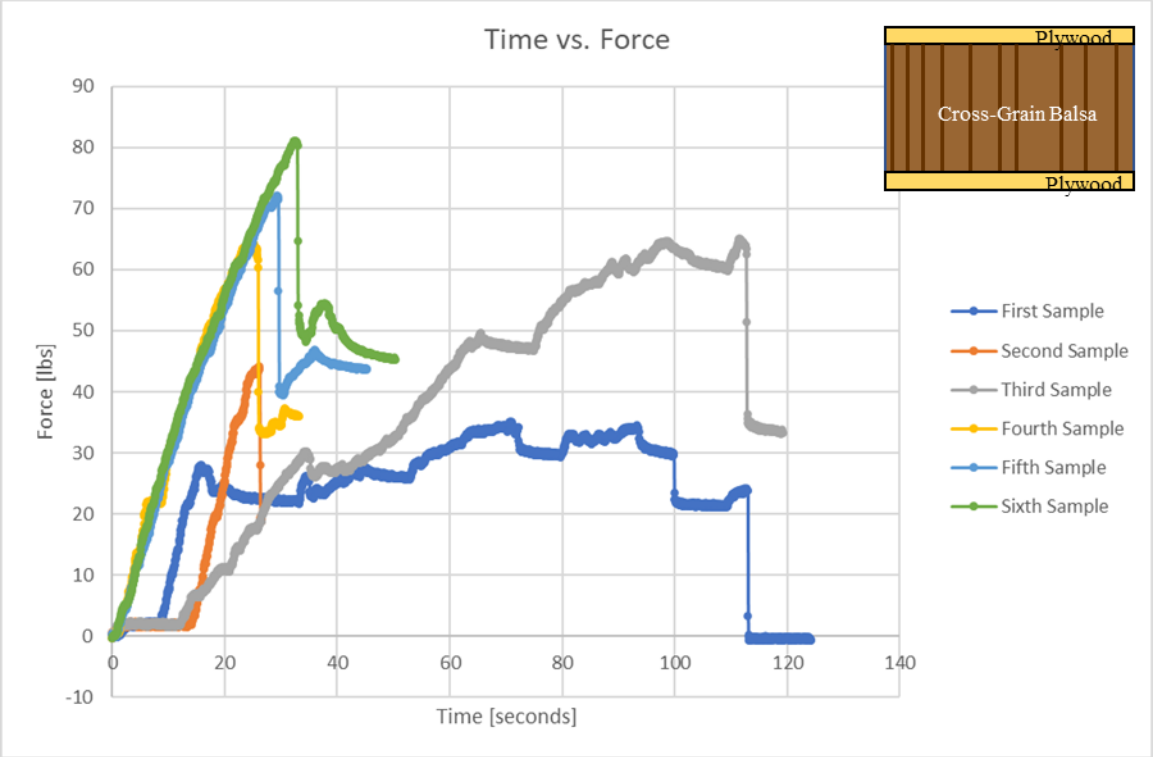

Figure 65: Time vs. Force for second cross-grain shear failure tests

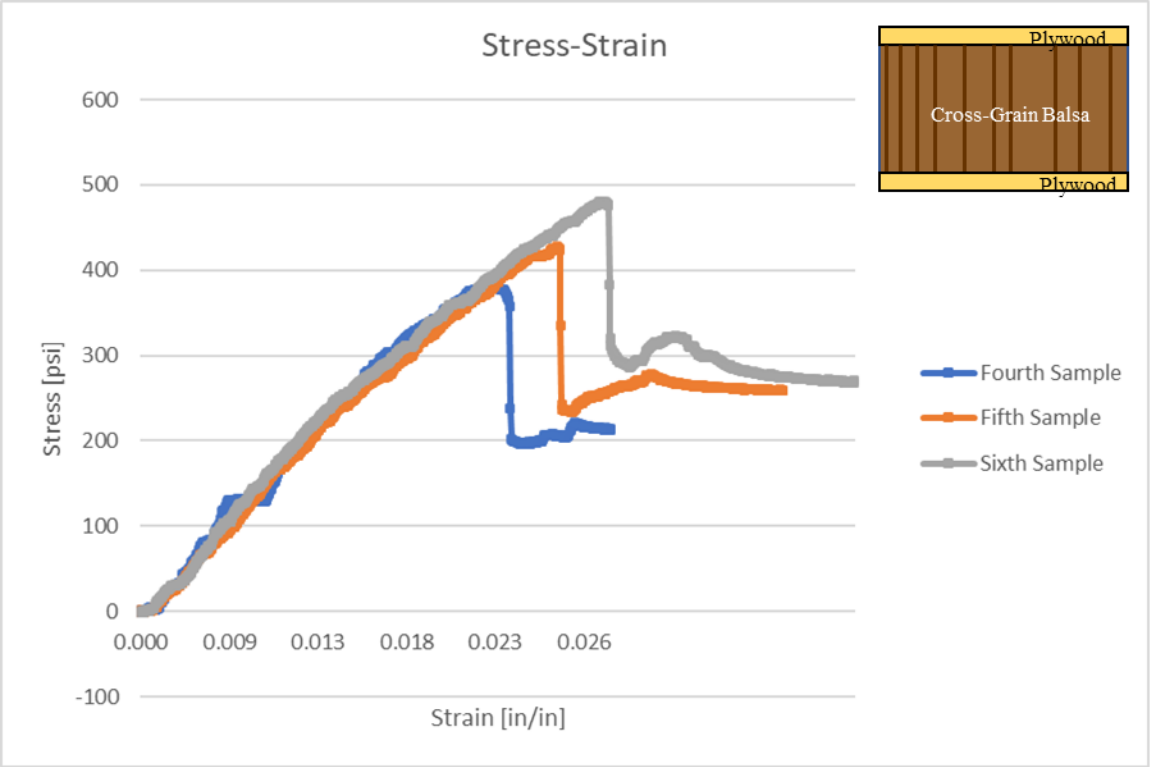

Figure 66: Stress-Strain for second cross-grain shear failure tests

Figure 65 shows the raw data collected by the Vernier Structure and Material Tester for time vs. force and Figure 66 shows the stress-strain graph created from the recorded data. The stress-strain graph shows an interesting step in the maximum stress between the samples. In Figure 66, one will notice slightly different trends in the different samples. In the third sample, the time to fracture force is much longer compared to four other samples. This was done to characterize the fracture modes and get pictures of the sample over the time. Applying force and waiting to make sure no breaking would occur and to get pictures as the test occurred caused the time for this test to be much longer than the rest of the tests. In the fifth sample, the first maxima that occurs at a time of approximately 18 seconds is where the fracture occurs, everything after was applying more load to exaggerate the fracture for taking pictures and to also see if the I-beam could handle more load after the shear web had broken.

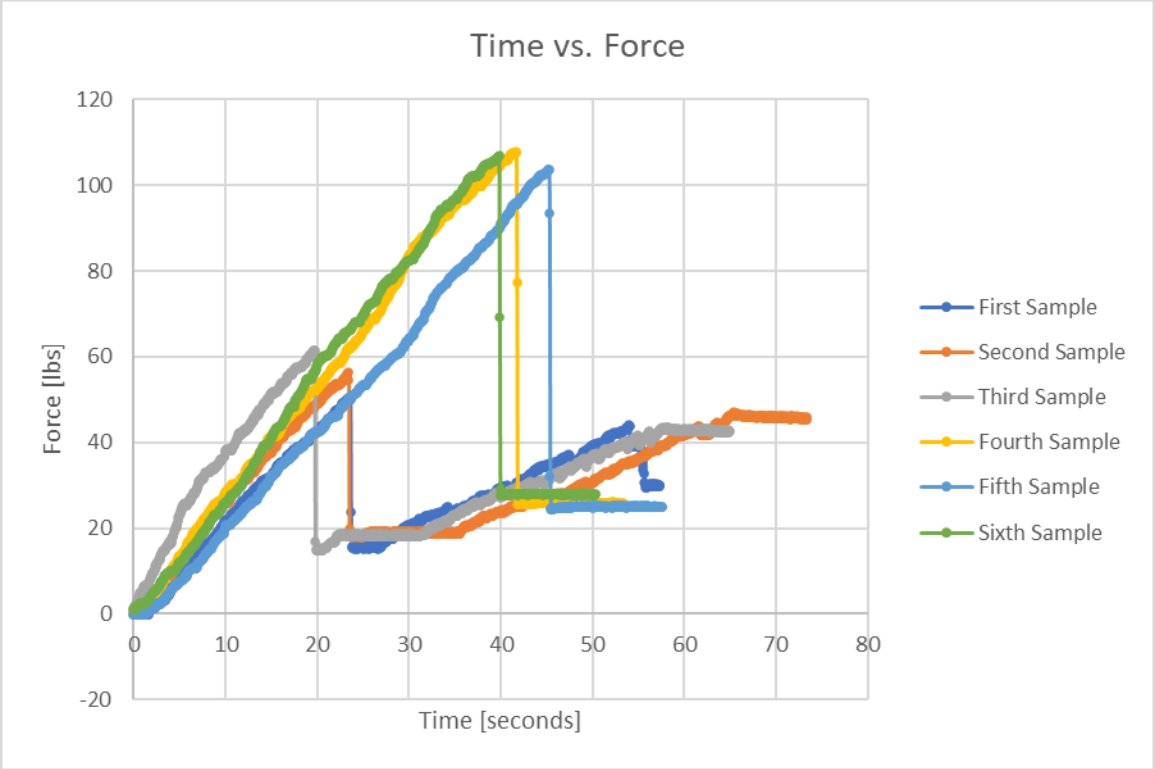

Figure 67: Time vs. Force for third cross-grain shear failure tests

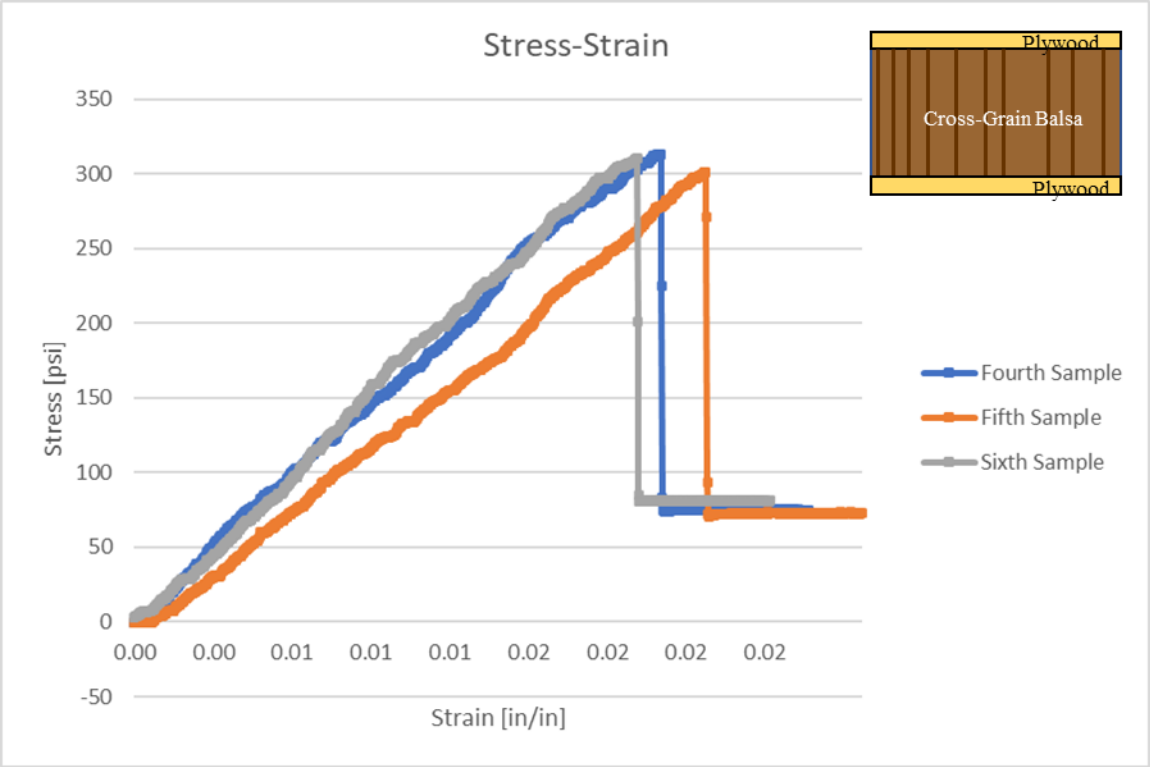

Figure 68: Stress-Strain for third cross-grain shear failure tests

Figure 67 shows the raw data graph of time vs. force for the third cross-grain shear failure tests and Figure 68 shows the stress-strain graph for these samples. The samples tested here have a degree of repeatability. In samples one, two, and three, the displacement values were not taken so a stress-strain graph could not be made. In samples one, two, and three, the samples all fracture at around the same force values and in samples four, five, and six, the samples all fracture at around the same value. This leads to the theory that these tests are repeatable if all of the material is recorded. Using different plywood and balsa wood will cause the breaking stress to be different for each sample.

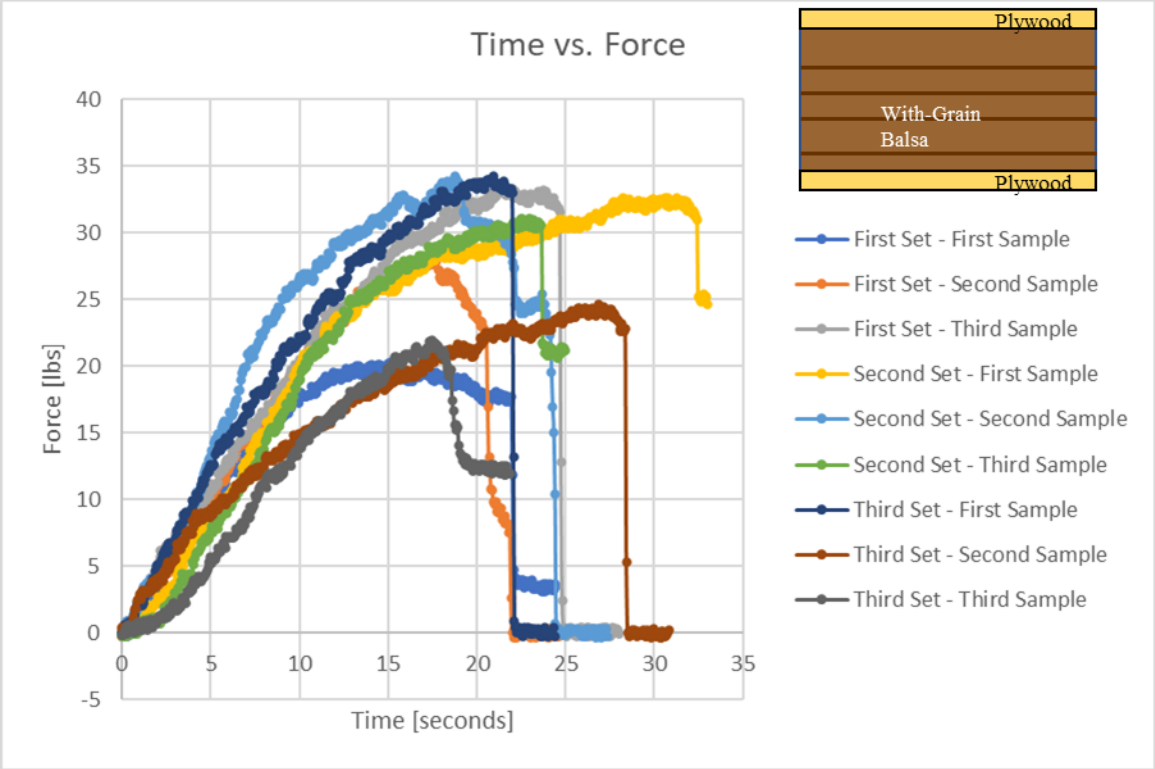

Figure 69: Time vs. Force for with-grain shear failure tests

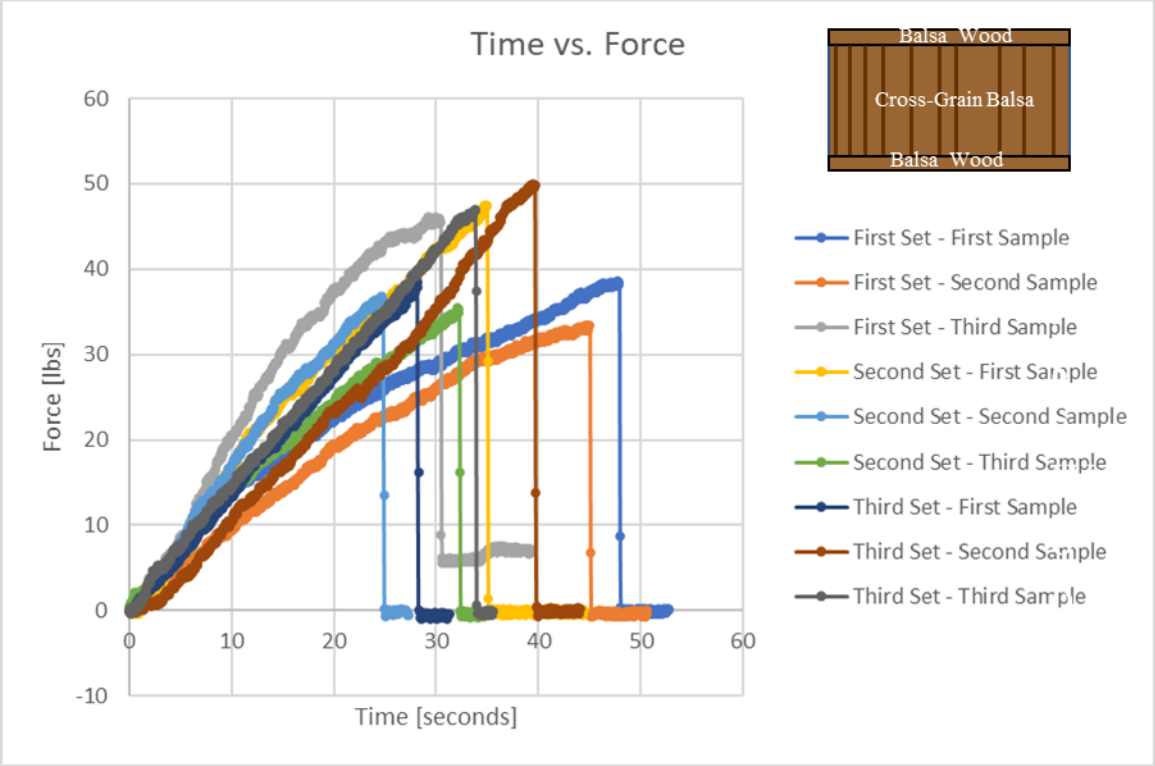

Figure 70: Time vs. Force for tensile failure tests

Figure 69 shows the raw data for time vs. force of the I-beams with plywood caps and a with-grain balsa shear web. The displacement sensor was not functional for these tests so only the raw data could be reported and compared. While this is not desirable, this will still allow the testing to continue as plan because with-grain balsa shear webs are never used in the construction of UAVs. For this reason, a visual understanding was the main goal of these tests. The data is still interesting though. The first set shows an increase in the fracture force with each sample starting at 20 lbs, going to 28 lbs, and then to 33 lbs. The second set shows better grouping with each sample breaking around 32 lbs. The third set does not show good grouping with the first sample breaking at almost 35 lbs, the seconds sample breaking at approximately 25 lbs, and the third sample breaking at approximately 22 lbs.

Figure 70 shows the raw for time vs. force of the I-beams with with-grain balsa wood caps and a cross-grain shear web. Again, the displacement sensor was not functional for these tests but fracture forces and stresses are able to be compare. A visual understanding of the failure mode is also obtained through these tests. In the first set, samples one and two both between 30 and 40 lbs, but the third sample breaks at approximately 45 lbs. In the second set, samples two and three both break around 35 lbs, but the first sample breaks at around 48 lbs. In the third set, samples two and three break at around 50 lbs, but the first sample breaks at approximately 40 lbs. It is interesting that every set of I-beams has one outlier in the fracture force. This is theorized to be due to the compounding imperfections in the balsa wood. Using balsa wood with different grain direction in the caps and shear increases the probability of imperfection in the material.

The other takeaway from the prototype I-beam testing is to get initial validation of the Wing Spar Analysis Program. When the geometry and material properties are applied to the code, the force that causes failure can be found for the various samples. The geometry of the 27 samples was input into the Wing Spar Analysis Program and the expected failure load was found. Table 3 and Table 4 show the experimental stress, expected stress, and percent different of prototype composite I-beam tests to allow for comparison between test samples.

Table 3: Prototype I-beam results for shear failure

Geometry	Test Specimen	Density [lb/ft^3]	Shear Stress [psi]	Expected Shear Stress [psi]	Percent Diference [%]
Shear Web: 0.125" x 0.5"	1	N/A	309	350	11.7
Caps: 0.125" x 0.5" plywood	2	N/A	322	350	8.0
5" long cross-grain	3	N/A	350	350	0.0
	4	N/A	504	350	44.0
	5	N/A	446	350	27.4
Shear Web: 0.125" x 0.35"	1	N/A	236	350	32.6
Caps: 0.125" x 0.5"	2	N/A	333	350	4.9
5" long cross-grain	3	N/A	263	350	24.9
	4	N/A	563	350	60.9
	5	N/A	631	350	80.3
	6	N/A	709	350	102.6
Shear Web: 0.125" x 0.75"	1	N/A	256	350	26.9
Caps: 0.125" x 1"	2	N/A	286	350	18.3
7" long cross-grain	3	N/A	312	350	10.9
	4	N/A	520	350	48.6
	5	N/A	501	350	43.1
	6	N/A	516	350	47.4
Shear Web: 0.125" x 0.5"	1	N/A	139	215	35.3
Caps: 0.125" x 0.5" plywood	2	N/A	193	215	10.2
5" long with-grain	3	N/A	230	215	7.0
Shear Web: 0.125" x 0.35"	1	N/A	285	215	32.6
Caps: 0.125" x 0.5"	2	N/A	299	215	39.1
5" long with grain	3	N/A	327	215	52.1
Shear Web: 0.125" x 0.75"	1	N/A	174	215	19.1
Caps: 0.125" x 1"	2	N/A	125	215	41.9
7" long with-grain	3	N/A	111	215	48.4

Figures 71 and 72 give visual representations of the table showing the stress values found from the various geometry cases with the expected failure stress represented by the horizontal red line.

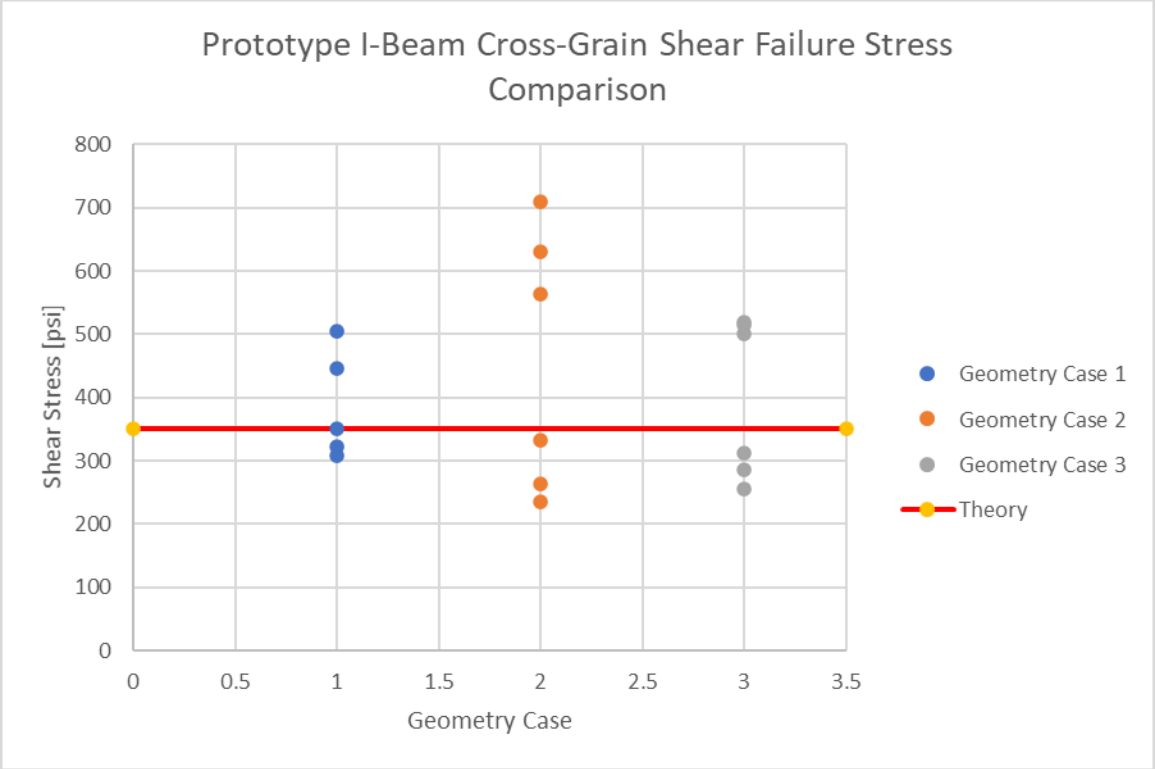

Figure 71: Prototype I-beam cross-grain shear failure stress comparison

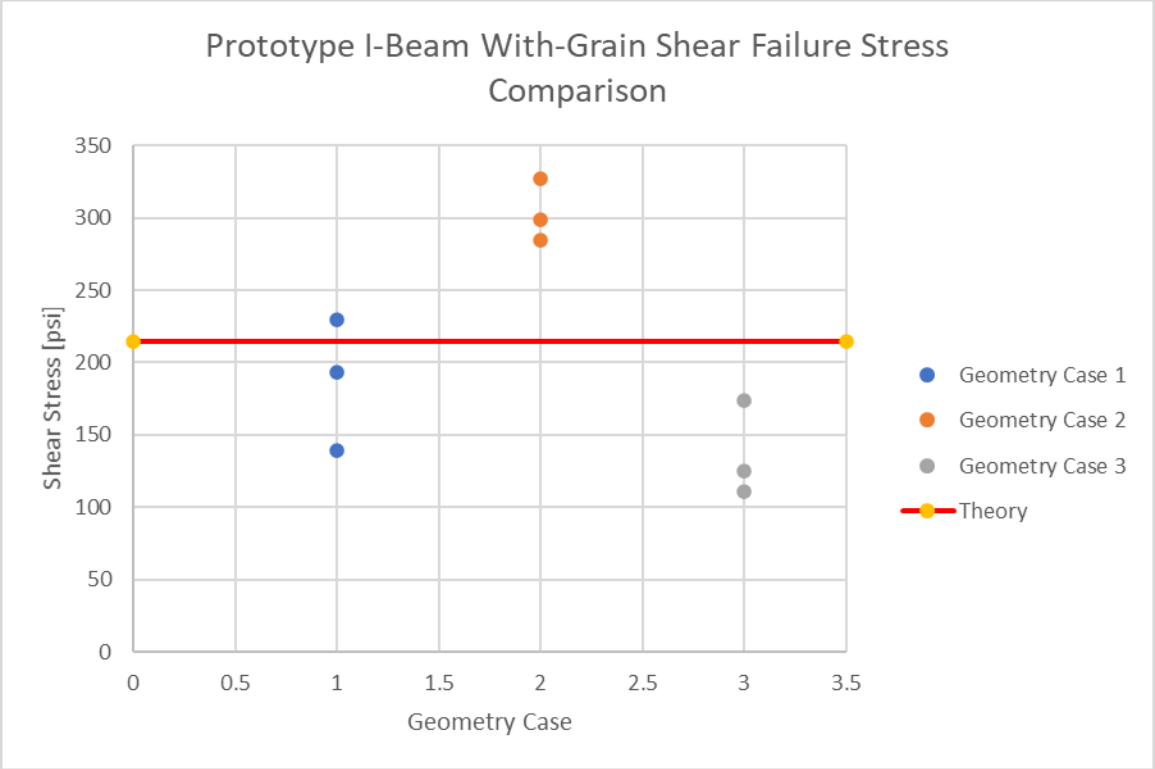

Figure 72: Prototype I-beam with-grain shear failure stress comparison

The first noticeable error in this analysis was not taking the density of the material. These tests were performed immediately after the tensile and shear testing of the balsa wood before a firm understanding of the relationship between density and strength was determined. Moving forward into composite I-beam testing with carbon and balsa, the density of the balsa shear webs will be recording. To move through this, the average value for ultimate shear stress of cross-grain balsa was found. While this is not a perfect solution, it does well for this application.

The results comparing the expected stress calculated from the Wing Spar Analysis Program and the max shear stress found through the tests give slight confidence in the Wing Spar Analysis Program for future use. To begin, a statistical analysis was performed to determine the standard deviation, confidence interval at 95%, and the root mean square (RMS) error. The following table shows the values found for this data for both cross-grain and with-grain shear failure.

Table 4: Statistical analysis of cross-grain shear failure data

Standard Deviation	140.4
Confidence Interval	66.7
RMS Error	154.0

Table 5: Statistical analysis of with-grain shear failure data

Standard Deviation	75.5
Confidence Interval	49.3
RMS Error	75.7

The positive trend in this data comes from looking at the percent different for the test samples between the Expected Shear Stress found from the Wing Spar Analysis Program and the shear stress that comes from the tests performed. The percent difference does have a large range from 0.0% - 102.6%, but this considers the extreme outliers in the data. If the three extrema points are taken out of the data, the range is from 0.0 % to 52.1%. With the extrema considers, this is an average percent difference of 33.8%. With these shear failure composite I-beams made from non-homogenous materials, the non-homogeneity effects are compounded. Large ranges in material properties as well as imperfections in the material become more probable and apparent when using two non-homogenous materials in a single composite I-beam. This leads to higher values in percent difference and the statistical analysis for this I-beam configuration. Future testing will use materials that are more understood and lower percent difference and statistical values are expected.

The same analysis performed in the shear failure composite prototype I-beams was performed with the tensile failure composite I-beams. The expected stress from the Wing Spar Analysis Program was compared with the experimental stress values found through testing. Table 6 and Figure 73 show the calculated versus experimental stress comparison for the tensile.

Table 6: Prototype I-beam results for tensile failure

Geometry	Test Specimen	Density [lb/ft^3]	Stress [psi]	Expected Stress [psi]	Percent Difference [%]
Shear Web: 0.125" x 1" balsa	1	Caps: 13.175 Shear Web: 12.920	217.8	260	16.2
Caps: 0.125" x 1" balsa	2	Caps: 13.175 Shear Web: 12.920	188.7	260	27.4
5" long cross-grain	3	Caps: 13.175 Shear Web: 12.920	409.6	260	57.5
Shear Web: 0.125" x 1.0" balsa	1	Caps: 13.238 Shear Web: 8.572	632.24	260	143.2
Caps: 0.125" x 1.0" balsa	2	Caps: 13.238 Shear Web: 8.572	498.82	260	91.9
7.5" long cross-grain	3	Caps: 13.238 Shear Web: 8.572	471.18	260	81.2
Shear Web: 0.25" x 1" balsa	1	Caps: 12.698 Shear Web: 13.016	310.6	260	19.5
Caps: 0.125" x 1" balsa	2	Caps: 12.698 Shear Web: 13.016	404.5	260	55.6
5" long cross-grain	3	Caps: 12.698 Shear Web: 13.016	379.7	260	46.1

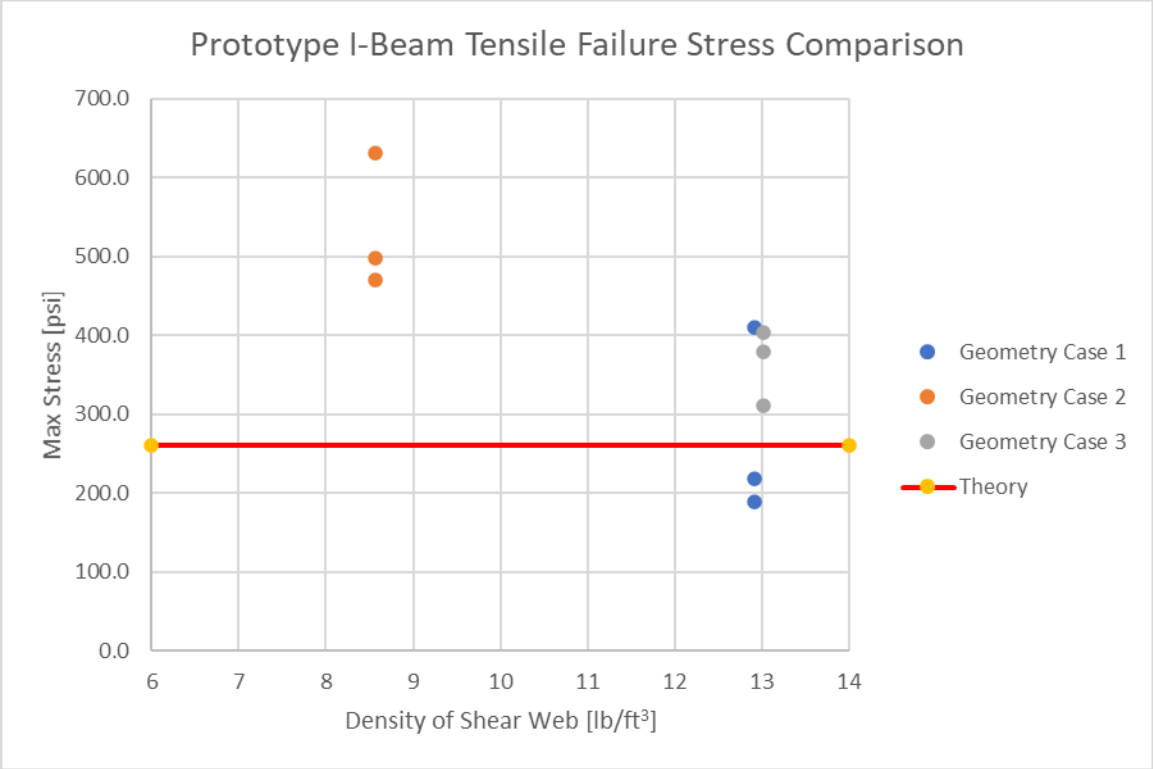

Figure 73: Prototype I-beam tensile failure stress comparison

The results from testing the I-beams designed to fail due to tension is less positive than the results for shear failure. Statistical analysis on the tensile stress was performed to determine the standard deviation, confidence interval at 95%, and the root mean square (RMS) error. The following table shows the results.

Table 7: Statistical analysis for tensile failure data

Standard Deviation	137.3
Confidence Interval	89.7
RMS Error	184.8

The percent difference in the expected stress and the experimental stress shows a large range from 16.2% to 143.3%. What is very interesting about this data though, is that the large percent differences come from the second set of I-beams with 0.125” x 1.0” cross-grain balsa wood shear web that is 7.5” long. The other two I-beam sets show a range of 16.2% to 57.5% which is in line

with the results from the shear failure I-beams. This large range in data is again attributed to the compounding non-homogeneity of balsa wood material properties. Even though an understanding of the material properties is known in regard to the density of the balsa wood, when the whole I-beam is made from balsa wood with different grain directions, these unknowns in the material properties are compounded on themselves. With this uncertainty of material, the percent different still gives reasonable confidence that with different materials and a good understanding of those materials properties, the Wing Spar Analysis Program can be used to analyze wing spars.

Composite I-Beam Testing Introduction

After prototype composite I-beam testing was finished, the next step was to perform three-point bending tests using materials used in UAVs. Composite I-beams made from uni-directional carbon fiber and cross-grain balsa were tested and analyzed to both understand the failure mode of the structure as well as validate the Wing Spar Analysis Program.

Composite I-Beam Experimental Setup

The composite I-beams are made from off-the-shelf unidirectional carbon fiber that has already been cured to keep consistency in material properties and geometry. The material is bought from CST Composites and gives consistent carbon fiber properties across the range of tests. The shear webs are made from cross-grain balsa wood pieces super glued together to create the desired length. Three different sets are made with five test samples in each set. Figure 74 shows the different samples used for this set of tests.

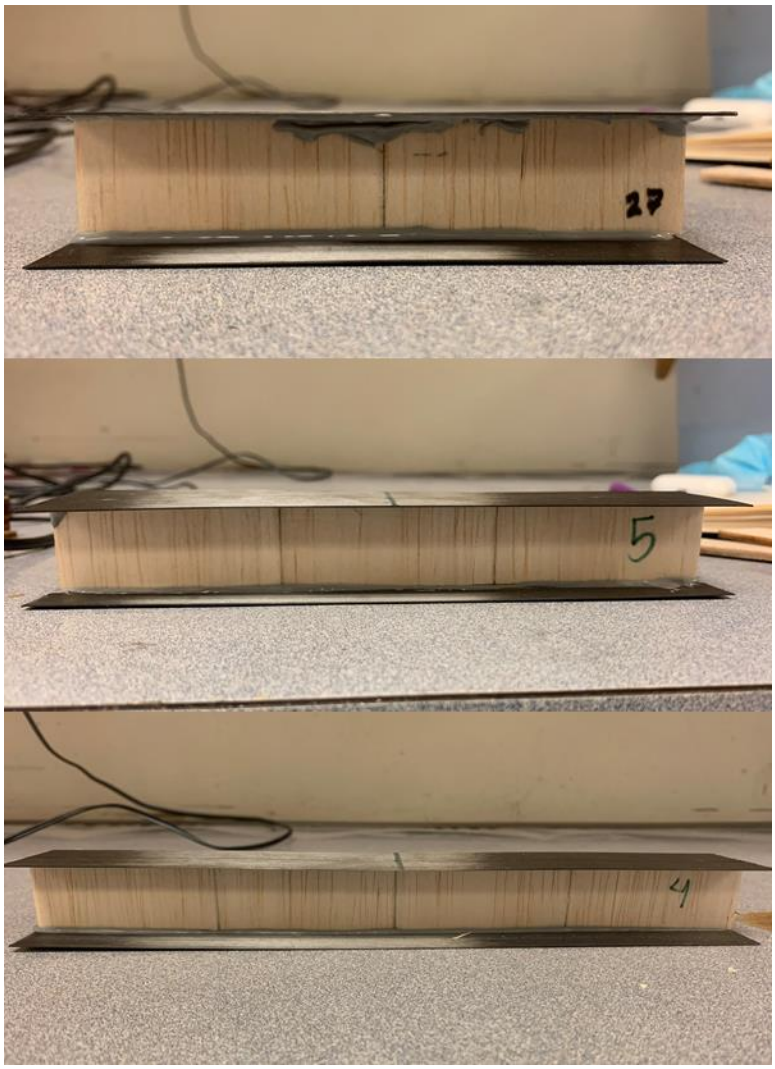

Figure 74: I-beams with carbon fiber caps and cross-grain balsa wood shear webs

The first set is made with unidirectional carbon fiber that is 0.020” thick, 1.56” inches wide, and 5.0” long. The balsa shear webs are made from balsa wood that is 0.125” thick, 1” tall, and 5.0” long. The second set is made from the same materials with the length changing to 7.5” long and the third set is made from the same materials with the length changing to 10.0” long.

To manufacture the I-beams, the unidirectional carbon fiber is cut into the desired length using a bandsaw and the cross-grain balsa wood is laser cut to 2.5” long segments. The balsa wood and carbon fiber are then sanded to get rid of the charred wood edges on the balsa wood and to give

a better bonding surface on the carbon fiber. The balsa wood is super-glued together and allowed to cure before bonding to the carbon fiber. Once the balsa wood is cured, LORD 320/322 Epoxy Adhesive is applied to the carbon fiber and a 3D-printed jig is placed for each 2.5" segment of balsa wood. The balsa wood is placed in the jig and pressure is applied to set the balsa wood to the carbon fiber. This is then set aside to cure for 6-8 hours to get the epoxy to handling time. Once cured, the jigs are removed and Lord 320/322 Epoxy Adhesive is applied to the other piece of carbon fiber. The jigs are placed onto the other piece of carbon fiber and the I-beam is placed together and set aside to cure for 24 hours to allow for full cure. The whole manufacturing process for one I-beam is approximately 30 hours, but the I-beams can be manufactured in large batches to have all samples ready to test in approximately a day and a half.

Figure 75: Composite I-beam manufacturing with 3D-printed jigs

The three-point bending tests are performed with the same Vernier Structure and Materials Tester with the same software and with the same methods as the prototype I-beam tests. The

improved data collection software was used to get both force and displacement measurements so the data could be manipulated to give stress and strain.

Composite I-Beam Experimental Methodology

The experimental methodology is as follows:

- Design I-beam components using Solidworks
- Cut out I-beam components using laser cutter
- Construct I-beam using given materials
- Mount I-beams to the Vernier Structure and Material Tester
    - Mark the center line longitudinally and laterally to allow for proper mounting
    - Allow for 1.00” space for I-beam to rest on support beams
    - Place the U-bolt in the center of the I-beam
- Plug Vernier Structure and Material Tester DAQ into computer with installed LabQuest 3 software and make sure it is reading data
    - Be sure to use “vstm_basic” file to record both Force and Displacement measurements
- Apply force until the force goes slightly positive then de-load slightly and zero the measurements
- Begin recording data
- Slowly turn the lever to apply load
- Once failure occurs, stop the data recording and de-load the Vernier Structure and Materials
    - For testing shear failure in cross-grain balsa wood shear webs, failure will appear as small cracks laterally in the shear web.

    - For shear failure in with-grain balsa wood shear webs, failure will appear as a long crack that propagates longitudinally down the I-beam. This will be a complete failure of the I-beam.
- Save data and export to a file that can be analyzed in Microsoft Excel
    - Save as a ".gmbl" file for the LabQuest 3 software
    - Export as a ".txt" file for analysis in Microsoft Excel
- This process is repeated for all of the samples

Composite I-Beam Results

The composite I-beams results are split into two sections; one visually inspecting the I-beams to physically understand what a shear failure looks like in the composite I-beam. This is done by looking at pictures taken with a high-power microscope and by analyzing the break with a high-speed camera.

The composite I-beams will then be analyzed using the data obtained from the Vernier Structure and Material tester. This data will be converted to give stress-strain graphs and the shear stress values found through experimentation will be compared to the calculated values from the Wing Spar Analysis Program.

Visual Analysis of Composite I-Beam Failure

The results for the composite I-beams are most important for both visually understanding how aircraft shear webs will fail and for validating the Wing Spar Analysis Program. First, the failures will be shown to get a visual understanding of what is happening. Figures 76 through 78 show the different failures in the composite I-beams.

Figure 76: 5" Composite I-Beam Failure

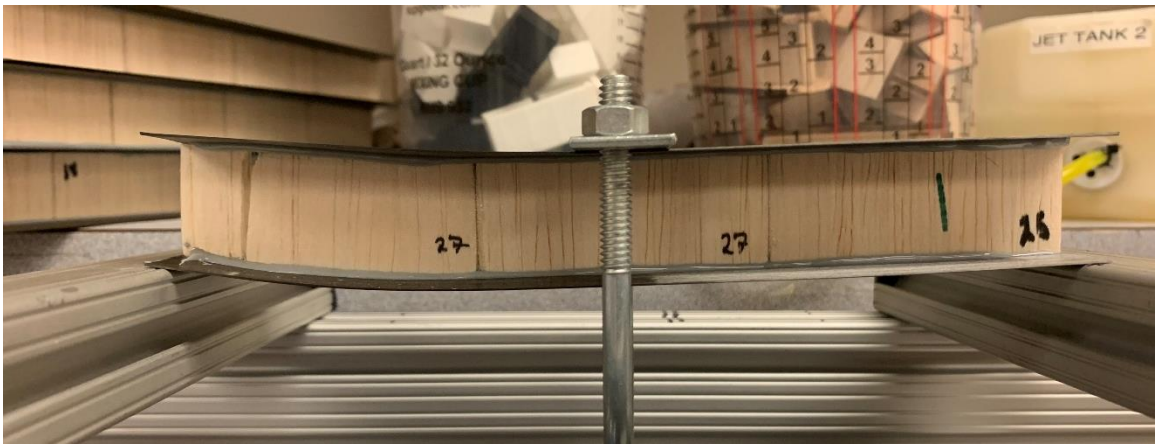

Figure 77: 7.5" Composite I-Beam Failure

Figure 78: 10" Composite I-Beam Failure

The vertical crack off-center occurs in every sample, but the side of the I-beam that the crack occurs on does vary from sample to sample. The other failure to notice is the failure in the epoxy bonding the balsa wood shear web to the carbon fiber caps. This is especially noticeable in the 10” I-Beam where one can see epoxy failure in both the bond between the bottom cap and balsa wood on the right side of the vertical crack and the bond between the top cap and the balsa wood on the left side of the vertical crack.

This failure mode was noticed in the prototype composite I-beams but was thought to be caused by the low strength of the super glue bond between the caps and shear web. Since this is has been found in the composite I-beams using high strength epoxy, investigations were done to see if the balsa-wood shear is failing first and causing the failure in the epoxy or if the epoxy is failing first and causing the failure in the balsa wood. Using a high-speed camera, footage was taken at 480 fps (frames per second) and analyzed frame by frame to see what section is failing first.

Based off the video footage, it appears that that failure in the balsa wood occurs first then causes the failures in the epoxy bond. This occurs very quickly; as soon as the crack begins to happen in the balsa wood shear web, the epoxy fails right after. Without using high-speed footage, this would not be seen. This leads to a new cause of concern. In the prototype I-beams, it was believed that once the shear web fails, the I-beam would not completely fail. With the near simultaneous failure of the shear web and epoxy bond, the I-beam can never reach loads that were achieved prior to the failure. If a shear failure occurs in flight, this would catastrophic for the aircraft.

After testing, the I-beams were inspected by looking at the failures and placing the fracture areas under a microscope to see what the failure looks like on a cellular level. Previously stated, one can see a combination fracture where the balsa shear web creates a vertical crack due to the

shear loading of the material and causes a delamination failure in the epoxy bond between the balsa wood shear web and the carbon fiber caps. After inspecting the test samples, the distance that the epoxy failure travels are directly related to the length of the beam. With the shorter 5” beam length, the failure in the epoxy does not travel away from the crack as far as the longer beams. The 5” beam shows the shortest epoxy delamination, shown in Figure 79, and the 10” beam shows the long epoxy delamination, shown in Figure 80.

Figure 79: Inspection of Failure in 5" I-Beam

When looking at Figure 79, you can see a crack along the bottom edge of the balsa shear web to the right of the crack. This is the start of the balsa pulling itself away from the epoxy, causing the failure along the bond. In Figure 79, you can also see the full failure of the balsa and epoxy bond in the top side.

Figure 80: Inspection of Failure in 10" I-Beam

When looking at Figure 80, you can see what the complete failure looks like between the balsa wood shear web and the epoxy. There is a noticeable gap between the failure of the balsa wood and the carbon fiber cap.

After visually inspecting the samples, some of the samples were broken down to inspect the balsa wood failure under a microscope. This is a way to see if there is a relationship between the localized cellular makeup of the balsa wood at the fracture location. The question raised is whether there is a large sap channel at the failure location that causes the balsa wood to fail in this specific location compared to a different location along the length of the beam.

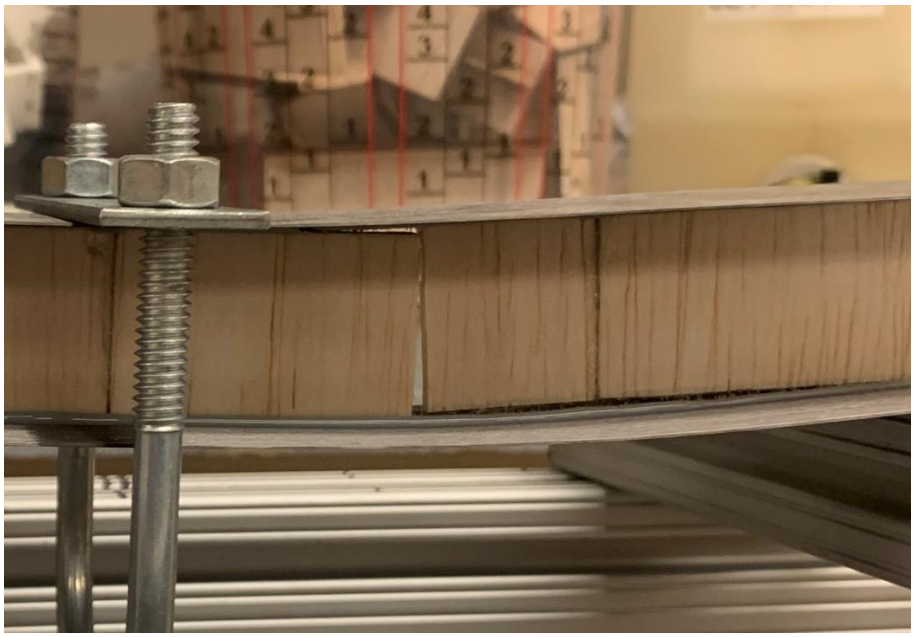

Figure 81: Failure of 10" - Sample 3 Composite I-Beam

Figure 82: View of 10" - Sample 3 I-Beam Failure Under Microscope

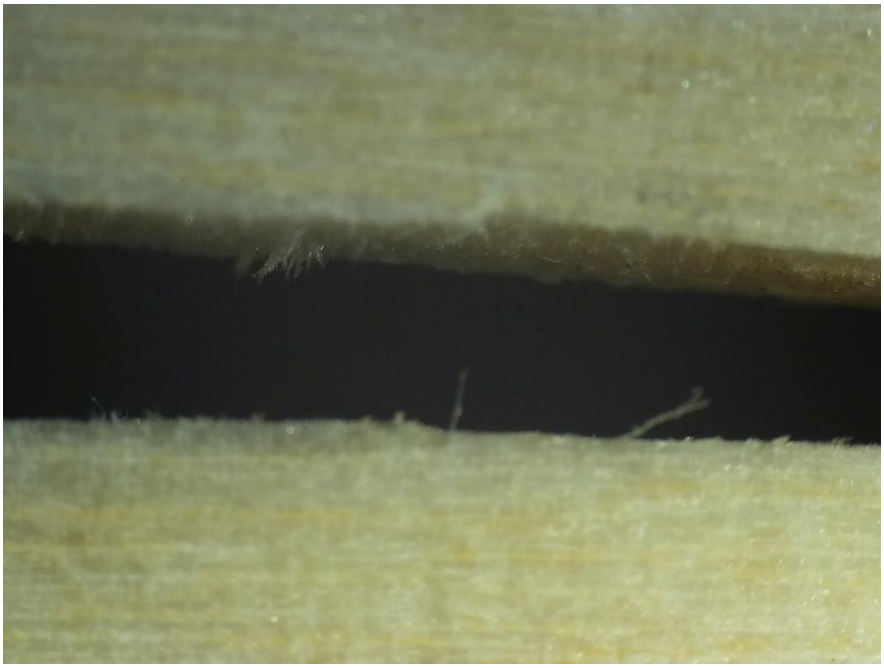

Figure 83: View of 10" - Sample 3 I-Beam Failure Under Microscope with Crack Expanded

These images, taken with an Opti-Tek Scope Model OT-S7, show the vertical crack produced from the shear load in Sample 3 of the 10” Composite I-Beam shown in Figure 74. This appears to be a clean break, but to get an even better understanding of the failure mode, the cellular make-up of the balsa wood along the crack needs to be inspected. By cutting the carbon fiber caps at the failure location, we can analyze the crack under the microscope.

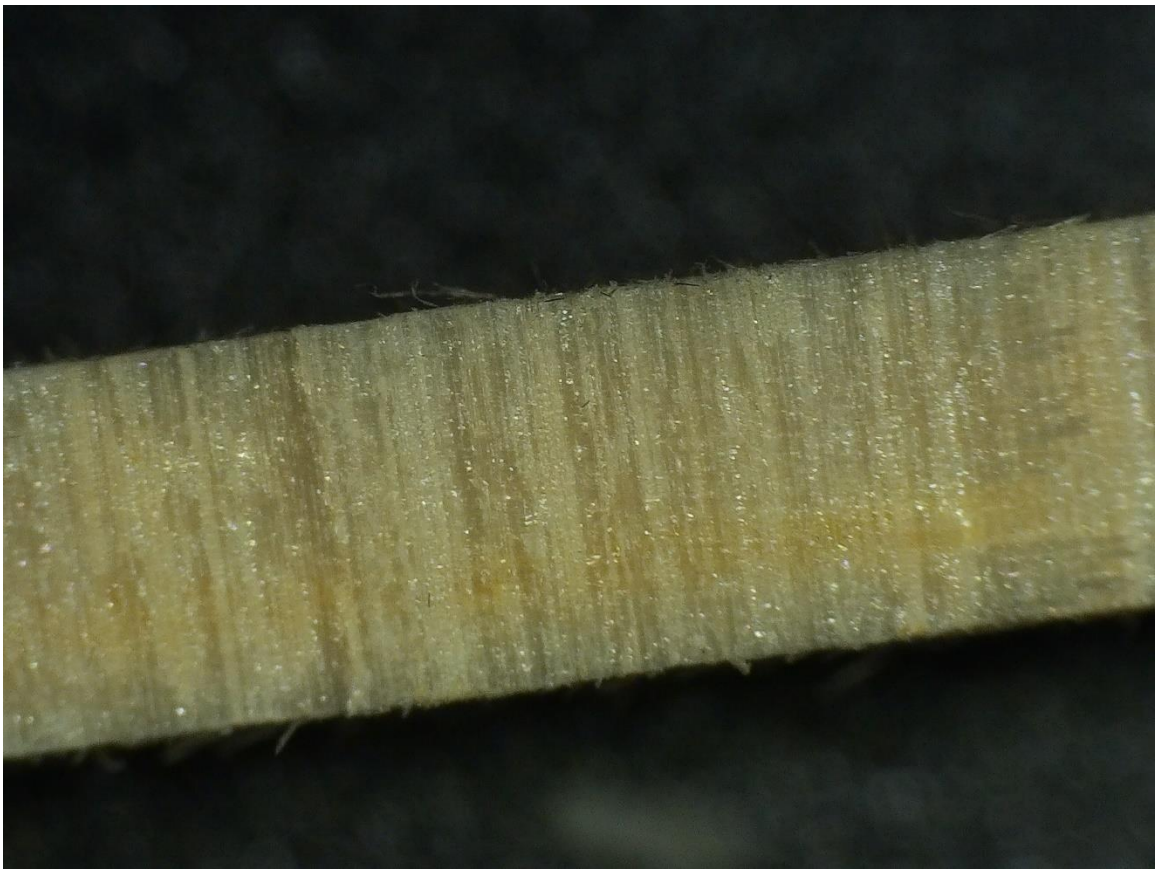

Figure 84: Sample 3 - 10" I-Beam Right Side Failure

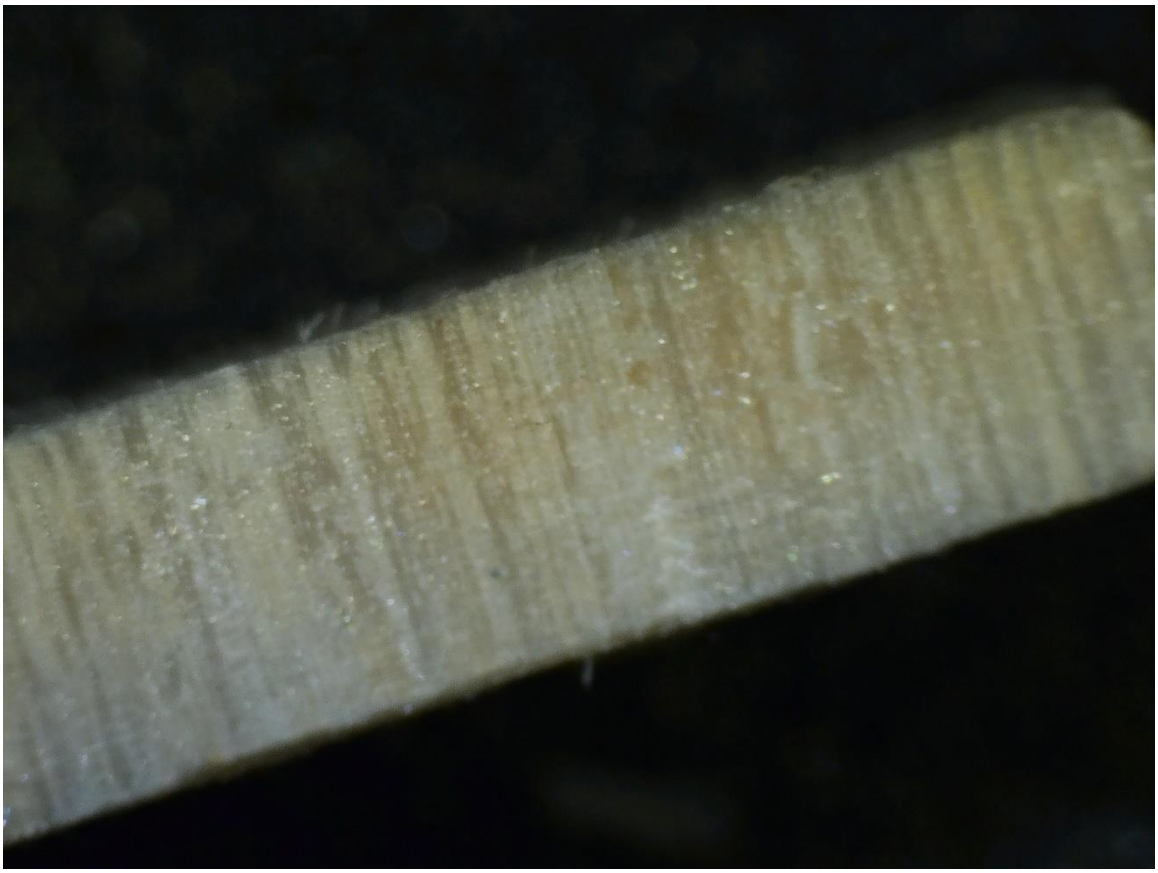

Figure 85: Sample 3 - 10" I-Beam Right Side Failure

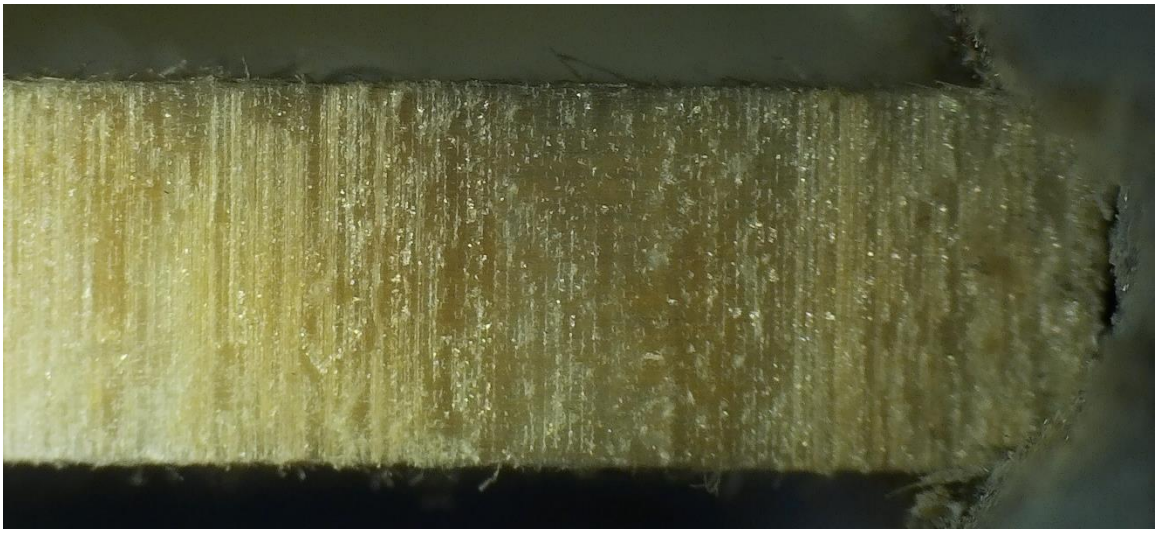

Figure 86: Sample 3 - 10" I-Beam Left Side Failure

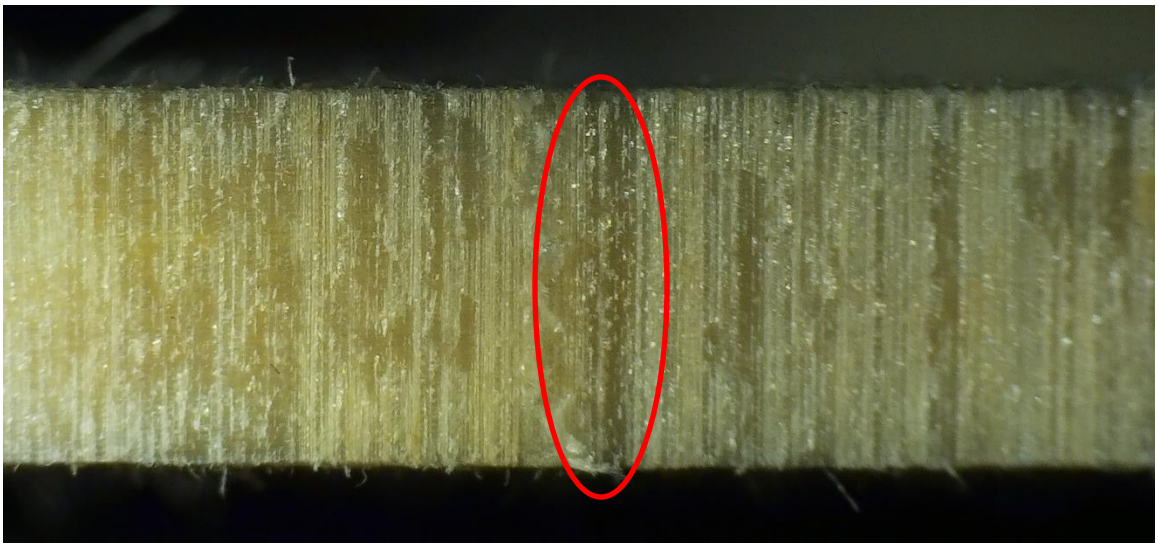

Figure 87: Sample 3 - 10" I-Beam Left Side Failure

When looking directly at the crack in the balsa wood under the microscope, one can see variation in the wood structure through the varying dark and light spots in the wood. These dark and light spots are noticed over multiple sample failures. It is believed that the varying dark and light spots are weak points in the balsa. When looking at Figure 86, a large dark spot is found near the bond between the balsa and the carbon fiber. Another dark spot is found in Figure 87 that appears to be darker than spots along the failure. Another interesting observation is that these varying dark and light spots are only noticed on the right side of the crack, on the left side, the material is more uniform in color. Using high-powered imaging tools would give a better understanding of this material. In the future, being able to acquire tools that could give more detailed visualization of the failure would clarify this material composition and non-homogeneity.

Numerical Analysis of Composite I-beams

From the raw data of force, time, and displacement, graphs for time vs. force and stress-strain were made. Figures 88 through 93 show the graphs for 5-inch, 7.5-inch, and 10-inch composite I-beams plotted together:

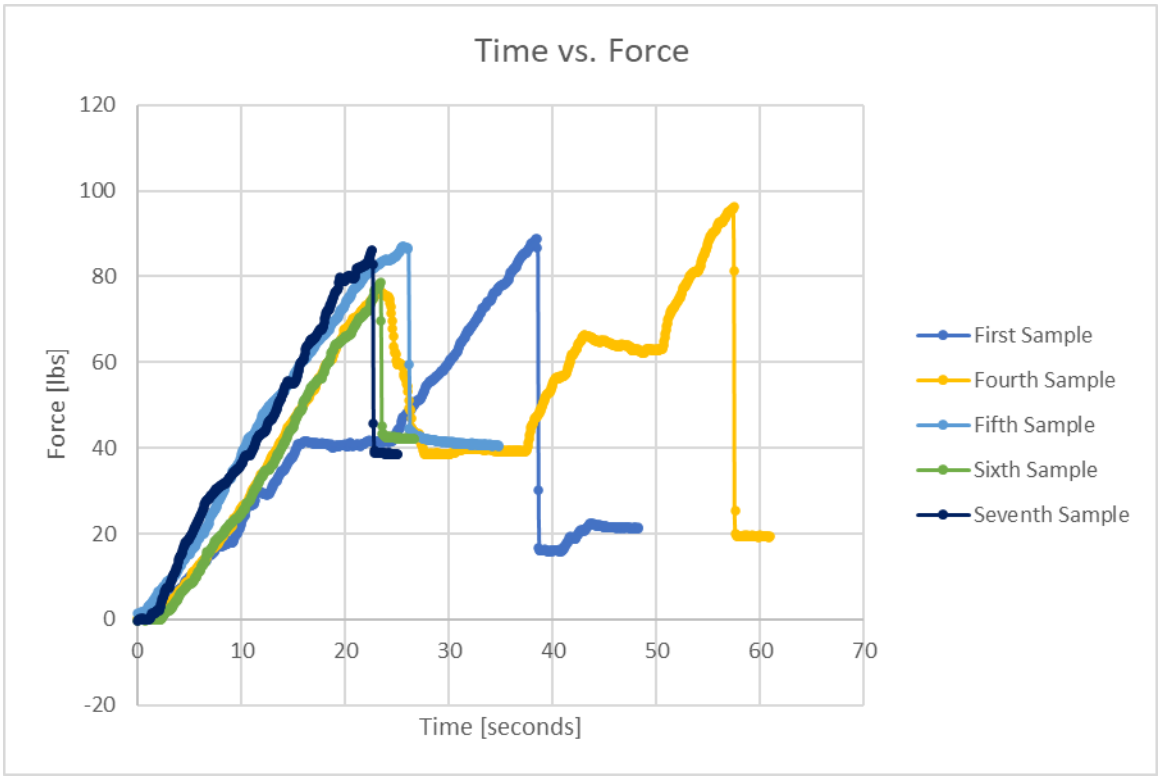

Figure 88: Time vs. Force for 5" Composite I-Beams

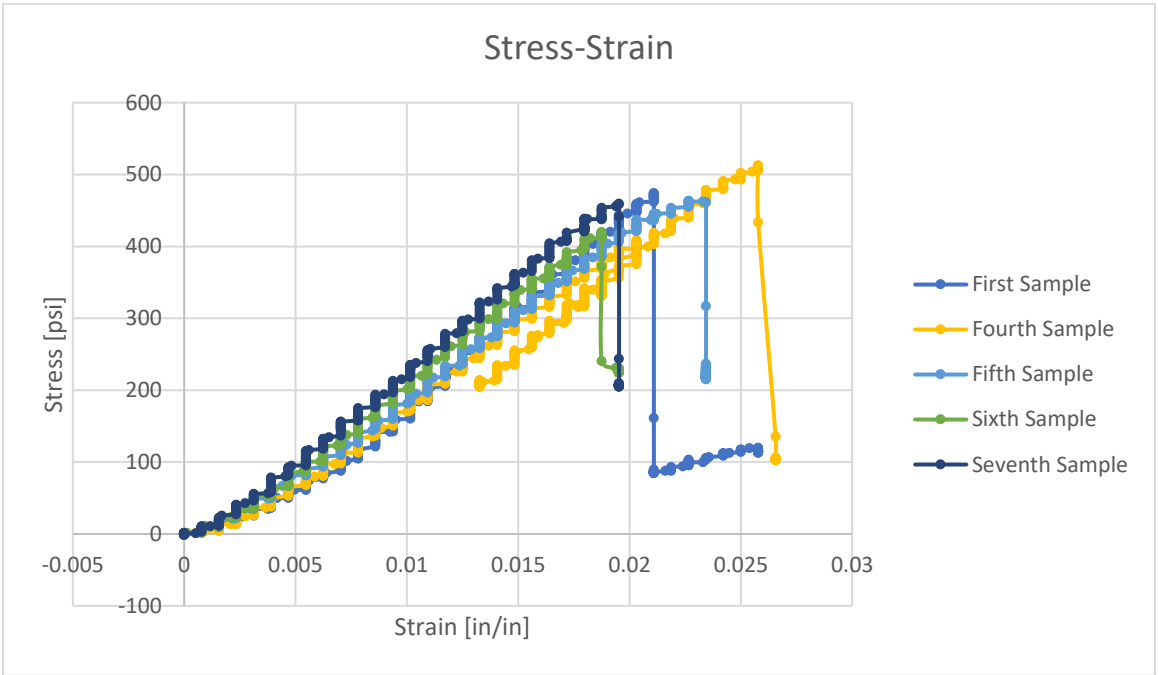

Figure 89: Stress-Strain for 5" Composite I-Beams

Figures 88 and 89 show the graphs for the 5”-long composite I-beams using unidirectional carbon fiber caps with cross-grain balsa shear webs. When looking at the time vs. force graphs, one can see that fracture force for all the I-beams are approximately the same value with one sample almost reaching 100 lbs. One trend that needs to be explained is why the times to fracture are so different. Due to the Vernier Structure and Material Tester being driven by user input, the time duration varies. The force vs. time graphs is a visual representation of the raw data for the tests. Because of this, the stress-strain graphs are better to compare across samples. All the values for stress are approximately the same value showing repeatability between the samples. One trend that is noticeable is in the fourth sample when the stress goes up and then dips back down. This is due to the testing environment where undergraduate and graduate students work. During the test, a student bumped into the sample causing this strange trend. It did not affect the test sample and the test was performed to completion.

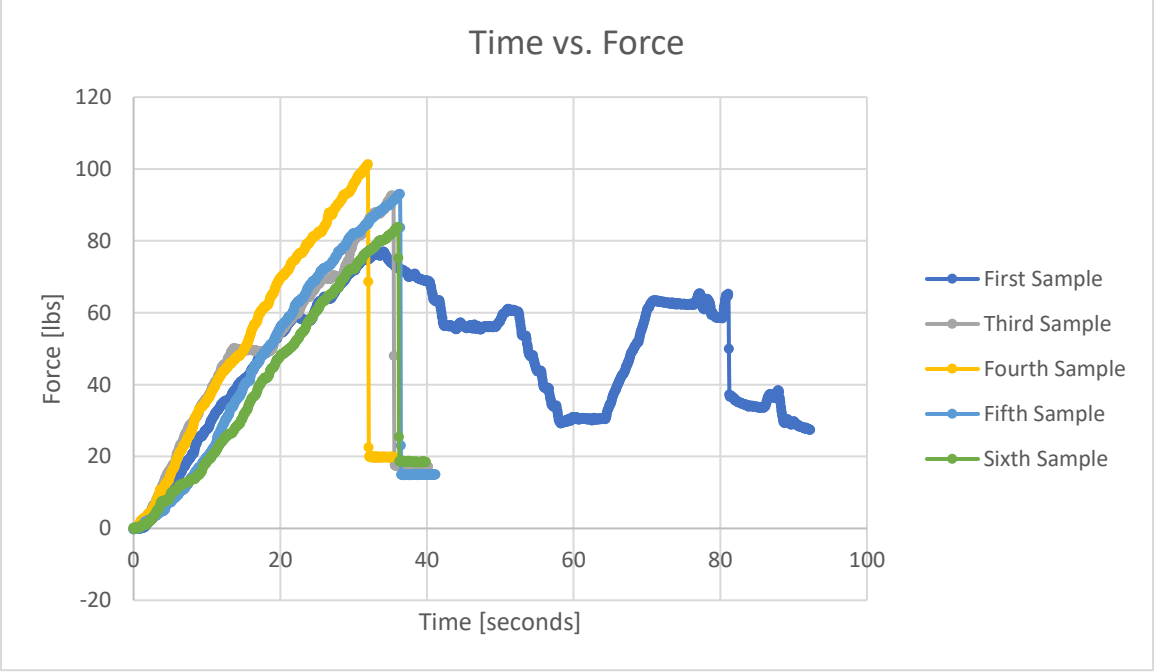

Figure 90: Time vs. Force for 7.5" Composite I-Beams

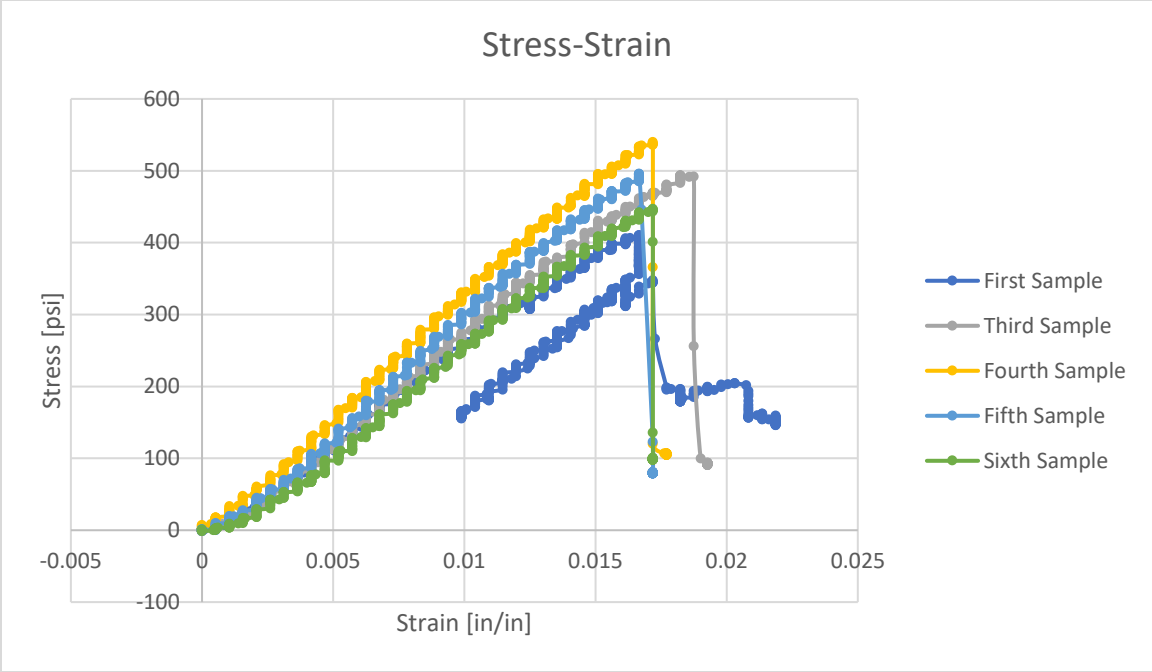

Figure 91: Stress-Strain for 7.5" Composite I-Beams

Figures 90 and 91 show the graphs for the 7.5”-long composite I-beams using unidirectional carbon fiber caps with cross-grain balsa shear webs. When looking at the time vs. force graphs, one can see that fracture force for all the I-beams are approximately the same value at in a range of 90-100 lbs. In the first sample, one can see a trend where the force increases and decreases across the time. The fracture occurs at the first maxima in the graph, the increase in force is due to experimenting with the sample to exaggerate the fracture for visual analysis. The force vs. time graphs is a visual representation of the raw data for the tests. Because of this, the stress-strain graphs are better to compare across samples. All the values for stress are approximately the same value showing repeatability between the samples. One trend that is noticeable is in the fifth sample when the stress goes up and then dips back. This is due to was discussed before in the testing environment. To exaggerate the fracture for visual analysis, the sample was adjusted in the test stand and more load was applied to obtain a visual understanding of the fracture.

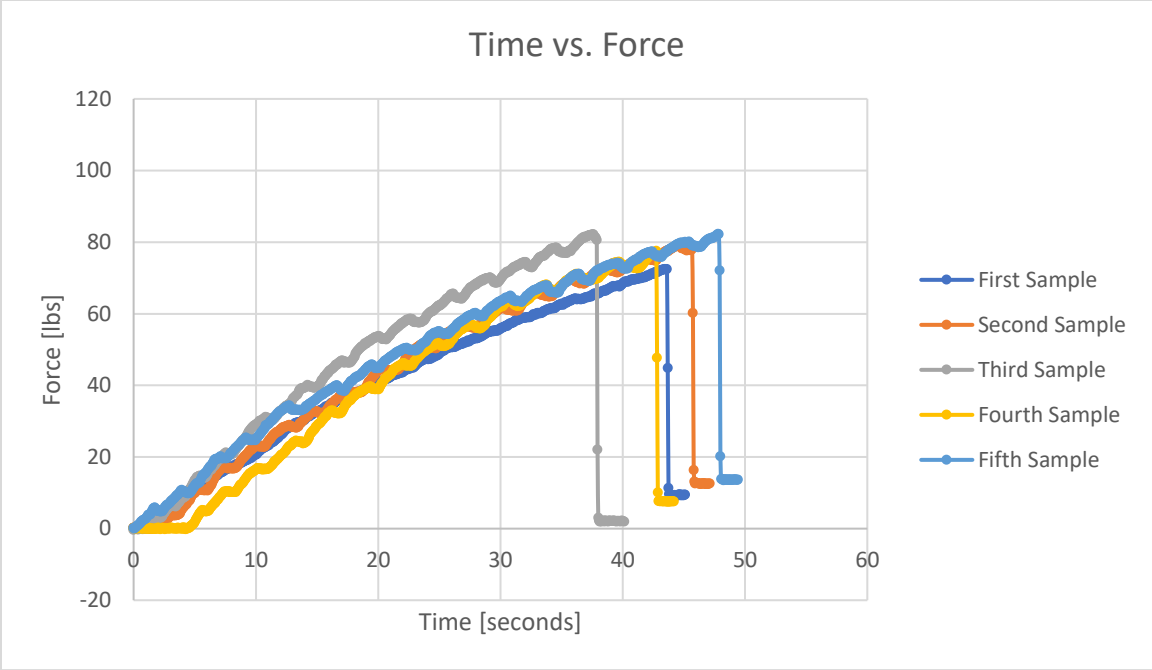

Figure 92: Time vs. Force for 10" Composite I-Beams

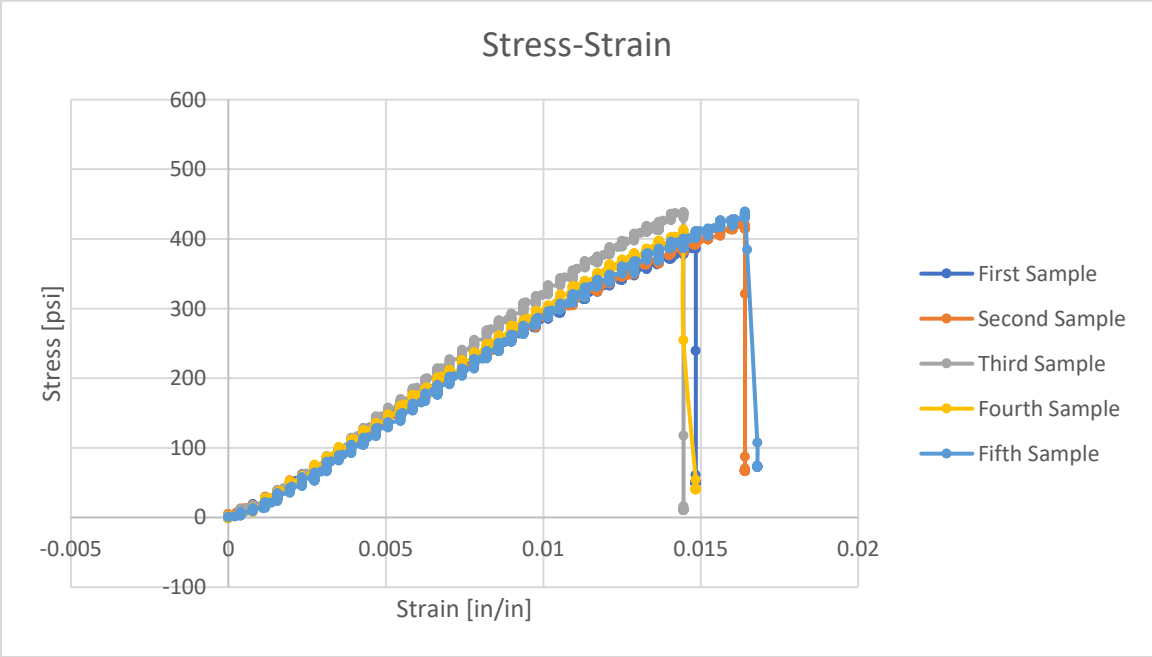

Figure 93: Stress-Strain for 10" Composite I-Beams

Figures 92 and 93 show the graphs for the 10”-long composite I-beams using unidirectional carbon fiber caps with cross-grain balsa shear webs. When looking at the time vs. force graphs, one can see that fracture force for all the I-beams are approximately the same value with the samples reaching to approximately 80 lbs. The force vs. time graphs is a visual representation of the raw data for the tests. Because of this, the stress-strain graphs are better to compare across samples. All the values for stress are approximately the same value showing repeatability between the samples. The stress-strain graphs for each sample are similar and show that repeatability is possible for the composite I-beams.

The graphs work well to understand the individual results of the samples tested, but the goal of this research is to make sure that the Wing Spar Analysis Program can simulate real world loading. To do that, the stress values found through the three-point bending tests were compared with the values calculated by the Wing Spar Analysis Program. The comparison was done using the percent difference between the expected and experimental values. Table 5 shows the maximum shear stress, the expected shear stress, and the associated percent difference to compare the test samples.

Table 8: Test Data from Composite I-Beams

Geometry	Test Specimen	Density of Balsa [lb/in^3]	Max Shear Stress [psi]	Expected Stress [psi]	Percent Difference [%]
Shear Web: 0.125" x 1"	1	7.619	418	350	19.4
Caps: 0.125" x 1.65" carbon	2	7.619	371	350	6.0
5" long cross-grain	3	7.619	377	350	7.7
	4	7.619	361	350	3.1
	5	7.619	409	350	16.9
	6	8.572	373	350	6.6
	7	8.572	408	350	16.6
Shear Web: 0.125" x 1"	1	7.619	362	350	3.4
Caps: 0.125" x 1.65" carbon	2	7.619	329	350	6.0
7.5" long cross-grain	3	7.619	436	350	24.6
	4	8.572	477	350	36.3
	5	8.572	433	350	23.7
	6	8.572	397	350	13.4
Shear Web: 0.125" x 1"	1	8.572	341	350	2.6
Caps: 0.125" x 1.65"	2	8.572	372	350	6.3
10" long cross-grain	3	8.572	387	350	10.6
	4	8.572	365	350	4.3
	5	8.572	387	350	10.6

Figure 94 gives a visual representation of the table showing the stress values found from the various geometry cases with the expected failure stress of 350 psi represented by the horizontal red line.

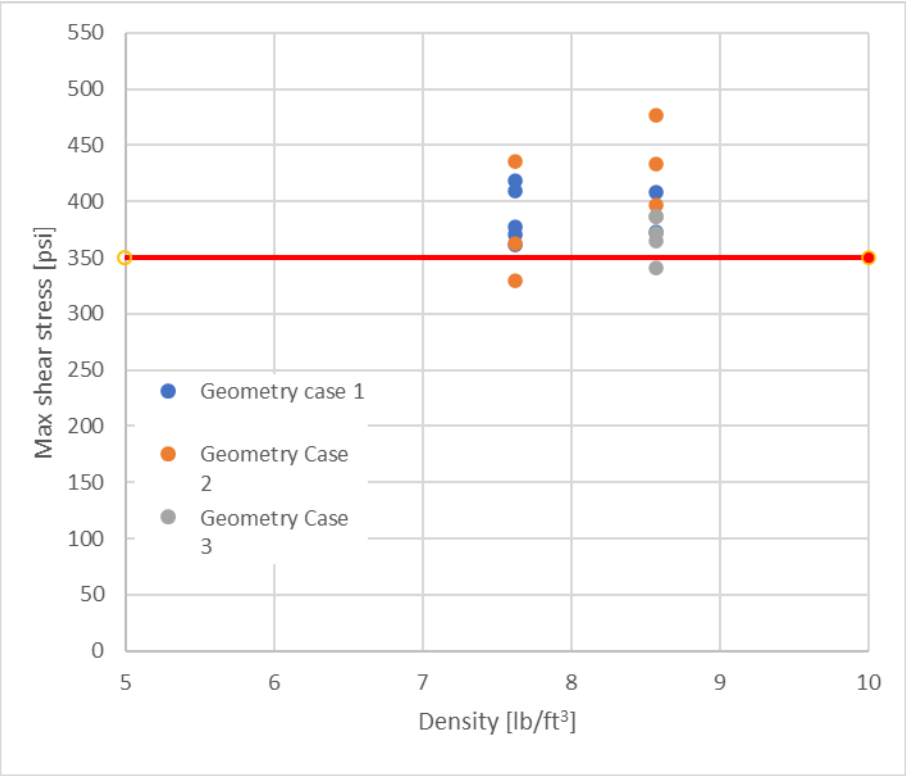

Figure 94: Figure comparing maximum shear stress with theoretical value

The results comparing the expected stress calculated from the Wing Spar Analysis Program and the max shear stress found through the tests are overwhelmingly positive. A statistical analysis was performed to determine the standard deviation, confidence interval at 95%, and the root mean square (RMS) error. The following table shows the values found for this data.

Table 9: Statistical analysis of composite I-beam data

Standard Deviation	36.5
Confidence Interval	16.9
RMS Error	52.7

A range in percent difference from 3.1% to 36.3% is found for all samples tested. If the extrema are removed from the range of values, a new range of 3.1% to 19.4%. The average percent difference for the composite I-beams is 12.1%. This percent difference is smaller than the prototype I-beams showing that using a standard material with recorded material properties in the caps, uni-directional carbon fiber, helps the Wing Spar Analysis Program by giving only one uncertainty in the calculations. The difference in expected vs experimental stress is only dependent on the material composition and non-homogeneity of the balsa wood.

With these tests performed, a database was made for the balsa wood material properties with their associated density. Because the shear strength of the balsa wood so heavily depends on the density of the balsa wood, a reference database was added to the Wing Spar Analysis Program to allow for future engineers to input the correct ultimate shear strength property depending on the density of the balsa wood measured by the engineer. Figure 95 below shows the database now in the Wing Spar Analysis program.

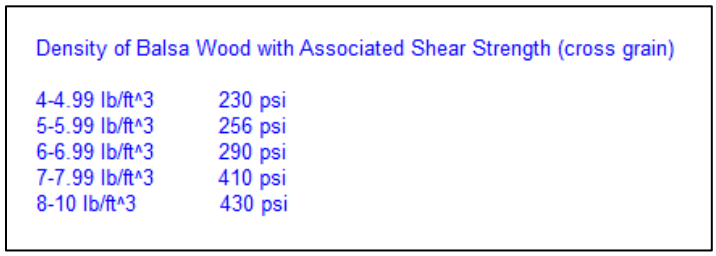

Figure 95: Shear strength database in Wing Spar Analysis Program

Composite I-Beam Results Summary

In conclusion, prototype composite I-beams were made using readily available materials that could be used in quick manufacturing processes. This included I-beams made from plywood caps with balsa wood shear webs and I-beams made from balsa wood with different grain orientations to account for the composites. The primary goal for these tests was to get a visual understanding of what a shear failure and tensile failure looks like with composite I-beams, but the

data was also recorded to allow for early comparisons with the Wing Spar Analysis Program. These tests succeeded in both counts by giving an understanding of what the failure modes looked like and giving reasonable confidence that the Wing Spar Analysis Program could give reliable calculations for composite I-beams.

After the prototype I-beam tests, I-beams were made with cross-grain balsa wood shear webs and unidirectional carbon fiber caps. These I-beams are used in the actual UAVs. These tests give confidence that the Wing Spar Analysis Program can be used for spar analysis with accuracy and repeatability. With an average percent difference of 12.1% between the expected and tested shear stress between 18 samples. These I-beams also give a visual understanding of what happens in the failure of the UAV spars. The shear web fails with a vertical crack which then causes the epoxy bond between the balsa wood and carbon fiber caps to fail due to the large differences in displacement.

CHAPTER VI

SUMMARY AND FUTURE WORK

The final chapter in this thesis will bring together all the testing and knowledge that has been gained throughout this research and paper. From all this knowledge a series of conclusions have been made along with recommendations about future work in the structural analysis of composite I-beams. The material properties of balsa and failure modes have been understood through basic tensile and shear testing. A relationship between the density and ultimate strength has been identified along with a relationship between the thickness and ultimate strength. The Wing Spar Analysis Program has been developed and validated using known solutions for common geometries and material properties to give an average percent difference of 12.1% between the expected and experimental failure stress. The understanding of the unique failure modes in composite I-beams for shear failure in the shear web and tensile failure in the caps has been achieved through testing of prototype and fully composite I-beams. Testing of the composite I-beams has been compared to the Wing Spar Analysis Program and has shown positive results that can be used for future design and analysis of composite I-beams for use in UAVs.

Summary

To begin, The Wing Spar Analysis Program was developed using the transformed area method to analyze composite I-beams. The transformed area method creates a homogenous material I-beam to calculate normal stress, shear stress, and strain along the length of an I-beam under a three-point bending loading scenario. This code was validated by using known solutions to

homogenous materials and known solutions to composite materials found through literature. The results of both calculations, using the program and known solutions, resulted in the same answers giving high confidence that the program could be used for future testing and analysis. The material testing of balsa wood allowed us to gain an understanding of the material properties of thin balsa, 0.125” to 0.25”, under both tensile and shear loading for grain direction parallel and perpendicular to the force direction. The results show a relationship between the density of balsa wood the ultimate strength of balsa wood, but also show a relationship between the thickness of balsa wood and ultimate strength. As the balsa wood increases in thickness, the non-homogeneity of the material becomes more present in the material composition. This increases the probability that imperfections in the balsa will occur causing weak points in the material. These weak points make the balsa weaker and unable to resist higher loads before fracture. These results gained have been used to develop a database of material properties that has been added to the Wing Spar Analysis Program for future design and analysis.

Prototype I-beams were manufactured using a laser cutter and glued together using CA super glue to create quick test samples. These test samples were used to gain a visual understanding of the failure modes for composite I-beams. One group of test samples used plywood caps with balsa wood shear webs to create a shear failure in the balsa wood. The second group of test samples was made using opposite orientation balsa for the shear web and caps to create a tensile failure in the balsa wood caps. These experiments showed that a failure in the cross-grain balsa shear web results in a vertical crack in the shear web with delamination in the bond between the caps and the shear web. A failure in the with-grain balsa shear web results in longitudinal crack down the length of the beam that is like shear buckling of the shear web. A tensile failure in the caps results a break in cap under tension creates a crack through the shear web and cap under compression. The force data from these tests was collected and compared with expected data with the Wing Spar Analysis Program and showed a wide range of percent difference between experimental and expected results.

While there is a wide range of percent difference, the results are repeatable. The large percent difference is attributed to the use of non-homogeneous materials and the compounding effects of the non-homogeneity in the composite I-beams.

Finally, composite I-beams that mimic the spars in UAVs were made using commercial-off-the-shelf carbon fiber caps with cross-grain balsa shear webs. These tests characterized the unique failure modes of composite I-beams while also providing data that was compared with the Wing Spar Analysis Program. Visually, a crack occurs in the balsa wood shear web that then causes failure in the epoxy bond between the balsa wood and carbon fiber caps. It was noticed that the I-beams could handle relatively high stresses, but when failure occurred, the I-beam was not able to recover and handle any more stress. The large amount of displacement after the initial fracture in the shear web causes the delamination in the epoxy bond with the data obtained and manipulated to show stress and strain, the results were compared with those reported from the Wing Spar Analysis Program. These results show an experimental uncertainty on the range of 2% - 15% which was better than expected. This research gives confidence that the Wing Spar Analysis Program can be utilized for composite I-beams undergoing flight loads for different flight envelops.

Goals Achieved

In the Introduction of this research, goals and objectives were described. If these goals and objectives were achieved, the research would be considered a success. The goals and objectives are as follows: The first goal for this research is to understand the structural properties, structural interaction, and failure modes in composite I-beams using carbon fiber caps and a balsa wood shear web. The second goal is to create an analysis tool that uses the transformed area method that can analyze composite I-beams with reasonable certainty for designing UAV wing spars.

The three main conclusions from this research are as follows:

1. The transformed area method works for the analysis of composite I-beams using carbon caps and balsa wood shear webs.
2. The unique failure modes of composite I-beams have been characterized. Mainly, a shear failure in the cross-grain balsa shear web appears as vertical cracks that causes delamination in the epoxy bond.
3. Balsa wood structural properties are heavily dependent on the thickness of the material.

This research has proven that the transformed area method works well for analyzing composite I-beams. Beyond this, with the addition of the material database for balsa wood, the Wing Spar Analysis Program can predict the failure mode of composite I-beams used in aircraft spars. Furthermore, this research has also given an understanding of the unique failure modes of composite I-beams using the balsa shear web. Moving forward, students and researchers will be able to understand the reasoning behind failures that occur in the wing during flight. Finally, it was found the non-homogeneity of balsa wood plays a large role in the strength of the material. As the thickness increases, the probability of imperfections in the material increase. This leads to the initial recommendations of never using balsa wood thicker than 0.125”-thick. Laminating balsa together could possibly be a better alternative compared to thick balsa shear webs when thickness is required for high g-loading.

Future Work

While there are many more opportunities for future research in UAV structural design, the most important takeaway comes from the realization that balsa wood structural properties are dependent on the thickness of the material. So many questions arise from this fact:

Why does the thicker material have these weaknesses? Is it something to do with the manufacturing process or the hand-selection by distributers?

Is this trend repeatable as the thickness is increased over 0.25”-thick?

Are the structural properties of balsa wood shear webs stronger when laminated together compared to solid balsa wood shear webs?

If they are stronger, is it better to laminate the balsa sheets together or stack them together with no lamination?

This idea that balsa wood structural properties are heavily dependent on the thickness of balsa is powerful in how shear webs are designed for UAVs. For years, engineers at Oklahoma State University have been designing shear webs using large pieces of balsa when it is required in high g-loading aircraft. This could mean that this process is incorrect. Future research, like what is done in this research, needs to be performed to understand why this trend occurs and if it is repeatable as the thickness keeps increasing. More importantly, the structural properties of laminated balsa needs to be characterized. A comparison between laminated balsa and solid balsa needs to be performed as well as a comparison between laminated balsa and balsa stacked together without lamination. It is possible that lamination could produce a shear plane that would fail before the balsa wood and cause premature failure of the wing.

The research performed here to understand the structural properties and structural interactions of balsa wood are good beginning research in the field of UAV structures. But this is just the beginning. This research has opened just as many new questions as it has answered. The research presented in the paper has opened the door for future engineers to begin developing the standards that all engineers will use in developing commercial UAVs for use in industry.

REFERENCES

[1] T. Megson, Aircraft Structures for Engineering Students, Oxford, UK: Butterworth-Heinemann, 2016.

[2] M. C. Niu, Airframe Stress and Analysis, Hong Kong: Conmilit Press Ltd., 2011.

[3] P. K. Johnson, "Shear Webs used in Wings," 2003. [Online]. Available: https://www.airfieldmodels.com/information_source/math_and_science_of_model_aircraft/rc_aircraft_design/shear_webs_in_model_aircraft_wings.htm. [Accessed 6 April 2021].

[4] D. Harding, "Dave Harding's Boehle (Bailey) Giant Blog," 15 March 2008. [Online]. Available: http://www.dhaerotech.com/giantblog3.htm. [Accessed 6 April 2021].

[5] A. Arena, "F5D Viper Construction," Stillwater.

[6] CST: The Composites Store, "Comparison Data for Pultruded Shapes," January 2011. [Online]. Available: https://www.cstsales.com/rod_comp.html. [Accessed March 2021].

[7] A. Da Silva and S. Kyriakides, "Compressive response and failure of balsa wood," *International Journal of Solids and Structures*, vol. 44, pp. 8685-8717, 2007.

[8] M. Borrega and G. J. Lorna, *Mechanics of Balsa (Ochroma Pyramidale) Wood,* Elsevier, 2015.

[9] ASTM International, "D143-14: Standard Test Methods for Small Clear Specimens of Timber," ASTM International, West Conshohocken.

[10] N. Kotlarewski, B. Gusamo, B. Bellevile and B. Ozarska, "Mechanical properties of Papua New Guinea balsa wood," *Holz als Roh- und Werkstoff,* 2015.

[11] D. Green, "Wood: Strength and Stiffness," in *Encyclopedia of Materials: Science and Technology*, Elsevier, 2001, pp. 9732-9736.

[12] R. Hibbeler, Mechanics of Materials, Pearson, 2013.

[13] "Aero Light Balsa," National Balsa, 2021. [Online]. Available: https://www.nationalbalsa.com/4_wide_sheets_s/85.htm. [Accessed 28 March 2021].

[14] J. Bodig and B. Jayne, Mechanics of Wood and Wood Composites, Malabar: Krieger Publishing, 1993.

[15] M. Arcan, Z. Hashin and A. Voloshin, "A Method to Produce Uniform Plane-stress States with Applications to Fiber-reinforced Materials," 1978.

[16] Z. Cai and R. J. Ross, "Mechanical Properties of Wood-Based Composite Materials," Forest Products Laboratory.

[17] "Plywood," Matweb, [Online]. Available: http://www.matweb.com/search/datasheet_print.aspx?matguid=bd6620450973496ea2578c283e9fb807. [Accessed 31 March 2021].

APPENDICES

OSU PROPRIETARY

Spar analysis using wing loading from a nonlinear vortex lattice technique for aerodynamic loads, and the bending equations for a composite spar using the Transformed Area Method.

Version history at bottom

Shear and Moment Calcs

$$\text{singf}(\text{power},a,x) := \begin{cases} \text{if power} = -2 \\ \quad \text{return } 1 \text{ if } x = a \\ \quad \text{return } 0 \text{ otherwise} \\ \text{if power} = -1 \\ \quad \text{return } 1 \text{ if } x \geq a \\ \quad \text{return } 0 \text{ otherwise} \\ \text{if power} = 0 \\ \quad \text{return } 1 \text{ if } x \geq a \\ \quad \text{return } 0 \text{ otherwise} \\ \text{if power} \geq 1 \\ \quad \text{return } (x-a)^{\text{power}} \text{ if } x \geq a \\ \quad \text{return } 0 \text{ otherwise} \end{cases}$$

$$w(x) := -F_2 \cdot \text{singf}(-1,0,x) + F_1 \cdot \text{singf}\left(-1,\frac{L}{2},x\right) - F_2 \cdot \text{singf}(-1,L,x)$$ Loading function

$$V(x) := F_2 \cdot \text{singf}(0,0,x) - F_1 \cdot \text{singf}\left(0,\frac{L}{2},x\right) + F_2 \cdot \text{singf}(0,L,x)$$ Shear function

$$m(x) := F_2 \cdot \text{singf}(1,0,x) - F_1 \cdot \text{singf}\left(1,\frac{L}{2},x\right) + F_2 \cdot \text{singf}(1,L,x)$$ Moment function

$$V_{max} := V(0)$$

$$M_{max} := m\left(\frac{L}{2}\right)$$

$$x := 0,1,..L$$

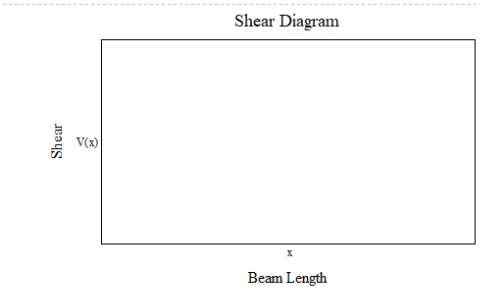

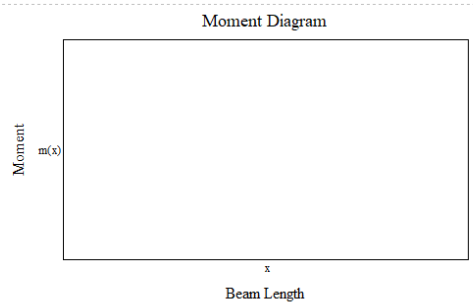

Shear and Moment Calcs

Spar Calculations

Transformed Area Method

Transformed Areas

$A_1 := h_1 \cdot b_1 =$

$A_2 := \frac{h_2 \cdot b_c \cdot E_c}{E}$ $A_{2real} := h_2 \cdot b_c$ $b_{c.new} := \left(\frac{E_c}{E}\right) \cdot b_c$

$A_3 := h_3 \cdot b_1 =$

$x_{NA} := \frac{A_1 \cdot \left(h_3 + h_2 + \frac{h_1}{2}\right) + A_2 \cdot \left(h_3 + \frac{h_2}{2}\right) + A_3 \cdot \frac{h_3}{2}}{(A_1 + A_2 + A_3)}$ Neutral Axis

$A_x := A_1 + A_2 + A_3$

$I_1 := \frac{b_1 \cdot h_1^3}{12} + A_1 \cdot \left[\left(h_3 + h_2 + \frac{h_1}{2}\right) - x_{NA}\right]^2$

$I_{2real} := \frac{b_c \cdot h_2^3}{12} + A_2 \cdot \left(x_{NA} - h_3 - \frac{h_2}{2}\right)^2$

For drawing spar

$x := 0, .1 .. b_1$

$ys_1 := h_3 + h_2$ $xp_1 := \frac{b_1}{2} - \frac{b_c}{2}$ $xpT_1 := \frac{b_1}{2} - \frac{b_c \cdot E_c}{2 \cdot E}$

$ys_2 := h_3$ $xp_2 := \frac{b_1}{2} - \frac{b_c}{2}$ $xpT_2 := \frac{b_1}{2} - \frac{b_c \cdot E_c}{2 \cdot E}$

$$I_2 := \frac{\frac{b_c \cdot E_c}{E} \cdot h_2^3}{12} + A_2 \cdot \left(x_{NA} - h_3 - \frac{h_2}{2}\right)^2$$

$$I_3 := \frac{b_1 \cdot h_3^3}{12} + A_3 \cdot \left(x_{NA} - \frac{h_3}{2}\right)^2$$

$$I := (I_1 + I_2 + I_3) \quad [in^4]$$

$$I_{real} := I_1 + I_{2real} + I_3$$

$$Q_c := A_1 \cdot \left[\left(h_3 + h_2 + \frac{h_1}{2}\right) - x_{NA}\right]$$

$$Q_t := A_3 \cdot \left(x_{NA} - \frac{h_3}{2}\right)$$

$$Q_{max} := A_1 \cdot \left[\left(h_3 + h_2 + \frac{h_1}{2}\right) - x_{NA}\right] + \overrightarrow{\left[(h_3 + h_2 - x_{NA}) \cdot b_c \cdot \frac{(h_3 + h_2 - x_{NA})}{2}\right]}$$

Angular Slope [radians]

$$\theta(x) := \left[\left(\frac{F_2}{2}\right) \cdot \text{singf}(2,0,x) - \left(\frac{F_1}{2}\right) \cdot \text{singf}\left[2,\left(\frac{L}{2}\right),x\right] + \left(\frac{F_2}{2}\right) \cdot \text{singf}(2,L,x) - \frac{F_1 \cdot L^2 \cdot x}{16}\right] \cdot \left(\frac{1}{E \cdot I}\right)$$

$$\theta_{midpoint} := \theta\left(\frac{L}{2}\right)$$

Deflection [inches]

$$\delta(x) := \left[\left(\frac{F_2}{6}\right) \cdot \text{singf}(3,0,x) - \left(\frac{F_1}{6}\right) \cdot \text{singf}\left[3,\left(\frac{L}{2}\right),x\right] + \left(\frac{F_2}{6}\right) \cdot \text{singf}(3,L,x) + \left[\left(\frac{-F_2 \cdot L^3}{6L}\right) + \left[\frac{F_1 \cdot \left(\frac{L}{2}\right)^3}{6 \cdot L}\right]\right] \cdot x\right] \cdot \left(\frac{1}{E \cdot I}\right)$$

$$\delta_{max} := \delta\left(\frac{L}{2}\right)$$

$$\delta_{max.percentage} := \frac{\delta_{max}}{L}$$

$$\sigma_t(x) := \frac{(m(x) \cdot x_{NA})}{I}$$

Normal Tensile Stress

$$\sigma_c(x) := \frac{\left[m(x)\cdot\left(h_1 + h_2 + h_3 - x_{NA}\right)\right]}{I}$$ Normal Compressive Stress

$\sigma_{maxT} := \sigma_t\left(\frac{L}{2}\right) =$ ▪ Max tensile stress

$\sigma_{maxC} := \sigma_c\left(\frac{L}{2}\right) =$ ▪ Max Compressive stress

$$\tau_{max}(x) := \left(\frac{V(x)\cdot Q_{max}}{I_{real}\cdot b_c}\right)$$ Max shear stress at NA [psi] (Transformed beam)

$$\tau_f(x) := \frac{V(x)\cdot Q_c}{I_{real}\cdot b_c}$$ Shear web joint with flange shear stress [psi] (Transformed beam)

Shear web buckling Criteria (Raymer eq. 14.37 ref NACA TN 3781)

$$\tau_{buckle} := 8\cdot E_c\cdot\left(\frac{b_c}{h_2}\right)^2$$

For drawing Cross sectional stresses and strains

$x_{xc_1} := 0$ $\quad \sigma t_1 := \frac{-M_{max}\cdot\left(x_{xc_1} - x_{NA}\right)}{I}$ $\quad \sigma_1 := \frac{-M_{max}\cdot\left(x_{xc_1} - x_{NA}\right)}{I}$ $\quad \varepsilon_1 := \frac{\sigma_1}{E}$

$x_{xc_2} := h_3$ $\quad \sigma t_2 := \frac{-M_{max}\cdot\left(x_{xc_2} - x_{NA}\right)}{I}$ $\quad \sigma_2 := \frac{-M_{max}\cdot\left(x_{xc_2} - x_{NA}\right)}{I}$ $\quad \varepsilon_2 := \frac{\sigma_2}{E}$

$x_{xc_3} := h_3$ $\quad \sigma t_3 := \frac{-M_{max}\cdot\left(x_{xc_3} - x_{NA}\right)}{I}$ $\quad \sigma_3 := \frac{-M_{max}\cdot\left(x_{xc_3} - x_{NA}\right)}{I}\cdot\frac{E_c}{E}$ $\quad \varepsilon_3 := \frac{\sigma_3}{E_c}$

$x_{xc_4} := h_3 + h_2$ $\quad \sigma t_4 := \frac{-M_{max}\cdot\left(x_{xc_4} - x_{NA}\right)}{I}$ $\quad \sigma_4 := \frac{-M_{max}\cdot\left(x_{xc_4} - x_{NA}\right)}{I}\cdot\frac{E_c}{E}$ $\quad \varepsilon_4 := \frac{\sigma_4}{E_c}$

$x_{xc_5} := h_3 + h_2$ $\quad \sigma t_5 := \frac{-M_{max}\cdot\left(x_{xc_5} - x_{NA}\right)}{I}$ $\quad \sigma_5 := \frac{-M_{max}\cdot\left(x_{xc_5} - x_{NA}\right)}{I}$ $\quad \varepsilon_5 := \frac{\sigma_5}{E}$

$x_{xc_6} := h_3 + h_2 + h_1$ $\quad \sigma t_6 := \frac{-M_{max}\cdot\left(x_{xc_6} - x_{NA}\right)}{I}$ $\quad \sigma_6 := \frac{-M_{max}\cdot\left(x_{xc_6} - x_{NA}\right)}{I}$ $\quad \varepsilon_6 := \frac{\sigma_6}{E}$

status := "0.5% Strain Warning" if $100\cdot|\varepsilon_1| > 0.5$

"0.5% Strain Warning" if $100\cdot|\varepsilon_6| > 0.5$

"COMPRESSIVE FAILURE !" if $\sigma_{maxC} > \sigma_{ult\_c}$

"TENSILE FAILURE !" if $\sigma_{maxT} > \sigma_{ult\_t}$

"SHEAR FAILURE !" if $\tau_{max}(1) > \tau_{ult}$

"SHEAR BUCKLING ! " if $\tau_{max}(1) > \min(\tau_{buckle})$

"Within Limits" otherwise

Spar Calculations

Detailed Geometry

TEST SETUP INPUT

Applied force from test stand

$F_1 \equiv$

$L \equiv$ Length of beam [inches]

$F_2 \equiv \frac{F_1}{2}$ Resultant forces

Shear-Moment Diagram for Beam

$x := 0, 1, ..L$

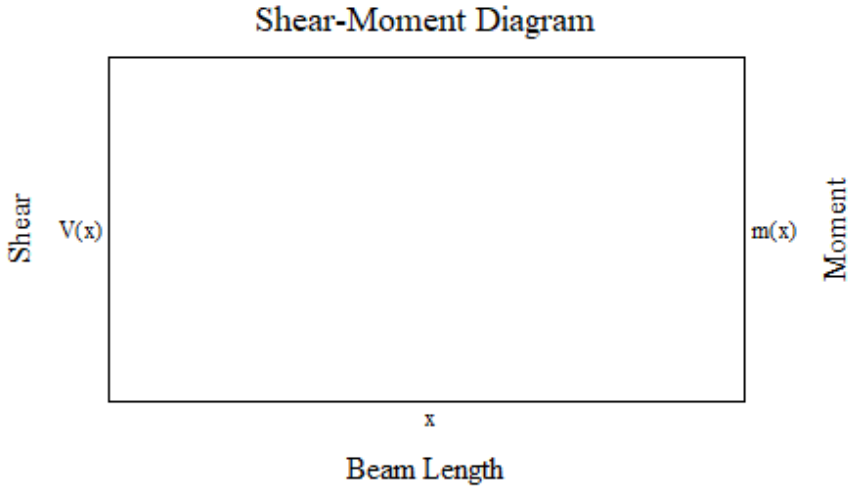

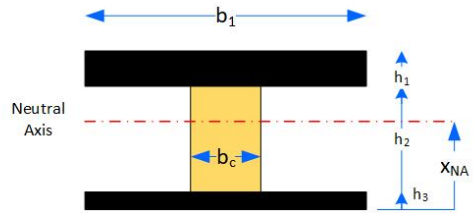

SPAR INPUTS

$h_1 \equiv$ ▮ Spar cap thickness (compression) [in] (0.005" is the approx thickness of one layer of carbon uni-tape)

$h_2 \equiv$ ▮ Core Height [in]

$h_3 \equiv$ ▮ Spar cap thickness (tension) [in] (0.005" is the approx thickness of one layer of carbon uni-tape)

$b_1 \equiv$ ▮ cap width [in]

$b_c \equiv$ ▮ core width [in]

$E \equiv \quad =$ ▮ Youngs Modulus of spar cap material [psi] - carbon is 135*145*1000

$E_c \equiv$ ▮ Youngs Modulus of core material [psi]

$\sigma_{ult\_c} =$ ▮ Ultimate compressive strength (cap) [psi]

$\sigma_{ult\_t} =$ ▮ Ultimate tensile strength (cap) [psi]

$\tau_{ult} =$ ▮ Ultimate shear strength (core) [psi]

Real Beam

Transform Beam

$V_{max} =$ ▮ Max Shear Force [lb]

$M_{max} =$ ▮ Max Bending Moment [in-lb]

$\tau_{max}(1) =$ ▮ Max shear stress

$\tau_f(1) =$ ▮ Max shear stress in bond

$\sigma_{maxT} =$ ▮ Max bending stress Tension [psi]

$\sigma_{maxC} =$ ▮ Max bending stress Compression [psi]

status = ▮

Beam Deflection

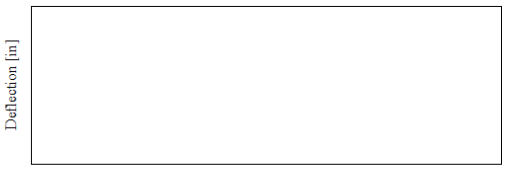

Max Bending Stress

Max Shear Stress

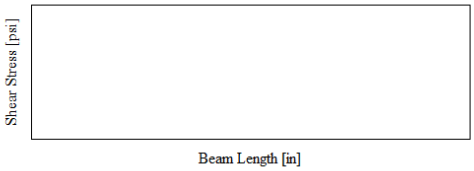

Write to File

data := augment(x_{xc}, σ)

$100 \frac{\sigma_{maxT}}{E} =$ ▮ Max tensile strain [%] (1% is large for beam theory assumptions)

$100 \frac{\sigma_{maxC}}{E} =$ ▮ Max compressive strain [%] (1% is large for beam theory assumptions)

$\delta_{max} =$ ▮ Max Deflection [in]

$\delta_{max.percentage} =$ ▮ Max Deflection [%]

$\theta_{midpoint} \cdot 57.3 =$ ▮ Max Anglular Deflection [deg]

$x_{NA} =$ ▮ Neutral Axis [in]

Transform Spar

Normal Stress

Real Spar

Normal Stress

P:...\Wing\SPAR\data.txt

data

Version History

1.0	Original program		26 April 2020
	1.1	Added shear stress calculations	29 April 2020
	1.2	Added 0.5% strain warning	03 May 2020
2.0	Added variable core height to allow poly-tapered beams		03 May 2020
	2.1	Added core shear buckling criterion	13 May 2020

Divinycell	
shear strength	145 psi
tensile strength	319 psi
E	11.6 ksi

Balsa	
shear strength (with grain)	304 psi
tensile strength	2161/1900 psi
compressive strength	1895 psi
E (cross grain)	7614 psi
E (with grain)	493128 psi

**For now assume balsa shear strength x-grain is 3x with grain (greed01d.pdf)

% Strain

%

Density of Balsa Wood with Associated Shear Strength (cross grain)

4-4.99 lb/ft^3	230 psi
5-5.99 lb/ft^3	256 psi
6-6.99 lb/ft^3	290 psi
7-7.99 lb/ft^3	410 psi
8-8.99 lb/ft^3	430 psi
9-9.99 lb/ft^3	360 psi
10+ lb/ft^3	430 psi

REFERENCES

[1] T. Megson, Aircraft Structures for Engineering Students, Oxford, UK: Butterworth-Heinemann, 2016.

[2] M. C. Niu, Airframe Stress and Analysis, Hong Kong: Conmilit Press Ltd., 2011.

[3] P. K. Johnson, "Shear Webs used in Wings," 2003. [Online]. Available: https://www.airfieldmodels.com/information_source/math_and_science_of_model_aircraft/rc_aircraft_design/shear_webs_in_model_aircraft_wings.htm. [Accessed 6 April 2021].

[4] D. Harding, "Dave Harding's Boehle (Bailey) Giant Blog," 15 March 2008. [Online]. Available: http://www.dhaerotech.com/giantblog3.htm. [Accessed 6 April 2021].

[5] A. Arena, "F5D Viper Construction," Stillwater.

[6] CST: The Composites Store, "Comparison Data for Pultruded Shapes," January 2011. [Online]. Available: https://www.cstsales.com/rod_comp.html. [Accessed March 2021].

[7] A. Da Silva and S. Kyriakides, "Compressive response and failure of balsa wood," *International Journal of Solids and Structures*, vol. 44, pp. 8685-8717, 2007.

[8] M. Borrega and G. J. Lorna, *Mechanics of Balsa (Ochroma Pyramidale) Wood,* Elsevier, 2015.

[9] ASTM International, "D143-14: Standard Test Methods for Small Clear Specimens of Timber," ASTM International, West Conshohocken.

[10] N. Kotlarewski, B. Gusamo, B. Bellevile and B. Ozarska, "Mechanical properties of Papua New Guinea balsa wood," *Holz als Roh- und Werkstoff,* 2015.

[11] D. Green, "Wood: Strength and Stiffness," in *Encyclopedia of Materials: Science and Technology*, Elsevier, 2001, pp. 9732-9736.

[12] R. Hibbeler, Mechanics of Materials, Pearson, 2013.

[13] "Aero Light Balsa," National Balsa, 2021. [Online]. Available: https://www.nationalbalsa.com/4_wide_sheets_s/85.htm. [Accessed 28 March 2021].

[14] J. Bodig and B. Jayne, Mechanics of Wood and Wood Composites, Malabar: Krieger Publishing, 1993.

[15] M. Arcan, Z. Hashin and A. Voloshin, "A Method to Produce Uniform Plane-stress States with Applications to Fiber-reinforced Materials," 1978.

[16] Z. Cai and R. J. Ross, "Mechanical Properties of Wood-Based Composite Materials," Forest Products Laboratory.

[17] "Plywood," Matweb, [Online]. Available: http://www.matweb.com/search/datasheet_print.aspx?matguid=bd6620450973496ea2578c283e9fb807. [Accessed 31 March 2021].

VITA

ZACHARY TAYLOR WATKINS

Candidate for the Degree of

Master of Science

Thesis: MODELING AND FAILURE ANALYSIS OF COMPOSITE I-BEAMS FOR UAV WING SPAR DESIGN

Major Field: Mechanical and Aerospace Engineering

Biographical:

Education:

Completed the requirements for the Master of Science in your major at Oklahoma State University, Stillwater, Oklahoma in May 2021.

Completed the requirements for the Bachelor of Science in Mechanical Engineer at University of Oklahoma , Norman, Oklahoma in 2019

Experience:

Graduate Research Assistant to Dr. Andy Arena, Department of Mechanical and Aerospace Engineering, Oklahoma State University, August 2019 – May 2021. Responsibilities included: designing, manufacturing, and testing composite unmanned aerial vehicles and their accompanying systems.